JOURNAL OF OPTOELECTRONICS AND ADVANCED MATERIALS Vol. 9, No. 12, December 2007, p. 3655 - 3701

Review Paper

Laser photoacoustic spectroscopy: principles, instrumentation, and characterization

D. C. DUMITRAS*, D. C. DUTU, C. MATEI, A. M. MAGUREANU, M. PETRUS, C. POPA
Department of Lasers, National Institute for Laser, Plasma, and Radiation Physics, 409 Atomistilor St., PO Box MG-36, 077125 Bucharest, Romania

Laser photoacoustic spectroscopy has emerged over the last decade as a very powerful investigation technique, capable of measuring trace gas concentrations at sub-ppbV level. Recent achievements in this field have made it possible to fully characterize the method and improve the design of instrument components in view of the task they are expected to fulfill. The basic principles of laser photoacoustic spectroscopy are reviewed and compared with those of other spectroscopic techniques. Photoacoustic signal generation is discussed, covering different aspects regarding resonant cells, that are resonance frequencies, dissipation processes, quality factor, pressure amplitude, cell constant, optimal PA cell geometry, voltage signal, and saturation effects. Noises and other limiting factors which determine the ultimate detection sensitivity are presented, and various types of noises are measured. The interfering gases play an important role both in limiting the sensitivity of the method and in the multicomponent analysis of the atmosphere. We therefore discuss the experimental measures for reducing the influence of interfering gases in a single component measurement and the methods used in multicomponent analysis. Based on a general schematic, the main components are described in detail. Special emphasis is laid on the home-built, frequency-stabilized, line-tunable CO_2-laser source and the resonant photoacoustic cell. All of the parameters that are characteristic of the photoacoustic cell, including the limiting sensitivity of the system, are measured and compared with the best results reported by other authors. Approaches to improving current sensor performance are also discussed. Other aspects of a functional photoacoustic instrument, such as the gas handling system and data acquisition and processing, are outlined. As a typical application, we present a precise measurement of the absorption coefficients of ethylene at CO_2 laser wavelengths. While the values obtained for the 10-μm band excellently agree with other measurements reported in the literature, important differences were found for the absorption coefficients in the 9-μm band. Other applications are briefly reviewed in the last section.

(Received November 26, 2007; accepted December 4, 2007)

Keywords: Laser photoacoustic spectroscopy, PA signal, Noises, Frequency-stabilized CO_2-laser, PA cell, Trace gas measurements, Absorption coefficients of ethylene

1. Introduction

The photoacoustic (PA) (formerly also known as optoacoustic) effect consisting in sound generation from the interaction of light and matter was discovered by Alexander Graham Bell [1]. He noticed that focused intensity-modulated light (chopped sunlight) falling on an optically absorbing solid substance produced an audible sound. In the next year, light absorption was detected through its accompanying acoustic effect not only in solids, but also in liquids and gases by Bell [2], Tyndall [3], Röntgen [4], and Preece [5]. They found the sound was stronger when the substance was placed in a sample cell (then called "photophone" and later "spectrophone"). It was Bell again that first described the resonant amplification of the PA signal [2]. The PA effect was also investigated at different light wavelengths. Bell and Preece were among the first to notice a PA signal for an aerosol when they experimented with cigar smoke. The advances of photoacoustic spectroscopy up to the invention of the laser were reviewed by Kaiser in 1959 [6].

Over the last four decades, technological developments in the field of lasers and high-sensitivity pressure detection systems (microphones and electronics) have contributed to the substantial progress of photoacoustic spectroscopy. The introduction of laser light sources emitting highly monochromatic and collimated intense beams have opened up new areas of research. Lasers provide the advantage of high spectral power density owing to their intrinsic narrow linewidth in the range of MHz. This laser linewidth is usually much smaller than the molecular absorption linewidth (GHz region at atmospheric pressure), and therefore it is not an important issue in most measurements. A true revival of PA spectroscopy was due to Kerr and Atwood [7], who made the earliest experiments with a laser illuminated PA detector in 1968, and Kreuzer [8], who first measured gas concentrations using a PA detector and a laser in 1971. Later experiments by Kreuzer and collaborators [9, 10] effectively demonstrated the extremely high sensitivity attainable by this method. To improve the detection of atmospheric pollutants, Dewey *et al*. [11] used in 1973 an acoustic resonance chamber and reached amplification factors higher than 100. In 1977 the feasibility of *in situ* aerosol measurements, which were important for atmospheric applications, was first reported by Bruce and Pinnick [12] and Terhune and Anderson [13]. Subsequently, many experimental and theoretical works

have been reported in the literature, proving the applicability of the method not only in spectroscopy, but also in various fields of physics, chemistry, biology, medicine, and engineering. The potential of laser photoacoustic spectroscopy (LPAS) has been discussed in several review articles [14-24] and books [25-34].

The most important features for a gas sensor include high sensitivity and selectivity, large dynamic range, high accuracy and precision, good temporal resolution, ease of use, versatility, reliability, robustness, and multicomponent capability. Gas chromatographs are neither sensitive nor fast enough. Although there is no ideal instrument that would fulfill all the requirements mentioned above, a spectroscopic method and particularly the simple setup of LPAS provide several unique advantages, notably the multicomponent capability, high sensitivity and selectivity, wide dynamic range, immunity to electromagnetic interferences, convenient real time data analysis, operational simplicity, relative portability, relatively low cost per unit, easy calibration, and generally no need for sample preparation. LPAS is primarily a calorimetric technique and, as such, differs completely from other previous techniques, as the absorbed energy can be determined directly, instead of via measurement of the intensity of the transmitted or backscattered radiation. In conjunction with tunable lasers, the *in situ* monitoring of many substances occurring at ppbV (parts per billion volume) or even pptV (parts per trillion volume) concentrations is a routine task today. PA detection provides not only high sensitivity but also the necessary selectivity for analyzing multicomponent mixtures by the use of line-tunable IR lasers, e.g., CO lasers [35] or CO_2 lasers [19].

CO_2 laser photoacoustic spectroscopy offers a sensitive technique for detection and monitoring of trace gases at low concentrations. The CO_2 laser is of special interest, as it ensures high output power in a wavelength region (9-11 μm) where more than 250 molecular gases/vapors of environmental concern for atmospheric, industrial, medical, military, and scientific spheres exhibit strong absorption bands [36]. This laser, however, can be only stepwise tuned when operated in cw. Nevertheless, it is an ideal source to push the sensitivity of PA gas detection into the concentration range of ppbV or even lower. Instruments based on LPAS have nearly attained the theoretical noise equivalent absorption detectivity of 10^{-10} cm^{-1} in controlled laboratory conditions [37]. This high sensitivity cannot be achieved in real detection conditions due to the coherent photoacoustical background signal and interfering background absorption of normal atmospheric constituents.

At present many research groups are actively involved in the development of LPAS systems for various applications in different disciplines, including nondestructive evaluation of materials, environmental analysis, agricultural, biological, and medical applications, investigation of physical processes (phase transitions, heat and mass transfer, kinetic studies), and many others. Our facility, which was originally designed for ethylene analysis at the low parts per billion level, is adaptable with minor modifications to a broad range of gases and vapors having absorption spectra in the infrared (IR).

In this paper, the basic principles of laser photoacoustic spectroscopy are reviewed and compared with other spectroscopic techniques. Photoacoustic signal generation is discussed at length, covering different aspects relative to resonant cells, resonance frequencies, dissipation processes, quality factor, pressure amplitude, cell constant, optimization of PA cell geometry, voltage signal and saturation effects. Noise and other limiting factors, which determine the ultimate detection sensitivity, are described in detail, and measurements of various types of noise are presented. We discuss the experimental measures for reducing the influence of interfering gases in a single component measurement and the methods used in multicomponent analysis. The main components are lengthily described based on a general schematic. Special consideration is given to the home-built, frequency-stabilized, line-tunable CO_2-laser source and the resonant photoacoustic cell. All of the parameters that characterize photoacoustic cells, including the limiting sensitivity of the system, are measured and compared with the best results reported by other authors. Approaches to improving the current sensor performance are also tackled. Other aspects of a functional photoacoustic instrument, such as the gas handling system and data acquisition and processing are outlined. As a typical application, we present a precise measurement of the absorption coefficients of ethylene at CO_2 laser wavelengths. The last section is a succinct review of various applications.

2. Basic principles

A gaseous molecule that absorbs electromagnetic radiation is excited to a higher electronic, vibrational or rotational quantum state. The excited state loses its energy by radiation processes, such as spontaneous (fluorescence) or stimulated emission, and/or by collisional relaxation, in which energy is converted into translational energy. Radiative emission and chemical reactions do not play an important role in the case of vibrational excitation, because the radiative lifetimes of the vibrational levels are long compared with the time needed for collisional deactivation at pressures used in photoacoustics (~1 bar), and the photon energy is too small to induce chemical reactions. Thus, in practice the absorbed energy is completely released via either fluorescence (at low pressures) or collisions. The latter give rise to a gas temperature increase due to energy transfer to translation as heat, appearing as translational (kinetic) energy of the gas molecules. The deposited heat power density is proportional to the absorption coefficient and incident light intensity. The nonradiative relaxation process occurs when the relaxation time can compete with the radiative lifetime of the excited energy levels. Radiative decay has a characteristic lifetime of 10^{-7} s at visible wavelengths as compared with 10^{-2} s in IR at 10 μm. For nonradiative decay these values depend on pressure (the decay time τ is inversely proportional to pressure) and may vary strongly

at atmospheric pressures (10^{-3}-10^{-8} s) depending on the gas nature and the involved energy level.

There are three techniques of linear laser spectroscopy, based on measurement of different physical quantities:

- the absorption method and the cavity ringdown spectroscopy (intensity);
- the radiative method (fluorescence); and
- the photothermal (calorimetric) method (pressure, temperature).

The most important optical process, as far as spectroscopic trace gas detection is concerned, is based on the extinction of radiation by molecular absorption. The absorption features and strengths specific of each molecule make it possible to identify trace gases and determine their concentrations. Absorption coefficients are typically on the order of 1 cm^{-1} (one wave number). The absorption of trace gas molecules in a gas mixture may be monitored by detecting the attenuation of the laser beam over a fixed absorption path length L. According to the Beer-Lambert law, the transmitted laser power in the absence of saturation is given by:

$$P(L) = P(0)\exp(-\alpha_p L) = P(0)\exp(-\alpha c L) \qquad (1)$$

where $P(0)$ and $P(L)$ are the laser powers before and after the absorption cell, respectively; α_p (cm^{-1}) is the absorption coefficient at a given pressure of the gas at a specific laser wavelength: $\alpha_p = \alpha c$; α (cm^{-1} atm^{-1}) is the gas absorption coefficient (the absorption coefficient normalized to unit concentration), and c (atm) is the trace gas concentration. Also, $\alpha_p = N_{tot}\sigma$, where σ (cm^2) is the absorption cross section per molecule and $N_{tot} = 2.5\times10^{19}$ molecules cm^{-3} is the number of absorbing molecules per cubic centimeters at 1013 mbar and 20 ^oC. It results:

$$c = -\frac{1}{\alpha L}\ln\frac{P(L)}{P(0)} = -\frac{1}{\alpha L}\ln\left(1-\frac{\Delta P}{P(0)}\right) \cong \frac{1}{\alpha L}\frac{\Delta P}{P(0)} \qquad (2)$$

which is valid for $\Delta P/P(0) << 1$ (optically thin sample), where $\Delta P = P(0) - P(L)$. For a given L, the detection limit is given by the smallest relative change $\Delta P_{min}/P(0)$ that can be measured in the transmitted signal. For dilute mixtures and modest absorption path lengths, the desired signal is the small difference between two large values so that high quantitative accuracies in signal intensities are required. The most sensitive method employs frequency modulation and harmonic detection. The sensitivity depends on the linewidth, and for atmospherically broadened lines Reid *et al.* [38] have reached $\Delta P_{min}/P(0) \cong 10^{-5}$ in a diode laser spectrometer (1050-1150 cm^{-1}). With a path length of 100 m, the result is a sensitivity of 10^{-9} cm^{-1}, which corresponds to concentrations of 3 ppbV of a weakly absorbing molecule such as SO_2 (ν_1 band), or 0.01 ppbV of a strongly absorbing molecule such as CO. Assuming the same detectable attenuation $\Delta P_{min}/P(0) \cong 10^{-5}$, a path length L = 1 m, and an absorption coefficient α = 30.4 $cm^{-1}atm^{-1}$ (typical of fundamental absorption in the mid-IR), one obtains a minimum detectable absorption coefficient $\alpha_p = 10^{-7}$ cm^{-1}. This number corresponds to a concentration of 3.3 ppbV at atmospheric pressure. Conventional absorption techniques, which require precise measurements of the difference between two nearly equal signals, are, however, unable to realize the full potential of the higher power levels now attainable. Improvement may be obtained by: increasing the path length L in a multipass or intracavity arrangement, or using wavelength modulation, i.e., by modulating the wavelength of the incident intensity across a molecular absorption line. In multipass transmission absorption spectroscopy, a multipass transmission cell (White cell) filled with analyte gas with mirrors at each end is used. The beam is folded back and forth through the cell, creating an extended yet defined optical path length within a confined space.

Cavity ringdown spectroscopy confines gas in an optically reflective cavity where laser radiation is introduced. Radiation amplitude decays at a certain rate in the absence of absorption. An absorbing sample gas in the cavity increases the rate of decay, thus indicating the presence of an absorbing species. The advantages of the method are high sensitivity and a small sample volume, while indirect measurement is an important drawback: as the measured parameter is the rate of light intensity decay, decay caused by absorption by the analyte of interest has to be distinguished from the one caused by the mirrors and other cavity-dependent losses.

In linear detection, sensitivity is limited by laser power fluctuations, and a considerable improvement can be obtained by the dark background methods, in which one measures a quantity that is directly proportional to absorption, rather than that part of the laser beam which is absorbed. In the visible, this can be done by monitoring the fluorescence from the upper level of the transition. In the infrared, however, the spontaneous emission rate is too low, and most of the excess vibrational energy is converted to heat through inelastic collisions.

The fluorescence method requires that a certain part of the excitation should relax through radiative channels. This condition is fulfilled by detecting atoms and molecules in the UV, visible, and near-IR spectral regions. As a principal advantage of the fluorescence techniques, the observed signal is proportional to the concentration of the measured species and the accuracy, therefore, depends on the magnitude of the signal relative to detector noise. The sensitivity is so high, that it makes it possible to detect single atoms in the laser beam.

The basic principle of all photothermal (PT) techniques is the absorption of light in a sample leading to a change in its thermal state. This may be a change in temperature or another thermodynamic parameter of the sample that is related to temperature. Measurement of either the temperature, pressure or density change that occurs due to optical absorption is ultimately the basis for all PT spectroscopic methods. PT analysis can be considered as an indirect absorption measurement, since the measured quantity is not an optical signal. (It should be noted here that the classical absorption measurement is not a direct measurement either. Though the measured value in this case is an optical one, namely the transmitted light,

the absorbed light quantity is derived from the difference of the incident energy and the transmitted one). The sample heating which produces the PT signal is directly correlated to the absorbed electromagnetic energy. Unlike in conventional transmission spectroscopy, neither scattered nor reflected light contributes to the signal. Although a PT effect can be induced by any light source, lasers are nowadays the preferred source of excitation for two reasons: (i) To a first approximation, the PT signal is proportional to the temperature rise in the sample and thus proportional to the absorbed energy. (ii) For many applications, the selectivity of a PT analysis, as with any other absorption method, depends on the tunability of the excitation wavelength.

PA spectroscopy is an indirect technique in that an effect of absorption is measured rather than absorption itself. Hence the name of photoacoustic: light absorption is detected through its accompanying acoustic effect. The advantage of photoacoustics is that the absorption of light is measured on a zero background; this is in contrast with direct absorption techniques, where a decrease of the source light intensity has to be observed. The spectral dependence of absorption makes it possible to determine the nature of the trace components. The PA method is primarily a calorimetric technique, which measures the precise number of absorbent molecules by simply measuring the amplitude of an acoustic signal. In LPAS the nonradiative relaxation which generates heat is of primary importance. In the infrared spectral region, nonradiative relaxation is much faster than radiative decay.

PA spectroscopy relies on the PA effect for the detection of absorbing analytes. The sample gas is in a confined (resonant or nonresonant) chamber, where modulated (e.g., chopped) radiation enters via an IR-transparent window and is locally absorbed by IR-active molecular species. The temperature of the gas thereby increases, leading to a periodic expansion and contraction of the gas volume synchronous with the modulation frequency of the radiation. This generates a pressure wave that can be acoustically detected by a suitable sensor, e.g., by a microphone. The advantages of the PA method are high sensitivity and small sample volume; besides, the acoustic measurement makes optical detection unnecessary. The main drawback is caused by the sensitivity to acoustic noise, because the measurements are based on an acoustic signal.

A concise comparison of the linear laser spectroscopy methods is presented in Table 1 [27].

Table 1. Comparison of linear laser spectroscopy methods.

Method / Characteristics	Absorption	Fluorescence	PA
Spectral range	UV – far IR	UV and visible	UV – far IR
Sensitivity (cm^{-1})	$10^{-5} – 10^{-9}$	Up to single atoms	$10^{-7} – 10^{-10}$
Time resolution (s)	1	$1 – 10^{-12}$	$1 – 10^{-3}$
Necessary conditions	-	Radiative channels of relaxation	Nonradiative channels of relaxation

The favorable properties of LPAS are essentially determined by the characteristics of the laser. The kind and number of detectable substances is related to the spectral overlapping of the laser emission with the absorption bands of the trace gas molecules. Thus, the accessible wavelength range, tunability, and spectral resolution of the laser are of prime importance. With respect to minimum detectable concentrations (LPAS sensitivity), a laser with high output power P_L is a benefit, because the PA signal is proportional to P_L. The broad dynamic range is an inherent feature of LPAS and therefore is not affected by the choice of the radiation source. In contrast to remote-sensing methods, LPAS is a detection technique applied locally to samples enclosed in a PA cell. In order to still obtain some spatial resolution, either the samples have to be transported to the system, or the system has to be portable. The temporal resolution of LPAS is determined by the time needed for laser tuning and the gas exchange within the cell. Thus, a small volume PA cell and a fast tunable laser are a plus.

The availability of suitable laser sources plays a key role, as they control the sensitivity (laser power), selectivity (tuning range), and practicability (ease of use, size, cost, and reliability) that can be achieved with the photoacoustic technique. The CO_2 laser perfectly fits the bill for a trace gas monitoring system based on LPAS. This IR laser combines simple operation and high output powers. The frequency spacing between two adjacent CO_2-laser transitions range from 1 to 2 cm^{-1}. By contrast, the typical width of a molecular absorption line is approximately 0.05 to 0.1 cm^{-1} for atmospheric conditions. Since this is not a continuously tunable source, coincidences between laser transitions and trace gas absorption lines are mandatory. Fortunately, this does not hamper its applicability to trace gas detection, as numerous gases exhibit characteristic absorption bands within the wavelength range of the CO_2 laser which extends from 9 to 12 μm when different CO_2 isotopes are used. The CO_2 laser spectral output occurs in the wavelength region where a large number of compounds (including many industrial substances whose adverse health effects are a growing concern) possess strong characteristic absorption features and where absorptive interferences from water vapors, carbon dioxide, and other major atmospheric gaseous components may influence the measurements.

The PA effect in gases can be divided into five main steps (Fig. 1):

1. Modulation of the laser radiation (either in amplitude or frequency) at a wavelength that overlaps with a spectral feature of the target species; an electrooptical modulation device may also be employed, or the laser beam is modulated directly by modulation of its power supply; the extremely narrowband emission of the laser allows the specific excitation of molecular states; the laser power should be modulated with a frequency in the range $\tau_{th} >> 1/f >> \tau_{nr}$, where τ_{th} is the thermal relaxation time, and τ_{nr} the nonradiative lifetime of the excited energy state of the molecule.
2. Excitation of a fraction of the ground-state molecular population of the target molecule by absorption of the incident laser radiation that is stored as vibrational-rotational energy; the amount of energy absorbed from the laser beam depends on the absorption coefficient, which is a function of pressure.
3. Energy exchange processes between vibrational levels (V-V: vibration to vibration transfer) and from vibrational states to rotational and translational degrees of freedom (V-R, T transfer); the energy which is absorbed by a vibrational-rotational transition is almost completely converted to the kinetic energy of the gas molecules by collisional de-excitation of the excited state; the efficiency of this conversion from deposited to translational energy depends on the pressure and internal energy level structure of the molecule; vibrational relaxation is usually so fast that it does not limit the sensitivity; however, notable anomalies occur in the case of diatomic molecules, such as CO, where vibrational relaxation is slow in the absence of a suitable collision partner, and of the dilute mixtures of CO_2 in N_2, where the vibrational energy is trapped in slowly relaxing vibrational states of N_2; the kinetic energy is then converted into periodic local heating at the modulation frequency.
4. Expansion and contraction of the gas in a closed volume that give rise to pressure variation which is an acoustic wave; the input of photon energy with correct timing leads to the formation of a standing acoustic wave in the resonator.
5. Monitoring the resulting acoustic waves with a microphone; the efficiency with which sound is transmitted to the microphone depends on the geometry of the cell and the thermodynamic properties of the buffer gas.

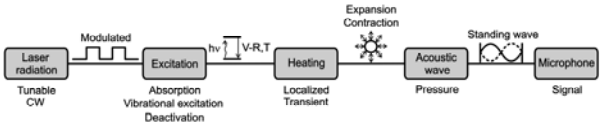

Fig. 1. Schematic of the physical processes occurring during optical excitation of molecules in photoacoustic spectroscopy.

From kinetic gas theory it can be estimated that a molecule performs 10^9-10^{10} collisions per second at 1 bar pressure. This means that at atmospheric pressure the photon energy is transformed into an acoustical signal in about 10^{-5}-10^{-6} s. For most polyatomic molecules signal production is even faster. The time needed by the pressure wave to travel from the laser beam area to the microphone in the acoustic cell is therefore in most cases longer than the vibrational relaxation time. For a distance of a few centimeters this transit time is about 10^{-4} s. The time delay between excitation and detection of the pressure wave, however, is influenced not only by energy transfer processes and the transit time, but also by the response time of the gas-microphone system, being about 10^{-4} s or longer [16].

A typical setup of a resonant LPAS, as used in the authors' laboratory for gas studies, is shown in Fig. 2. The continuous wave laser radiation is amplitude-modulated by a mechanical chopper operating at an acoustic resonance frequency of the PA cell. It is then focused by a lens and directed through the resonant PA cell. The transmitted laser power is monitored with a power meter (signal P in Fig. 2). Inside the cell the radiation produces pressure modulation recorded by microphone as an acoustical signal S, which is processed by a lock-in amplifier locked to the chopper frequency. The normalized absorption can then be deduced as S/P ratio.

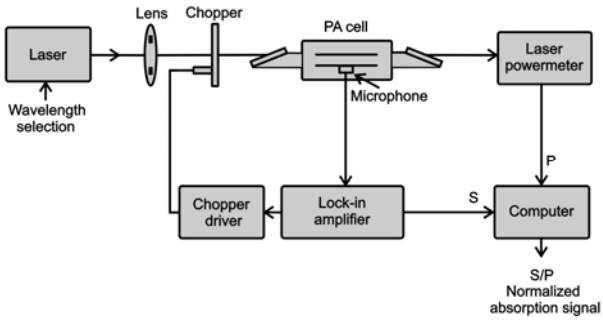

Fig. 2. Typical laser photoacoustic setup for trace gas measurements.

The power reading after beam passage through the PA cell can only be used for "transparent" gas samples. Let us evaluate if this condition is fulfilled. If the absorption is assumed to follow the Beer-Lambert law (Eq. 1), in the case of small absorption, the fractional absorption of the laser beam in the PA cell is given as $\Delta P/P(0) \cong \alpha Lc$ (Eq. 2). The quantity αLc is known as the optical density of the gas in the resonator tube (this quantity is also called absorbance). Therefore, the PA signal proportional to ΔP depends linearly on the absorption coefficient, and its dependence on gas concentration is also linear. At αLc = 0.06, a deviation of ~3% results from the linear behavior (~10% for αLc = 0.07). An optical density of 0.06 (an ethylene concentration of 65 ppmV for L = 30 cm, the length of our cell) may thus be regarded as the upper limit of the linear range of a PA detector. Consequently, the PA signal can be modeled as a linear function of concentration

in the full range from a few pptV to 65 ppmV ethylene, so that the range spans over 7 orders of magnitude! Taking into account typical values for the absorption coefficients of the species to be measured (e.g., for ethylene at concentrations in the range 1ppbV-10 ppmV, $\alpha c \cong 3\times10^{-8}$-$3\times10^{-4}$ cm^{-1}) and usual lengths of the PA cells (~30 cm), the fractional absorption is very small (10^{-6}-10^{-2}), which means that in the worst case less than 1% of the incident laser power is absorbed in the sample gas inside the PA cell. It follows that the powermeter measures the real value of the laser power inside the PA cell (we have "transparent" gases).

Another advantage of photoacoustic spectroscopy as a tool for trace gas analysis is that very few photons are absorbed as the laser beam passes through the sample cell. As a result, notwithstanding the losses from absorption in the windows, the transmitted beam typically has sufficient power for analyzing samples in successive cells, via a multiplexing arrangement. A multiplexed photoacoustic sensor can be used to monitor many different samples simultaneously so that one instrument can be deployed to monitor up to 20 different locations within a clean room, industrial plant or other facility [39].

Following the terminology introduced by Miklos *et al*. [22], the name 'PA resonator' will be used for the cavity in which the resonant amplification of the PA signal takes place. The term PA cell (or PA detector; both terms are used in the literature to describe the device in which the PA signal is generated and monitored) is reserved for the entire acoustic unit, including the resonator, acoustic baffles and filters, windows, gas inlets and outlets, and microphone(s). Finally, PA instrument (PA sensor) stands for a complete setup, including the PA cell, light source, gas handling system, and electronics used for signal processing.

It is interesting to mention that the *reverse* PA effect, called "sonoluminiscence", consists in the generation of optical radiation by acoustic waves, while the *inverse* PA effect is the generation of sound due to optical energy being lost from a sample, instead of being deposited in a sample as in the usual PA effect [17].

3. Photoacoustic signal

3.1 Resonant cells

A PA cell can be operated either in nonresonant mode or at an acoustic resonance frequency specific to the PA resonator. In the so-called nonresonant mode, the modulation frequency is much lower than the first acoustic resonance frequency of the PA resonator. In this case, the wavelength of the generated acoustic wave is larger than the cell dimensions. Thus, the generation of standing acoustic waves is not possible. A nonresonant PA cell lacks any means of energy accumulation in the acoustic wave, i.e., the induced pressure fluctuations are a function of the energy absorbed on that cycle alone and, in fact, any acoustic energy remaining from previous cycles tends only to produce noise on the desired signal. The main drawbacks of the nonresonant scheme are the low modulation frequency, which makes the system susceptible to $1/f$ noise, and the relatively large background signal generated by absorption in the windows of the cell and by radiation scattered to the walls. Nevertheless, the acoustically nonresonant cell has an advantage in low-pressure operation, as the signal, and hence the signal-to-noise ratio, remains constant as pressure is decreased, whereas for the resonant cell, it drops almost linearly with decreasing pressure (Fig. 3). Also, the background signal, which limits the sensitivity of the nonresonant cell at atmospheric pressure, has been found to depend approximately linearly on pressure and would be less troublesome in low-pressure operation [40].

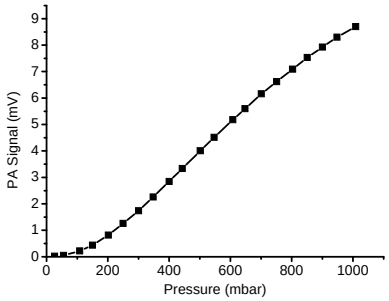

Fig.3. PA signal dependence on total gas pressure in the cell (1ppmV ethylene in nitrogen).

Nonresonant operation can compete with enhanced resonant operation only at much lower frequencies and smaller cell volumes; however, a number of practical difficulties have been cited. At low frequencies, gas inlet-outlet ports act as pneumatic short circuits for the induced pressure [41]. Excess acoustic energy in previous cycles of the modulated light can produce noise in the nonresonant signal, while in resonant operation this type of noise is avoided because the energy in each cycle contributes to a standing wave [42]. For the small, nonresonant cell, attachment of the microphone can lead to difficulties in extracting the optimum pressure response signal [43].

With increasing modulation frequency, the acoustic wavelength equals the cell dimensions at a certain point, and the resonant modes of the cell can be excited, leading to an amplification of the signal. The signal can be boosted manifold by: a) designing the sample cell as an acoustic resonance chamber, so that the pressure fluctuations produced by spatially and temporally nonuniform excitation contribute to standing acoustic waves within the chamber, and b) minimizing dissipation of the acoustic energy and modulating the laser beam spatially and temporally at a frequency which coincides with one of the natural resonant acoustic frequencies of the chamber. The system becomes an acoustic amplifier in the sense that the energy existing in the standing wave is many times higher than the energy input per cycle, and the signal is amplified by a quality factor Q. The final signal amplification obtainable depends on the resonator losses. After an initial transient state, during which energy is accumulated in the standing acoustic wave, a steady state is reached in which the energy lost per cycle by various dissipation processes

is equal to the energy gained per cycle by absorption of infrared laser photons. Resonance properties mainly depend on the geometry and size of the cavity. For an acoustically resonant PA cell, important parameters will include gas characteristics such as heat capacity, thermal conductivity, viscosity, energies and relaxation times of the molecular vibrations and the sound velocity which determines the resonant frequencies of the cavity. Other parameters govern the loss mechanisms that determine the quality factors of the resonances and also cause small shifts in the resonant frequencies.

A comparison of the microphone signals for nonresonant operation at 100 Hz and resonant operation at 564 Hz is depicted in Fig. 4 (a) and (b), respectively, together with the chopper waveforms. For nonresonant operation, the laser beam was amplitude-modulated with a duty cycle (pulse duration divided by the pulse period) of 25%, and the PA signal exhibits ringing at the resonant frequency on top of the 100-Hz square wave. For resonant operation, the laser beam was amplitude-modulated with a duty cycle of 50% and the microphone output was simply a coherent sine wave. In Fig. 4 (b), the data were recorded with a concentration of 1 ppmV of ethylene in the PA cell.

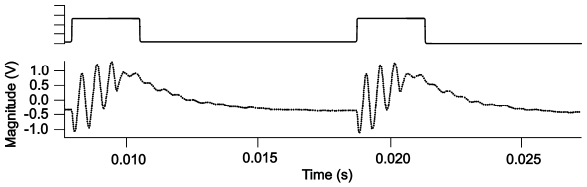

(a)

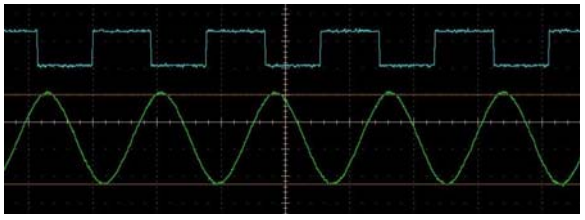

(b)

Fig. 4. Microphone signals for: (a) nonresonant operation of the PA cell [23]; (b) resonant operation of the PA cell (our cell), recorded with a Tektronix DPO 7104 Digital Oscilloscope, horizontal scale 1 ms/div, vertical scales 1 V/div. (rectangle wave) and 0.5 V/div. (sine wave amplified x 100).

3.2 Resonance frequencies

Several distinct resonances can be generated if the dimensions of a cavity are comparable with the acoustic wavelength. The standing wave patterns and resonance frequencies depend on the shape and size of the PA resonator. The most frequently used resonator is the cylinder, the symmetry of which coincides well with that of a laser beam propagating along the cylinder axis. The natural acoustic resonance frequencies of a lossless cylindrical resonator (fully reflecting walls) are determined as a solution of the wave equation in cylindrical coordinates [16]:

$$f_{kmn} = \frac{v_s}{2}\left[\left(\frac{k}{L}\right)^2 + \left(\frac{\alpha_{mn}}{\pi r}\right)^2\right]^{1/2} \tag{3}$$

where v_s is the sound velocity, L and r are the length and radius of the cylinder, the k, m, n indices (non-negative integers) refer to the values of the longitudinal, azimuthal, and radial modes, respectively, and α_{mn} is the n-th root of the derivative of the m-th Bessel function:

$$\frac{\mathrm{d}J_m(z)}{\mathrm{d}z} = 0 \tag{4}$$

($\alpha_{00} = 0$, $\alpha_{01} = 3.8317$, $\alpha_{02} = 7.0153$, $\alpha_{10} = 1.8412$, $\alpha_{11} = 5.3311$, $\alpha_{12} = 8.5360$, etc.). For the first longitudinal mode, $k = 1$, $m = 0$, $n = 0$ and $f_{100} = f_0 = v_s/2L$.

In deducing Eq. (3), it was assumed that there was no phase shift on reflection of the pressure wave from the cavity walls caused either by wall compliance or boundary layer effects. If we depart from the assumption of complete wall rigidity, the boundary layer can be seen to cause significant frequency deviations from the above formula. To evaluate the frequency from Eq. (3), we must know the sound velocity, which may vary with frequency and pressure due to molecular relaxation effects and the nonideal behavior of the gas.

In reality, frequencies at the resonances are somewhat smaller. The corresponding resonance frequencies for PA resonators with open-open ends can be obtained from the following expression [44]:

$$f_0 = \frac{v_s}{2(L + \Delta L)} \tag{5}$$

where the quantity ΔL is the so-called end correction, which should be added to the length of the pipe for each open end. Physically, the end correction can be understood as an effect of the mismatch between the one-dimensional acoustic field inside the pipe and the three-dimensional field outside that is radiated by the open end. The end correction can be approximated by the following expression: $\Delta L \cong 0.6r$, where r is the radius of the pipe [22]. More precisely, the end correction slightly decreases with frequency; therefore the resonance frequencies of an open pipe are not harmonically related but slightly stretched. In our experimental setup, the resonance frequency for 0.96 ppmV of ethylene in pure nitrogen is 564 Hz at $L = 30$ cm. By taking $v_s = 343$ m/s in nitrogen at 22°C (the sound velocity in nitrogen of 330 m/s at 0°C was corrected for the room temperature), we have $\Delta L \cong 0.2$ cm for the two open ends of our PA resonator and $\Delta L \cong 0.6r$ ($r = 0.35$ cm).

In an ideal gas, the sound velocity is given by:

$$v_s = (\gamma RT / M)^{1/2} \quad (6)$$

where $\gamma = C_p/C_v$ is the ratio of specific heats at constant pressure and volume, R is the ideal-gas constant, T is the absolute temperature, and M is the molecular weight. The sound velocity in an ideal gas only depends on temperature and remains unchanged at pressure modifications if γ is constant. In the case of ideal gases, γ = 1.4 for diatomic gases and γ = 1.33 for triatomic gases. Experimentally, the following values have been measured: 1.404 for N_2, 1.401 for O_2, 1.404 for CO, 1.32 for H_2O, 1.31 for NH_3, 1.31 for CH_4, and 1.25 for C_2H_4.

For nonideal gases, the sound velocity can be approximately calculated by the following formula:

$$v_s = [\gamma(RT + 2Bp)/M]^{1/2} \quad (7)$$

where B is the second virial coefficient and p is the pressure.

Little attention has been given to the role of the buffer gas (defined as the optically nonabsorbing gaseous component in photoacoustic detectors). In principle, the molecular weight and the thermodynamic and transport properties of the buffer gas should have a significant impact on the photoacoustic signal. One would also expect the energy transfer between the absorbing species and the buffer gas to play an important role in PA detection [45, 46]. In a mixture of ideal gases, the sound velocity $\bar{v}_s$ and consequently the resonant frequencies of a PA resonator depend on the effective specific heat ratio and the average mass of the mixture:

$$\bar{v}_s = (\bar{\gamma} RT / \overline{M})^{1/2} \quad (8)$$

where the specific heat ratio $\bar{\gamma}$ and the average molecular weight $\overline{M}$ are:

$$\bar{\gamma} = \frac{xC_p^b + (1-x)C_p^a}{xC_v^b + (1-x)C_v^a} \quad (9)$$

$$\overline{M} = xM^b + (1-x)M^a \quad (10)$$

Here C_p^b, C_v^b, C_p^a and C_v^a are the heat capacities of the buffer and absorbing gases, respectively; M^b and M^a are their molecular weights; and x is the fractional concentration of the buffer gas. When the molecular weight of the buffer gas is increased, the resonance frequency of the PA resonator shifts to lower values. In conclusion, the resonance frequency is a sensitive function of temperature and gas composition, both of which influence the speed of sound.

At a fixed temperature, v_s also depends on the water content in the air [47]:

$$v_s = v_{s0}^{'}\left[1 - \frac{p_w}{p_{air}}\left(\frac{\gamma_w}{\gamma_{air}} - \frac{5}{8}\right)\right] \quad (11)$$

Here γ_w and γ_{air} are the ratios of the specific heats of water vapor and air. The partial pressures of water and air are denoted as p_w and p_{air}. The sound velocity in dry air is written as $v_{s0}^{'}$. The increase of the resonance frequency of a 30-cm long longitudinal resonator at ambient temperature is 0.90 Hz for 1 % of water vapors added to the gas. For all practical purposes, the variation of the resonance frequency with the CO_2 concentration is negligible: -0.15 Hz per 1000 ppmV. For a given water vapor concentration, the resonance frequency provides information about the gas temperature inside the resonator. In most cases, the PA cell resonance frequency has to be determined experimentally.

Since the resonance frequency is proportional to the sound velocity, the temperature dependence of the sound velocity is directly mirrored by the resonance frequency. The sound velocity in air has a temperature coefficient of about 0.18%/°C, thus a frequency shift $\delta f \cong 0.0018 f_0 \Delta T$ is expected for a temperature change ΔT (°C) [22]. The true resonance frequency may therefore deviate from the fixed modulation frequency by δf. Then the PA signal will not be excited at the peak of the resonance, but slightly to one side. Since a detuning from the resonance peak by 0.46 (Δf(10%)/Δf(FWHM) = 16/35) results in a 10% drop of the PA signal (see Fig. 5), the detuning should be smaller than $\pm 0.23 f_0/Q$ for 10% signal stability. This stability can be ensured, if the condition $Q\Delta T \le 128$ ($\delta f \le 0.23\Delta f$ or $0{,}0018 f_0 \Delta T \le 0.23\Delta f$ or $Q\Delta T \le 0.23/0.0018$) is fulfilled ($\Delta T \le 7.9$°C in our case for Q =16.1). The corresponding condition for PA signal stability of 2% can be written as $Q\Delta T \le 64$ ($\Delta T \le 4$°C in our case). These examples clearly show that low-Q photoacoustic resonators are not sensitive to temperature variations and consequently do not need temperature stabilization or active tracking of the resonance to adjust the modulation frequency.

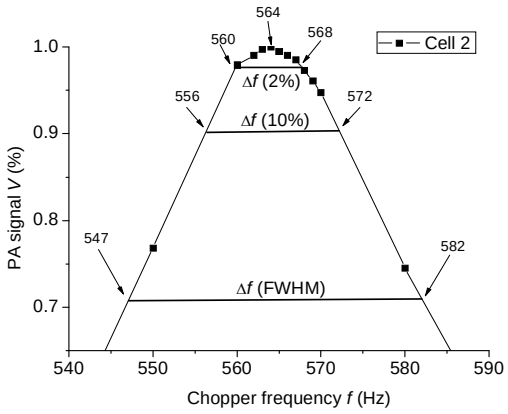

Fig. 5. Resonance curve of our PA cell showing the full width at half maximum (FWHM) and the full widths for a signal drop of 2% and 10% from its maximum.

3.3 Dissipation processes

The various dissipation processes occurring in an acoustic cavity were first discussed at length by Kamm in 1976 [42]. The energy accumulation attainable in a standing wave of a resonant cavity is many times larger than the energy loss occurring during a single period of an acoustic oscillation. This acoustical amplification effect is limited, however, by various dissipation processes. The losses can be divided into surface effects and volumetric ones [48]. The surface losses are due to the interaction of the standing wave with the internal resonator surface and may be subdivided into the following dissipation processes:

(1) compliance of the chamber walls;
(2) dissipation at the microphone diaphragm;
(3) losses due to wave scattering at surface obstructions such as gas inlet/outlet, microphones, and windows;
(4) viscous and thermal dissipation in the boundary layer at the smooth internal surfaces.

In a carefully designed high quality resonator, the contribution of the first three effects can be minimized. The dominant contribution is caused by the viscous and thermal boundary layer losses. Throughout the major portion of the resonator volume the expansion and contraction of the gas occur adiabatically. We neglect heat conduction and viscous losses in the volume of the gas because the acoustic power loss from these effects is very small. However, the wall consists of a material with a thermal conduction coefficient much greater than that of the gas. Thermal dissipation occurs because expansion and contraction of the gas do not proceed adiabatically near the walls, where the process will change to isothermal. The temperature variation changes exponentially from the adiabatic propagation regime in the gas to a zero value at the wall. This leads to heat conduction within a transition region (thermal boundary layer), which is responsible for the thermal dissipation process. Outside a thin boundary layer with thickness d_h, near the wall, the thermal losses can be neglected:

$$d_h = \left(\frac{2K}{\rho \omega C_p} \right)^{1/2} \tag{12}$$

Here K is the thermal conductivity of the gas, ρ is the density of mass, C_p is the molar heat capacity, and $\omega = 2\pi f$ is the angular frequency.

The viscous dissipation can be explained by the boundary conditions imposed by the walls. At the surface, the tangential component of the acoustic velocity is zero, whereas inside the cavity, it is proportional to the acoustic pressure gradient. Thus, viscoelastic dissipation occurs in a transition region with a thickness d_v, which is called the viscous boundary layer:

$$d_v = \left(\frac{2\mu}{\rho \omega} \right)^{1/2} \tag{13}$$

where μ is the viscosity coefficient.

Equations (12) and (13) are only valid if d_h and d_v are much smaller than the radius of the PA resonator (d_h, $d_v << r$), which yields a lower frequency limit. The upper frequency limit is reached when the wavelength of sound is comparable to the cross-sectional dimensions of the tube ($\lambda_s = v_s/f_0 \cong r$). The magnitude of d_h and d_v can be calculated by using the properties of nitrogen at standard pressure (p = 1 atm) and room temperature: $K = 2.552 \times 10^{-2}$ W/(m K), $\mu = 1.76 \times 10^{-5}$ Pa s, $C_p = 1.04 \times 10^3$ J/(kg K), $\rho = 1.142$ kg/m^3 and $\gamma = C_p/C_v = 1.4$. As a result, the values for the thermal and viscous boundary layer thicknesses are, respectively: $d_h = (2K/\rho\omega_0 C_p)^{1/2} = 2.6(f_0)^{-1/2}$ (mm Hz$^{1/2}$) $\cong$ 0.110 mm (at f_0 = 564 Hz) and $d_v = (2\mu/\rho\omega_0)^{1/2} = 2.2(f_0)^{-1/2}$ (mm Hz$^{1/2}$) $\cong$ 0.093 mm (at f_0 = 564 Hz). Therefore, at atmospheric pressure and audio frequencies, both boundary layers are only a fraction of a millimeter thick.

The volumetric or bulk losses are caused by processes that tend to establish equilibrium in the propagating wave. These damping processes are:

(1) free space viscous and thermal dissipation;
(2) diffusion effects;
(3) radiation effects; and
(4) relaxational damping (dissipative relaxation processes within polyatomic gases).

Friction due to compressional motion and the transformation of organized energy into heat due to temperature gradients are responsible for the free space viscous and thermal losses. These two processes are often called Stokes-Kirchhoff losses and are small compared with surface damping. Diffusion and radiation effects are normally very small. Nevertheless, radiation losses through openings, e.g., pipes connecting the resonator to buffer volumes, cannot be neglected. The radiation losses can be reduced by increasing the acoustic input impedance of the openings. This is achieved by terminating the cavity resonator at the openings with acoustic band-stop filters, which prevent sound escape from the resonator. Relaxational effects can add a significant contribution in diatomic and polyatomic molecules. The reason for the relaxational losses is the phase difference between gas pressure and density in the dispersion region, leading to an irreversible conversion of sound energy into thermal energy.

3.4 Quality factor

The amount of signal enhancement that occurs when the laser is modulated at a resonance frequency is determined by the quality factor. At resonance, the amplitude of the PA signal is Q times larger than the amplitude far from the resonance frequency, i.e., the amplification is equal to the value of the Q factor. The quality factor of the system, Q, is the ratio between the energy stored in a specific mode (the acoustic wave) and the energy losses per cycle of this acoustic wave:

$$Q = \frac{2\pi \text{ accumulated energy}}{\text{energy lost over one period}} \tag{14}$$

For high Q values the quality factor can be deduced dividing the resonance frequency by its bandwidth at the 0.707 amplitude point:

$$Q = \frac{f_0}{\Delta f} = \frac{\omega_0}{\Delta \omega} \tag{15}$$

where f_0 and Δf are the resonance frequency and the full-width value of the resonance profile ($\omega_0 = 2\pi f_0$ and $\Delta\omega = 2\pi\Delta f$). The full width is measured between the points where the amplitude of the resonance profile is at $1/\sqrt{2}$ the peak value amplitude (half-maximum values of the intensity). Therefore, Δf is also called the full width at half maximum (FWHM). Q is typically between 10 and 50 for longitudinal resonators, but can be as high as 1000 for spherical cavities.

Also, the quality factor can be calculated as [42, 49]:

$$Q = \frac{2S}{2\pi r\left[d_\nu + (\gamma - 1)d_h\right]} \tag{16}$$

where S stands for the cross section of the resonator tube and r for the radius of the tube. By introducing the radius (r = 3.5 mm) of the PA resonator we used and the values for the thermal and viscous boundary layer thicknesses determined in the previous section, Eq. (16) yields Q = 14.2, in agreement with the experimentally determined value (Q = 16.1).

The overall Q factor for a resonance may be found by summing all the losses, expressed as $1/Q_i$:

$$\frac{1}{Q_{tot}} = \sum_i \frac{1}{Q_i} \tag{17}$$

In practice, we only include three contributions: viscous and thermal dissipation in the boundary layer at the smooth internal surfaces (surface loss), free space viscous and thermal dissipation, and relaxation losses (volumetric losses).

3.5 Pressure amplitude

The transformation of the absorbed laser energy into heat is usually modeled by a simple relaxation process, while the well-known acoustic-wave equation is applied to calculate the sound-pressure field. The laws of fluid mechanics and thermodynamics can be used to model the acoustic and thermal wave generation in gases. The governing physical equations are the laws of conservation of energy, momentum, mass, and the thermodynamic equation of state. The physical quantities characterizing the acoustic and thermal processes are the temperature T, pressure p, density ρ, and the three components of the particle velocity vector $\mathbf{v}$. By eliminating the variables T, ρ, and $\mathbf{v}$ (and by neglecting the influence of the thermal and viscous interactions of the gas), a linear (inhomogeneous) wave equation can be derived for the acoustic pressure changes, p [22]:

$$\frac{\partial^2 p(\mathbf{r},t)}{\partial t^2} - v_s^2 \nabla^2 p(\mathbf{r},t) = (\gamma - 1)\frac{\partial H(\mathbf{r},t)}{\partial t} \tag{18}$$

where $H(\mathbf{r},t)$ is the heat density deposited in the gas by light absorption. The term on the right-hand side of the equation describes the heat input changes over time. When the heat input is constant, this term is zero and no pressure wave is generated. Thus, the heat input must be modulated, which requires that the laser radiation be also amplitude or frequency modulated. A modulated laser beam generates periodic sound due to the periodic localized heating of the gas. From an acoustic point of view, the PA cell is a linear acoustic system, which responds as a whole to the disturbance generated by light absorption. The differential equation (18) is not valid for capillary tubes with a small diameter ($2r \approx d_\nu, d_h$) nor for gases with exceptionally high viscosity or heat conductivity.

When the absorbing gas can be modeled by a two-level system consisting of the vibrational ground and the excited state, Meyer and Sigrist [19] found that the amplitude of heat production rate, H, is given by:

$$H(\mathbf{r},t) = \alpha_p I(\mathbf{r},t) \tag{19}$$

where $I(\mathbf{r},t)$ is the intensity of the laser beam. This equation is valid only when the laser beam is slowly chopped in the kHz range or below, and in the absence of optical saturation.

If the cross-sectional dimensions of a resonator are much smaller than the acoustic wavelength, the excited sound field develops a spatial variation only along the length of the resonator, i.e., a one-dimensional acoustic field is generated. A narrow pipe (or tube) can be regarded as a one-dimensional acoustic resonator. A pressure wave propagating in the pipe will be reflected by an open end with the opposite phase. Through multiple reflections a standing wave pattern with pressure nodes will be formed. Therefore, open pipes should have resonances when the pipe length is equal to an integer multiple of the half wavelength.

Bernegger and Sigrist [49] proved that the plane acoustic wave propagation can be modeled by the one-dimensional analogue of the electrical current flow in a transmission line. According to this theory, a cell constant C (Pa cm/W) only dependent on the geometry of the cell (it includes the losses of the PA resonator), which relates the pressure amplitude p with the absorbed laser power P_L, can be defined at resonance frequency:

$$p = C(\omega = \omega_0)\alpha_p P_L \tag{20}$$

where p (N/m^2 = Pa) is the pressure response of the cell, α_p (cm^{-1}) is the absorption coefficient at a given pressure of the gas at the laser wavelength, and P_L (W) is the laser

power. The units of C are given in Pa cm/W based on the usual dimensions of p, α_p, and P_L. Here, the angular frequency is $\omega_0 = 2\pi f_0$, where f_0 is the resonance frequency; for a longitudinal resonant cell, the first resonance frequency is $f_0 = v_s/2L$ (Eq. 3), so that $\omega_0 = \pi v_s/L$. C is usually determined by calibration measurements, where one single absorbing substance with known absorption spectrum is investigated.

Equation (20) implies that for a reasonably small laser power (no saturation), slow modulation frequency ω_0 ($\omega_0 \tau << 1$, where τ is the thermal relaxation time characteristic for the cooling of the gas to equilibrium), and small absorption ($\alpha_p L << 1$), the sound pressure amplitude depends linearly on the absorption coefficient and the laser power.

3.6 Cell constant

For a given PA cell geometry ("high-Q" case), Kreuzer [50] deduced that:

$$C(\omega_0) = \frac{(\gamma - 1) LQG}{\omega_0 V} \tag{21}$$

where V is the volume of the PA resonator and G a geometrical factor (depending on the transverse beam profile but not on the cell length) on the order of 1 Pa m^3/W s (Bijnen *et al*. [51] found a value G = 1.2 Pa m^3/W s for their specific experimental conditions). Since the quantities in Eq. (21) are independent of the laser power and absorption coefficient, these factors can be regarded as characteristic setup quantities for PA resonators. The quantity C describes the sensitivity of the PA resonator at a given resonance frequency. It is widely known as the 'cell constant'. It depends on the size of the resonator, the frequency, and the Q factor of the resonance selected for PA detection. It also depends on the spatial overlap of the laser beam and the standing acoustic wave pattern. Its 'cell constant' name is therefore misleading, as it characterizes the complete measurement arrangement (including the acoustic resonator with a selected resonance, microphone position, and laser beam profile with spatial location) rather than the mere PA cell. Moreover, it depends on frequency, and its value differs for different resonance modes. Therefore, it would more appropriately be called a 'PA setup constant' [22] rather than a 'cell constant'. However, since the name 'cell constant' is already established in the literature, we will continue to use it hereinafter.

As the cell constant is inversely proportional to an effective cross section defined by $S_{eff} = V/L$ and $\omega_0/Q = \Delta\omega$ (Eq. 15), it follows that:

$$C(\omega_0) = \frac{(\gamma - 1) G}{\Delta\omega S_{eff}} \tag{22}$$

Based on this formula, we can estimate the magnitude of the cell constant. By introducing in Eq. (21) or Eq. (22) the values for our medium-Q resonator (r = 3.5 mm, L = 30 cm, Q = 16.1 and f_0 = 564 Hz; $S_{eff} \cong$ 0.4 cm^2, Δf = 35 Hz), it follows C = 4720 Pa cm/W, which is almost twice as much as the experimentally measured value (2500 Pa cm/W). If an open resonator is built into a closed PA cell, then the pressure generated by the PA effect will be distributed over the entire closed volume. Therefore, the total volume of the PA cell must be taken into account instead of the volume of the resonator. A PA resonator optimized for high-Q performance (S_{eff} ~80 cm^2, Q ~1000 at f_0 = 1 kHz) has a cell constant of about 800 Pa cm/W. The cell constant of a low-Q resonator is a complicated function of several parameters, and therefore cannot be determined with sufficient accuracy by calculation. It has to be determined experimentally by calibration measurements using certified gas mixtures (see Section 8).

The possibilities for improving the cell constant of acoustic resonators are limited [22]. The only parameter that can really be changed over a broader range is the effective cross section of the cell. A reduction of the cell diameter will increase the cell constant. A lower limit is set by the diameter and divergence of the laser beam employed. The cell constant for modulated measurements is inversely proportional to the FWHM value of the resonance profile. Unfortunately, the half width cannot be reduced indefinitely, because it scales approximately with the surface-to-volume ratio of the resonator. As the cross section of the cell is reduced, the surface-to-volume ratio increases. It is therefore impossible to achieve small cross sections and a small bandwidth (high Q) simultaneously. The smallest diameter used in practical systems is several millimeters, the largest about 10 cm.

Combining Eqs. (20) and (21), we have:

$$p = \frac{(\gamma - 1)\alpha_p LP_L QG}{\omega_0 V} \tag{23}$$

It should be noted that the amplitude of the PA pressure signal is a function of (1) the heat capacity of the mixture (γ), (2) laser power (P_L), (3) modulation frequency (ω_0), (4) vibrational relaxation times of the absorbing gas, and (5) damping effects of the buffer gas (Q). The first four factors contribute to the power going into the sound wave, and the last mechanism determines the Q of the resonances. From Eq. (23) it follows that the amplitude of the pressure wave (the PA pressure signal) is proportional to the absorption coefficient and laser power, but inversely proportional to the modulation frequency and effective cross section V/L of the PA resonator. Thus, the signal increases with decreasing resonator dimensions and modulation frequency. As the noise increases with a decrease of these parameters, there is a maximum in the signal-to-noise ratio (SNR) for a certain combination of cell size and modulation frequency.

For resonant operation, the modulation frequency is tuned to one of the resonance modes of the PA resonator, i.e., $\omega = \omega_m$. Not only the m-th mode, but all the other modes of the acoustic resonator are excited as a result. The resonance amplitude is proportional to Q, while the amplitudes of the other resonances are inversely

proportional to the quantity $\omega^2 - \omega_m^2$. Therefore, distant resonances will not be excited efficiently. Certain resonances can be suppressed for special symmetry conditions, e.g., azimuthal modes cannot be excited if the cylindrical laser beam propagates exactly along the cylinder axis.

The measured PA signal also depends on the exact position of the microphone in the resonator. The signal detected by the microphone is proportional to the integral average of the pressure over the microphone membrane. Since mostly miniature microphones are applied in photoacoustics, the integral can be approximated by the value of the pressure amplitude at the microphone location.

Angeli *et al*. [52] reported a dependency of the cell constant on the kind of calibration gas. They concluded that the cell constant could not be determined unambiguously by a calibration measurement using a single absorbing species, indicating the "nonabsolute" character of photoacoustic spectroscopy. This result would have severe implications and would render analyses of multicomponent gas mixtures very difficult or impossible. Fortunately, Thöny and Sigrist [53] proved that detailed investigations including a number of different gases and measurements on numerous laser transitions contradict those observations and revealed the expected independence of the cell constant within the measurement errors.

3.7 Optimization of the PA cell geometry

Since the PA signal is inversely proportional to the cell volume and modulation frequency, high PA signal levels can be obtained by taking a small cell volume (< 10 cm^3) and low modulation frequencies (< 100 Hz). However, noise sources (intrinsic noise of the microphone, amplifier noise, external acoustic noise) show a characteristic $1/f$ frequency dependence, and therefore the SNR of such a gas-microphone cell is usually quite small. The SNR of a PA cell can be increased by applying higher modulation frequencies (in the kHz region) and acoustic amplification of the PA signal. For this reason, resonant PA cells operating on longitudinal, azimuthal, radial, or Helmholtz resonances have been developed. Furthermore, resonant cells can be designed for multipass or intracavity operation.

A qualitative behavior for Q and ω_0 can be derived from simple geometrical considerations. So, for Q, the energy stored in a specific mode is proportional to the cell volume ($\propto r^2L$), while the energy losses per cycle of the acoustic wave are proportional to the cell surface ($2\pi rL$) and to the thicknesses $d_h \approx d_v = d \propto \omega_0^{-1/2} \propto L^{1/2}$. Therefore:

$$\omega_0 \propto L^{-1}, \tag{24}$$

$$Q(\omega_0) \propto (r^2L/rLL^{1/2}) \propto rL^{-1/2}, \tag{25}$$

and

$$C(\omega_0) \propto (L)(rL^{-1/2})/(L^{-1})(r^2L) \propto r^{-1}L^{1/2}. \tag{26}$$

which is represented graphically in Fig. 6. These equations show that the product $Q(\omega_0)C(\omega_0)$ is nearly independent of the cell dimensions for any kind of resonant PA cell. The operation of the cell in a longitudinal mode is more advantageous because it makes it possible to optimize the resonance frequency and the Q-factor independently, which cannot be achieved in the case of radial resonance.

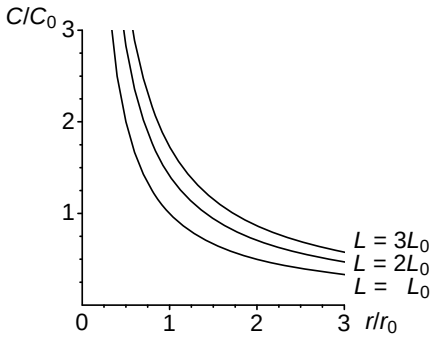

Fig. 6. Graphical representation of Eq. (26): dependence of the normalized cell constant on tube radius and resonator length.

Cell geometries with large diameter-to-length ratios designed to excite the resonance in the radial or azimuthal acoustic modes possess high Q values and high resonance frequencies, but have low cell constants. PA cells with high Q values are sensitive to long-term drifts (e.g., due to thermal expansion if the temperature is not carefully controlled), so that they require an active locking of the modulation frequency on the resonance frequency of the cell. In a longitudinally excited resonator, a smaller acoustic gain, as a consequence of a relatively low Q value, is compensated for by the signal gain due to the smaller diameter.

According to Eqs. (24-26), to obtain a higher acoustic signal in a longitudinally excited resonator with a low Q-factor (a higher C), it is necessary to have a resonator with a large length and a small diameter. Yet, narrowing the tube diameter and increasing the tube length are restricted by the divergence of the laser beam over the length of the cell. The maximum length is limited by the minimum frequency at which the cell is to be operated or by the maximum absorption coefficient α_{max} that is to be detected ($L << 1/\alpha_{max}$). The minimum possible diameter is set by the beam diameter or the volume-to-surface ratio that is needed to minimize adsorption and desorption at the cell walls. A too small diameter of the PA cell gives rise to high PA background signals due to absorption of the wings of the gaussian laser beam profile. On the other hand, a high quality factor is required in order to decrease the background signal caused by window heating. In conclusion, the optimization of the PA cell geometry depends on the specific experimental conditions and the application for which it is designed.

3.8 Voltage signal

When the resonance contributions are included, the photoacoustic voltage signal can be obtained at a given operating frequency simply by multiplying the pressure response (Eq. 20) by the microphone responsivity ($V = pS_M$ and $\alpha_p = \alpha c$):

$$V = \alpha C S_M P_L c \tag{27}$$

where: V (V) is the photoacoustic signal (peak-to-peak value); α (cm^{-1} atm^{-1}), the gas absorption coefficient at a given wavelength; C (Pa cm W^{-1}), the cell constant; S_M (V Pa^{-1}), the microphone responsivity; P_L (W), the cw laser power (unchopped value; 2x measured average value); and c (atm), the trace gas concentration (usually given in units of per cent, ppmV, ppbV or pptV). This equation reveals that the photoacoustic signal is linearly dependent on laser power. Thus, sensitive measurements benefit from using as much laser power as is reasonably available. Moreover, the signal is directly dependent on the number of molecules in the optical path (trace gas concentration), which means that this technique is truly a "zero-baseline" approach, since no signal will be generated if the target molecules are not present.

Equation (27) is valid as long as absorption is small ($\alpha_p L << 1$), and the modulation frequency is higher than the inverse of the molecular diffusion time but lower than the inverse of the molecular relaxation time. The PA signal is linearly dependent on the absorption coefficient, cell constant, microphone responsivity, incident laser power, and absorbent trace gas concentration. Thus, by doubling Q (and consequently C), or the microphone responsivity, or the laser power, or the number of absorbing molecules in the optical path, the voltage will also double. The peak-to-peak value of the signal is obtained by multiplying by $2\sqrt{2}$ the rms voltage amplitude measured by the lock-in amplifier. As a rule, another parameter is used to characterize the PA cell, namely:

$$R = C S_M \tag{28}$$

where R (V cm/W) is the (voltage) responsivity of the PA cell or the calibration constant. The cell constant C is multiplied by the responsivity of the microphone given in V/Pa units. A comparison of different PA cells can be made independently of the application in terms of this figure of merit. However, the cell characterization can be used only if a calibrated microphone is available. In this way, Eq. (27) becomes:

$$V = \alpha R P_L c \tag{29}$$

To increase the detection sensitivity, we have to ensure: a) a cell constant as large as possible (optimization of the PA resonator); b) a large microphone responsivity; c) a laser power as high as possible, provided that saturation does not become a limiting factor; d) a narrow bandwidth of the lock-in amplifier, and e) a high absorption coefficient of the trace gas to be measured at the laser wavelength. It is also useful to increase the number n of microphones (connected in series), but this number is limited by the dimensions of the PA cell. The summation of the signals from the single microphones results in an n-times higher effective PA signal, because the total responsivity $S_{M\,tot}$ is increased n-fold, i.e.:

$$S_{M\,tot} = n S_M \tag{30}$$

On the other hand, the incoherent noise only increases by $\sqrt{n}$. One thus obtains:

$$\mathrm{SNR}_{\mathrm{tot}} = \sqrt{n}\,\mathrm{SNR} \tag{31}$$

The minimum measurable voltage signal $V = V_{min}$ is obtained at SNR = 1, where the minimum detectable concentration $c = c_{min}$ can be recorded:

$$c_{\min} = \frac{V_{\min}}{\alpha P_L R} \tag{32}$$

The sensitivity of PA instruments increases with the laser power, as $V \propto \alpha P_L$. However, the voltage signal does not depend on the length of the absorption path. Furthermore, in contrast to other techniques based on absorption spectroscopy, the response of the acoustic detector is independent of the electromagnetic radiation wavelength as long as the absorption coefficient is fixed. According to theoretical considerations, extremely low detection limits on the order of $\alpha_{min} = \alpha c_{min} \cong 10^{-10}$ cm^{-1} for 1 W incident laser power have been predicted [18] and experimentally proved [37]. Such sensitivity makes it possible to detect many trace constituents in the sub-ppbV range. Theoretical calculations (see Section 2) predict the linearity of the signal response over a concentration range as broad as 7 orders of magnitude. This wide dynamic range, characteristic of LPAS, is important for air pollution monitoring, as it helps conduct measurements in polluted areas at the source (emission) as well as in rural areas (immission) [35].

3.9 Saturation effects

A PA signal may become saturated due to either a large concentration of the measured analyte or high laser power levels. We showed in Section 2 that, in the case of ethylene, the signal starts to saturate at a concentration of 65 ppmV. As a matter of fact, Thöny and Sigrist [53] observed weak saturation effects on 10P(14) CO_2 laser transition for a concentration of 100 ppmV of ethylene. The degree of saturation is gas dependent. We found (Section 2) that a deviation of ~3% from linear behavior resulted in an optical density $\alpha Lc = 0.06$.

By increasing laser intensity, the excitation pumping rate of the molecules grows higher, and a molecule is more likely to absorb a nearby photon before it relaxes to the ground state. So, as the molecules in the excited state increase in numbers, the number of molecules which can

absorb laser radiation is reduced. The gas actually becomes as though more transparent to laser radiation, and the effective absorption coefficient per unit laser power is lowered; this is called laser power saturation. Saturation due to nonlinear absorption of the laser power only occurs in focused high-power laser beams or when the PA cell is placed intracavity in a laser, so that the laser power can be on the order of tens of watts or even higher than 100 W. The pumping rate to a higher vibrational-rotational level is proportional to the laser light intensity; in the case of saturation it exceeds the collisional de-excitation rates.

Harren *et al*. [37] studied the saturation effects by placing the PA cell intracavity of a waveguide CO_2 laser. Extracavity, the ratio between 10P(14) and 10P(16 line) is 5.96 ± 0.2 (see Table 7). Intracavity, this ratio becomes 2.8 $\pm$ 0.3 (47% from its extracavity value) at an intracavity laser power of 130 W (for a laser beam waist of 0.282 mm, that is at a laser intensity higher than 200 kW/cm^2). By lowering the intracavity laser power, this ratio increases to its extracavity value. This effect is caused by saturation of the transitions in C_2H_4 at the 10P(14) CO_2 laser line. Depletion from the vibrational excited level (ν_7) via other vibrational levels (e.g., ν_{10}) through collisions becomes slow in comparison with the pump rate due to the high intracavity power. When the laser beam waist is increased to 1.02 mm (laser intensity is decreased to 15.9 kW/cm^2), the ratio of the absorption coefficients of C_2H_4 on the 10P(14) and 10P(16) CO_2 laser lines increased to 4.7 ± 0.5 (78% of its extracavity value). To compensate for the saturation effect, these authors used an absorption coefficient of 23.7 cm^{-1}atm^{-1} (78% of 30.4 cm^{-1}atm^{-1} at an intracavity power of 100 W) for C_2H_4 at the 10P(14) CO_2 laser line.

By using an intracavity arrangement where the CO_2 laser power was varied between 10 and 70 W, Groot [54] measured the saturation parameter of ethylene for several laser lines. The relation of the effective absorption coefficient α_e to the intrinsic absorption coefficient α is given by $\alpha_e = \alpha/(1 + P/P_s)$, where P_s (W) is the laser power saturation parameter and represents a measure for the relaxation rate. At $P = P_s$, the absorption coefficient decreases to half its initial value. The following values were obtained for P_s: 178 W for the 10P(8) line; 102 W for 10P(10); 112 W for 10P(12); 51.8 W for 10P(14); 101 W for 10P(16); 128 W for 10P(18), and 112 W for 10P(20). The strongest saturation effect was observed for the 10P(14) line, where the absorption coefficient is the largest. The saturation for this line at a laser power of 130 W corresponds to the equivalent absorption coefficient $\alpha_e = 0.285\alpha$. The stronger saturation in this case compared with the results of Harren *et al*. [37] could be accounted for by a tighter focusing of the laser beam (smaller beam waist). As a matter of fact, saturation is determined by the laser beam intensity (irradiance) rather than the laser power. Power saturation does not depend on the gas concentration in the PA cell (if the absorbing gas concentration is not too high).

4. Noises and limiting factors

In order to obtain an optimum signal-to-noise ratio (SNR), noise control and interfering signals have to be taken into account. These limiting factors are discussed in the following two sections.

Noise plays an important role in all photoacoustic measurements and is of particular importance in the detection of ultralow gas concentrations, because the noise level limits the ultimate sensitivity. In the photoacoustic literature, the detection level is usually defined by the signal-to-noise ratio, where the noise is given by the microphone signal measured with the laser light blocked. However, when light hits the PA cell, an additional background signal is generated which exists even when the absorbing species are not present in the detector. The background signal is often larger than the noise signal, and therefore the detection limit or sensitivity has to be defined by the signal-to-background ratio (SBR) in most experiments. Unfortunately, it is common practice to consider only the SNR. This procedure yields an extrapolated detection limit that may be far too small. The background signal is usually determined with a nonabsorbing gas, such as nitrogen, in the PA detector. It is influenced by many system properties, such as the pointing stability, the beam divergence, and the diameter of the laser beam.

For photoacoustic spectroscopy, “noise” often has a structure that is coherent with the signal from the target species, and therefore should more appropriately be treated as a background signal, not as noise. The background signal can be determined by measuring the acoustic signal in the absence of absorbers (i.e., with pure nitrogen), but with the same flow and in the same pressure conditions as those used for the sample gases.

The sensitivity-limiting factors which are encountered in LPAS can be classified into three categories:

a) Electrical noise, by which we mean any random fluctuation, whether electronic or acoustic, which does not have a fixed phase relation with the modulation of the laser intensity. It determines the ultimate detector sensitivity.

b) Coherent acoustic background noise, meaning a signal caused by the modulation process, but not attributable to the presence of the light beam in the PA cell. This signal is at the same frequency as, and locked in phase with respect to, the laser intensity modulation.

c) Coherent photoacoustic background signal. This signal, which is always present in the PA detector, is caused by the laser beam, yet not by light absorption in the bulk of the gas. Rather it is due to laser beam heating of the windows and of the absorbates at their surfaces, and heating of the PA resonator walls by the reflected or scattered light owing to imperfections of the focusing lens, windows and inner walls of the PA resonator. This signal is in phase with, and at the same frequency as, the laser intensity modulation. Therefore, it is not filtered out by the lock-in amplifier connected to the microphone. Thus, a background signal proportional to the laser power becomes the main factor that limits sensitivity. The

background signal in the PA cells may arise from several sources, some of which are listed below [56]:

(1) Window surface absorption: the molecules absorbed on the window surface and/or the window surface itself absorb the modulated laser radiation, and the resulting gas heating in the cell generates a pressure pulse.
(2) Window bulk absorption: even the highest quality ZnSe window substrates exhibit a residual window absorption of ~10^{-3} cm^{-1}.
(3) Off-axis radiation within the cell: light scattered from the windows and at the edge of the chopper blade may strike the inside walls of the PA resonator, where it may be absorbed and produce a signal.
(4) Light scattering or absorption due to microaerosols.
(5) Small amounts of contamination that may outgas from the cell materials, seals, and so forth.

The detection limit of the PA cell is determined by the combined effect of the intrinsic stochastic noise of the microphone, acoustic background noise, and photoacoustic background signal. Background signals are deterministic, and to the extent that they can be quantified and minimized, do not reduce the performance of the cell significantly. The detection limit is defined either at a signal-to-noise ratio of unity (SNR = 1) or at a signal-to-background ratio of unity (SBR = 1).

The amplifier input noise and microphone noise are gaussian in nature, that is, the amount of noise is proportional to the square root of the bandwidth in which the noise is measured. All of these noise sources are incoherent. The input noise of the SR830 lock-in amplifier used in our experiments is about 6 nV (rms)/$\sqrt{\text{Hz}}$. Microphone noise, which is manifested as a noise voltage present at the microphone output terminals, can be expressed as a product between the normalized noise pressure value owing to both thermal agitation of the diaphragm and cartridge responsivity at the corresponding frequency and the square root of the measurement bandwidth. The electrical noise of Knowles EK models electret microphones is 40 nV (rms)/$\sqrt{\text{Hz}}$. The overall random noise of multiple sources is determined by taking the square root of the sum of the squares of all the individual incoherent noise figures. For gaussian noise, the peak-to-peak value is about 5 times the rms noise value, while for the two other types of noises, the rms value must be multiplied by a factor of $2\sqrt{2} \cong 2.8$ to obtain the peak-to-peak amplitude. Electrical noise usually has a broadband frequency spectrum and can be reduced efficiently by narrowband filtering of the signal, as is done in the phase sensitive detection. A detection bandwidth of 0.25 Hz was set (a time constant of 1 second) in all of our measurements. Electrical noise can be reduced by using state-of-the-art (and therefore very expensive) lock-in amplifiers and/or by using longer time averaging (the noise decreases with the square root of the averaging time) at the cost of longer measurement times.

The two types of coherent background, however, are extremely narrowband signals at the same frequency as the modulation and hence cannot be filtered out. In addition, since the signal and the coherent photoacoustic background signal are both proportional to laser power, no improvement will be achieved as the laser power is increased.

Table 2 shows the magnitudes of these limiting factors in the case Brewster windows are used. We expressed each factor in several different sets of units [55]: voltage, pressure amplitude, equivalent absorption coefficient that would give the same pressure amplitude, and the concentration of ethylene that would be required to give that much absorption.

The limiting electrical noise measured at resonance frequency was V_N^e = 0.15 μV /$\sqrt{\text{Hz}}$. At atmospheric pressure, the acoustic background noise was V_N^{ac} = 3.1 μV (at resonance frequency) under normal working conditions. A photoacoustic background signal of V_N^b (nitrogen) = 2.3 μV/W was observed, in phase and at resonance frequency, as the cell was filled with pure N_2 at atmospheric pressure.

Table 2. Noises measured in our PA system.

Noise type	Root-mean-square (rms) value	Equivalent pressure[a]	Equivalent absorption[b]	Equivalent C_2H_4 concentration[c]
Electrical noise, V_N^e	0.15 μV/$\sqrt{\text{Hz}}$	5.3×10^{-6} Pa/$\sqrt{\text{Hz}}$	2.1×10^{-9} W cm^{-1}/$\sqrt{\text{Hz}}$	6.9×10^{-11} W /$\sqrt{\text{Hz}}$
Coherent acoustic background noise[d], V_N^{ac}	2.6 μV	9.2×10^{-5} Pa	2.6×10^{-8} W cm^{-1} [f]	8.6×10^{-10} W [g]
Coherent photoacoustic background signal[e], V_N^b	2.7 μV/W	9.6×10^{-5} Pa/W	2.7×10^{-8} cm^{-1} [h]	0.9×10^{-9} [i]

[a] The equivalent peak-to-peak pressure was obtained by dividing the peak-to-peak noise level to microphone sensitivity: $2\sqrt{2}\ V_N^i / S_M$, where V_N^i is either V_N^e, V_N^{ac} or V_N^b

[b] The equivalent absorption was obtained by dividing the peak-to-peak noise level to cell responsivity (see Section 8): $2\sqrt{2}\,V_N^i/R$, where V_N^i is either V_N^e, V_N^{ac} or V_N^b

[c] The equivalent C_2H_4 concentration was obtained by dividing the equivalent absorption to the C_2H_4 absorption coefficient at one atmosphere pressure of the gas at the 10P(14) laser wavelength (α_p = 30.4 cm^{-1})

[d] We expressed the coherent acoustical background noise in V independent of the bandwidth, as did Gerlach and Amer [55] and Beck [57] (and not in V/$\sqrt{Hz}$ as used by Harren *et al*. [37]); our measurements showed the acoustical background noise was independent of the lock-in bandwidth when the equivalent noise bandwidth (ENBW, the effective bandwidth for gaussian noise) of the low pass filter was varied between 0.08 Hz and 8 Hz (the lock-in time constant T was changed between 0.3 and 30 s, where ENBW = 1/(4T) for a slope of 6 dB/oct)

[e] The coherent photoacoustical background signal was measured in pure nitrogen at atmospheric pressure (1011 mbar) and at a temperature of 22 ^oC: 12 μV at a laser power of 4.4 W for 10P(14) line of the CO_2 laser; this signal was the same both in a static gas or at a flow rate of 50 ccmV

[f] The same as the limiting sensitivity of the cell, S_{cell} in Table 5

[g] With a laser power P_L = 4.4 W, the minimum measurable concentration of ethylene was 0.2 ppbV, the same as the limiting measurable concentration of ethylene, c_{lim} in Table 5

[h] The same as the minimum measurable absorption coefficient, α_{min} in Table 5

[i] The same as the minimum detectable concentration, c_{min} in Table 5

To determine the actual levels of noises that would be observed in practice, the random electrical noise level of 0.15 μV/$\sqrt{Hz}$, for example, must be multiplied by $B^{1/2}$. Also, to get the noise-equivalent absorption one must multiply 2.1×10^{-9} W cm^{-1}/$\sqrt{Hz}$ by $B^{1/2}P^{-1}$, where B is the bandwidth and P the laser power. In order to get an idea of the sensitivity that can be achieved for a representative trace gas, the equivalent ethylene concentration that would give the same signal level is also tabulated. To get the noise-equivalent ethylene concentration, multiply 6.9×10^{-11} W/$\sqrt{Hz}$ by $B^{1/2}P^{-1}$.

Our coherent acoustical background was 2.6 μV or 9.2×10^{-5} Pa, equivalent to an absorption of 2.6×10^{-8} W cm^{-1}. To get the equivalent absorption coefficient divide the latter number by P_L (5.9×10^{-9} cm^{-1}). This background signal is dependent on the location of the PA cell in relation to the sound sources associated with the modulation process.

The coherent photoacoustic background was 2.7 μV/W, or 9.6×10^{-5} Pa/W, assuming the beam was optimally aligned. This is equivalent to an absorption coefficient of 2.7×10^{-8} cm^{-1}, or an ethylene concentration of about 0.9 ppbV, independent of the laser power. Since the noise and coherent acoustical background can be made negligible by using high power, as is done in intracavity operation, this coherent photoacoustic background will be the ultimate limit of sensitivity.

In order to obtain a maximized signal-to-noise ratio, a resonance frequency under 1 kHz is necessary. Under 1 kHz, the noise level is determined by the 1/f amplifier noise, showing a frequency behavior of 1/ω. Together with $C \propto \omega_0^{-1/2}$ (because $C \propto Q/\omega_0$, $Q \propto (d_v, d_h)^{-1}$ and $(d_v, d_h) \propto \omega_0^{-1/2}$, see Sections 3.6, 3.4 and 3.3), we get a signal-to-noise ratio proportional to $\omega_0^{1/2}$. Above 1 kHz, where the 1/f amplifier noise is negligible, the signal-to-noise ratio is proportional to $\omega_0^{-1/2}$.

Below 1 kHz, the 1/f amplifier noise is the main source. Above 1 kHz, the frequency independent Brownian noise takes over. Since the pressure amplitude is inversely proportional to the square root of the resonance frequency ($p \propto C$, Eq. 20), a convenient resonance can be found between 500 and 1500 Hz. This limits the choice to a cell length of 100-300 mm. If optimal signal enhancement were the only argument, one would rather choose a large (300 mm) resonator ($C \propto L^{1/2}$, Eq. 26). Shorter resonator lengths are necessary in the case of an intracavity setup due to the limited space inside the cavity. Also, a fast time response of the cell requires a short cell length.

When the sample gas is flown continuously through the detector, acoustical noise can be produced, if the gas flow is turbulent, if acoustical noise from the surroundings is coupled directly into the detector sample space or into the tubes connected to the detector and then propagated into the detector, or if acoustic disturbances from the pump running the sample gas through the detector are propagated through the tubes. Thick detector and tube walls, small flow rates, mounting of the cell and chopper in separate sound insulating boxes, etc. must be chosen to suppress these noise contributions.

The background signal can be minimized by placing the windows at nodes of the mode being excited and by introducing buffer volumes at both ends of the cell. The ratio of buffer to resonator diameters must be large enough, and the buffer length has to be equal to one-fourth of resonator length.

5. Gas interference

Interference of other absorbing substances may impair the theoretical detection limit in a multicomponent analysis of the real atmosphere. Such interference may be caused by other molecular systems present in the environment or substances that are entrained by the carrier flux. If an interfering species is present in the environment, its effect can be minimized by either the introduction of scrubbers and cryogenic traps or the use of dual beam techniques using two PA cells. Sample-entrained interfering species present a more serious problem, since they will be present only near the source

and therefore cannot be eliminated by dual beam spectroscopy.

In ambient air, one finds CO_2 concentrations of 330-365 ppmV (0.033%-0.0365%) [18, 37, 47]. This level may rise to about 1% in the practical conditions of an agricultural application. This poses a serious practical problem. The CO_2 molecule possesses absorption vibrational band transitions $\nu_1 \rightarrow \nu_3$ ($10^00 \rightarrow 00^01$) and $2\nu_2 \rightarrow \nu_3$ ($02^00 \rightarrow 00^01$) which are weak, while the lower levels are barely populated at room temperature (~1%). However, due to the exact coincidence of these vibrational-rotational transitions with the CO_2 laser lines and the relatively high concentration of CO_2 in comparison with trace gases like C_2H_4, carbon dioxide is inevitably excited by CO_2 laser radiation, and the related photoacoustic signal may exceed the trace signal by many orders of magnitude. The absorption coefficient increases strongly with temperature, but is independent of the CO_2 concentration over a wide range. A 1.5% concentration of CO_2 has an absorption strength comparable to 1 ppmV of C_2H_4 (for CO_2 at the 10P(14) laser line, $\alpha(CO_2) = 2.1\text{x}10^{-3}$ $\text{atm}^{-1}\text{cm}^{-1}$ and $c(C_2H_4) = c(CO_2)\alpha(CO_2)/\alpha(C_2H_4) = 10^{-6}$ atm = 1 ppmV). At the 10P(14) line of CO_2, 360 ppmV of CO_2 has an absorption coefficient equal to that of 24.8 ppbV of C_2H_4. Similarly, at the 9R(30) line of CO_2 at 21°C, the same concentration of CO_2 has an absorption coefficient equal to that of 13.5 ppbV of NH_3.

Water vapor exhibits a broad continuum with occasional weak lines in the frequency range of the CO_2 laser (for H_2O at the 10P(14) laser line, $\alpha(H_2O) = 2.85\text{x}10^{-5}$ $\text{atm}^{-1}\text{cm}^{-1}$). The two dominant peaks are the absorption lines on 10R(20) and the most favorable for ambient air measurement, the 10P(40) laser transition. The absorption of 1% of water vapor in air (50% relative humidity at 18°C) at the 9R(30) line of CO_2 is about the same as that of 9.4 ppbV of C_2H_4 at the 10P(14) line or 5 ppbV of NH_3 [47]. However, at a constant temperature the absorption coefficient $\alpha(H_2O)$ depends on the water vapor concentration x and appears to obey the relation: $\alpha(H_2O) = \alpha_0 x$, where α_0 is a constant. The natural unpolluted atmosphere contains H_2O at a concentration level of ~1.5%.

Ammonia (a colorless, poisonous gas with a characteristic smell and well solvable in water) is vibrationally excited to the ν_2 state, usually by means of the *saR*(5, *K*) transitions at $\lambda = 9.22$ μm. These levels can be excited by the 9R(30) line of the CO_2 laser, where the absorption coefficient $\alpha(NH_3)$ has a value of 56 cm^{-1} atm^{-1} [47]. Ammonia is present in the atmosphere in concentrations ranging from below 0.1 ppbV over open water up to several tens of ppbV in areas with intensive livestock breeding.

Due to the additive character of the photoacoustic signal under normal atmospheric conditions, the presence of a large amount of water vapor and carbon dioxide impedes C_2H_4 detection in the low-concentration range (ppbV). Consequently, some means of selective spectral discrimination is required if ethylene is to be detected interference free in the matrix of absorbing gases. There are several ways to overcome this problem. The first is to remove CO_2 from the flowing sample by absorption on a KOH-based scrubber inserted between the sampling cell and the PA cell (a specific chemical reaction results: $KOH \rightarrow K_2CO_3$ and water). In this way, concentrations below 1 ppmV CO_2 (equivalent to a concentration of 0.07 ppbV of C_2H_4) can be achieved without influencing the C_2H_4 concentration.

Another method is a multicomponent analysis approach. The PA spectrum of an arbitrary gas mixture is represented by a linear combination of the absorption spectra of all constituents. Hence, the absorption spectra of all expected constituents that contribute to the total absorption have to be determined prior to the analysis of a multicomponent gas mixture. Let us assume a nitrogen atmosphere including a mixture of n absorbing gases at unknown concentration levels $c_1, c_2, \ldots, c_n$, low enough to assure linearity. The PA signal $V(\lambda)$ of the n absorbing compounds j ($j = 1, 2, \ldots, n$) with their concentration c_j and their wavelength-dependent absorption coefficients $\alpha_j(\lambda)$ is the sum of the individual signals from each compound. In some cases, the calculation becomes more complicated due to different phases of photoacoustic signals generated by the individual constituents of the mixture. For some components, e.g. CO_2, a temporal delay in the production of the PA signal may occur. This effect is known as kinetic cooling and results in a phase shift of the PA signal. In these circumstances, the PA signal has to be considered as the vector sum of the individual signals from each compound:

$$V(\lambda) = \sum_{j=1}^{n} V_j(\lambda) = RP_L(\lambda) \sum_{j=1}^{n} c_j \alpha_j(\lambda) \tag{33}$$

where R (V cm/W) is the cell responsivity. By sequentially tuning the laser to m different wavelengths (discrete CO_2-laser transitions) λ_i, $i = 1, 2, \ldots, m$, we obtain m measured photoacoustic signals V_i from which we derive a set of m linear equations for the unknown concentration levels c_j:

$$V_i(\lambda_i) = RP_i \sum_{j=1}^{n} \alpha_{ij}(\lambda_i) c_j = \sum_{j=1}^{n} a_{ij} c_j \tag{34}$$

where $P_i = P_L(\lambda_i)$, $a_{ij} = RP_i\alpha_{ij}$ (a constant for a given gas, a given wavelength and a given laser power), and $m \geq n$ (it should be noted that the system of linear equations is only well defined if the number m of laser transitions is higher than the number of gas components j); α_{ij} is the absorption coefficient of the j-th trace absorbant gas at wavelength λ_i, while P_i is the laser power at that wavelength. The measurements result in PA signals V_i from all components j in the gas mixture which absorb on the wavelength of the laser transition, λ_i. The minimum number of measurements at different laser wavelengths must be equal to at least the number of unknown trace gases, $m = n$. In this case we can define:

$$B = \begin{pmatrix} b_{11} \dots b_{1n} \\ : \quad : \\ b_{n1} \dots b_{nn} \end{pmatrix} = \begin{pmatrix} a_{11} \dots a_{1n} \\ : \quad : \\ a_{n1} \dots a_{nn} \end{pmatrix}^{-1} \tag{35}$$

Therefore,

$$c_j = \sum_{i=1}^{n} b_{ji} V_i \tag{36}$$

for j = 1, 2, ... , n. The coefficients b_{ji} have units of atm V^{-1}. If the number m of CO_2 laser lines used to carry out the analysis of a gas mixture is equal to or higher than the number n of absorbing components in the sample (whose CO_2 laser absorption coefficients are known), the unknown concentrations of each n component can be determined with the proper selection of laser lines. The solution of sets of simultaneous equations is generally required to estimate the concentrations of each species in a multicomponent mixture and select the optimal wavelengths for a fixed number of laser lines. The selection of CO_2 laser wavelengths for the optimum detection of a single species in the presence of interferences can usually be carried out by comparing the corresponding laser absorption profiles.

This method was used by Perlmutter *et al*. [58], who observed a minus sign of the calculated CO_2 concentration level. The minus sign stems from the fact that the absorption coefficients of CO_2 were taken to be positive in the numerical analysis. Actually the absorption coefficients of CO_2 present in nitrogen at low concentration levels (up to ~0.5%), at CO_2 laser transitions, are of negative sign. The absolute values are unchanged. This minus sign is associated with the kinetic cooling effect. They found experimentally that in a longitudinal resonant PA cell (chopping frequency = 1 kHz) the CO_2 gives a $180^o \pm 10^o$ out-of-phase PA signal relative to operation with normal gases like ethylene. This is true when CO_2 is present at concentration levels up to ~0.5% in nitrogen. At concentration levels higher than ~0.5%, the kinetic cooling phase deviation does not exceed ~180^o and highly depends on concentration, thus leading to an increasing PA signal level.

A crucial feature of photoacoustics on gas mixtures is the molecular dynamics involved in the conversion of internal molecular energy to heat [59, 60]. This is particularly important when dealing with mixtures involving CO_2 and N_2. The near degeneracy between the fundamental asymmetric stretch of CO_2 (2349 cm^{-1}) and the N_2 v = 1 vibration (2331 cm^{-1}) leads to a large cross section for resonant energy transfer. In a CO_2 laser, this mechanism is used to advantage by adding N_2 to the gas mixture in order to increase the pump rate by energy transfer from the vibrationally excited N_2 to CO_2 in the ground state. In our case, the situation is reversed. Thus, following absorption of CO_2 laser radiation, an excited CO_2 molecule transfers its excitation energy to N_2, where it resides for a long time owing to the metastable character of the excited N_2 levels (the lifetime of the vibrational level v = 1 is ≅ 1 ms at 1 atm; 1 atm = 101.325 kPa). Since the CO_2 molecule was initially taken out of an excited state, and the transition was a hot band transition, there now is a non-equilibrium situation among the CO_2 vibrational levels, and equilibrium is eventually restored at the expense of translational energy. Thus, following radiation absorption, a transient cooling of the CO_2 gas takes place, and the effect is therefore referred to as kinetic cooling. In trace gas detection, this means that the photoacoustic phase of the CO_2 signal will be significantly different from the phase of the trace gas signal, where no kinetic cooling is involved. The situation is further complicated if water is present in the gas mixture, since water molecules are effective in deexciting the metastable N_2 levels and hence in reducing the phase contrast. The presence of 1% water vapors speeds up the relaxation of vibrationally excited N_2, and this effect reduces the phase contrast to about 135^o down from 180^o. This phase contrast is a very important aid in the analysis of mixtures where one of the components is strongly dominant, since a quantitative analysis of the phase contrast may provide information about the H_2O concentration.

The presence of H_2O and CO_2 will always influence the measurement of C_2H_4 and NH_3 concentrations. These background gases absorb CO_2 laser radiation and produce simultaneously occurring photoacoustic signals. A comparison of the predicted amplitude and phase of the photoacoustic signal with experimental data is given in Fig. 7 [47].

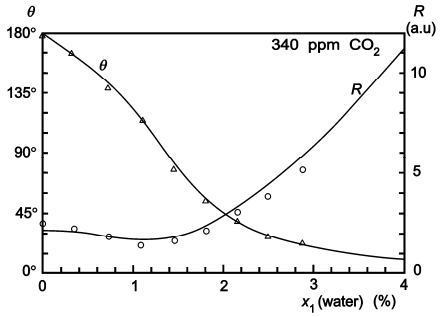

Fig. 7. Predicted amplitude R and phase θ for air with 340 ppmV CO_2 as a function of water vapor concentration. The corresponding experimental data are plotted for a frequency of 560 Hz and an excitation at 9R(28) CO_2 line (9.23 μm) [47].

In Fig. 8, the phase of the calculated heat production rate for a CO_2 – N_2 – O_2 – H_2O mixture is plotted as a function of the concentrations c_{CO_2} and c_{H_2O} [19]. The data used for this plot were those for 10R(20) CO_2 laser transition, i.e., I_0 = 20 W/cm^2, σ_{H_2O} = 3.5×10^{-23} cm^2 and σ_{H_2O} = 1.0×10^{-22} cm^2, and a chopper frequency f = 2650 Hz. As demonstrated in Fig. 8, the phase reversal only occurs within rather narrow concentration ranges. Thus, a heat-rate phase different from 0^o or 180^o is rarely expected for low H_2O and CO_2 concentrations.

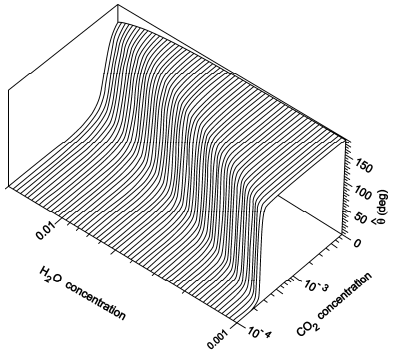

Fig. 8. Calculated phase of heat production rate for a CO_2 – N_2 – O_2 – H_2O mixture as function of the concentrations c_{CO_2} and c_{H_2O} and for c_{N_2} = 0.8 and c_{O_2} = 0.2 [19].

The multicomponent analysis can utilize the phase information of the photoacoustic response to suppress the CO_2 signal. A high concentration of CO_2 yields a phase shift of the signal with respect to the acoustic signal of ethylene. A combined signal for a CO_2-C_2H_4 mixture is less than the sum of both individual amplitudes (vectorially added). The zero phase of the two-phase vector lock-in amplifier is adjusted to pure C_2H_4 absorption, and thus a mixture of CO_2 and C_2H_4 in air is measured on two CO_2 laser transitions. One obtains four pieces of information, i.e. the CO_2-C_2H_4 mixture phase shift and absorption coefficients for both lines. From this, with known absorption coefficients for both lines, the CO_2 and C_2H_4 concentrations can be extracted [47]. A good estimate is obtained from the difference between the two measured signals V_a and V_b. Putting $V_a = R_a \exp(i\theta_a)$ and $V_b = R_b \exp(i\theta_b)$ the magnitude of the difference is found with the cosine rule:

$$|V_a - V_b| = \left[R_a^2 + R_b^2 - 2R_a R_b \cos(\theta_a - \theta_b)\right]^{1/2} \quad (37)$$

Here it is only the difference between the two phase angles that is required, so absolute calibrations can be avoided. This approach has the advantage that a high laser power can be used, and no partial failure of the scrubber can falsify the C_2H_4 concentration.

In a multicomponent mixture, this effect can be taken into account by measuring the amplitudes V_i of the PA signal at the laser transitions i as well as its phases θ_i, where the number i = 1... m stands for the discrete CO_2 laser transitions with the powers $P(\lambda_i) = P_i$. Thus, similar to Eq. (34) we have the following equation for the PA signal amplitude:

$$V_i \cos\theta_i = RP_i \sum_{j=1}^{n} c_j \alpha_{ij}(\lambda_i) \cos\theta_{ij} \quad (38)$$

with i =1... m, j = 1... n, $n \le m$, where c_j is the concentration of the gas component j and α_{ij} is the absorption coefficient of the gas compound j at the laser transition i. The phase θ_{ij} is a mathematical aid for easy calculation. It is nearly independent of the laser transition i for a certain gas component and can thus be written as θ_j. In our wavelength range it is only CO_2 which shows a phase $\theta_j = \pi$, whereas all the other gases studied so far show a phase θ_j = 0. In real measurements small deviations of the phases from the predicted ones occur due to measurement errors. Nevertheless, the approximation $\theta_{ij} = \theta_j = 0$ for all the other air compounds is well justified. It should be noted that the system of linear equations is only well defined if the number of gas components j is smaller than the number m of laser transitions, i.e., for $n \le m$. Based on measurements of the signals V_i, phases θ_j, and laser powers P_i, and knowing the absorption coefficients α_{ij} from literature data or calibration measurements, the unknown concentrations c_j can be derived by solving the above equation system. The algorithm of the data analysis has been described by Meyer, Sigrist [19]. For multicomponent mixtures an algorithm, e.g., a nonlinear Levenberg-Marquardt fit [62] is employed to fit the measured spectrum on the basis of calibration spectra of the individual compounds.

The concentrations of C_2H_4, CO_2, and H_2O in nitrogen at atmospheric pressure can be determined by measuring the PA signals using three CO_2 laser transitions, e.g., 10P(14), 10P(20) and 10R(20) [35]. The 10P(14) and 10R(20) transitions coincide with sharp peaks of the IR spectra of C_2H_4 (α = 30.4 $cm^{-1}atm^{-1}$) and H_2O ($\alpha = 8.36 \times 10^{-4}$ $cm^{-1}atm^{-1}$), respectively. The 10P(20) line that is used to measure CO_2 concentration ($\alpha = 2.2 \times 10^{-3}$ $cm^{-1}atm^{-1}$) could be replaced by many other transitions without much change in sensitivity, because CO_2 is relatively spectrally flat.

Rooth *et al*. [47] determined the H_2O, CO_2, and NH_3 contents in ambient air by using four laser transitions (10R(20) is used to compute water vapor concentration using the absorption coefficient at the actual gas temperature; the influence of the CO_2 absorption on the measurement of H_2O is also taken into account by using the 9R(18) and 9R(28) lines; the difference in the two signals yields the CO_2 concentration with the help of Eq. (37); the fourth line, 9R(30) together with 9R(28) provides the NH_3 concentration). Nägele and Sigrist [61] recorded the PA signal on two transitions for each compound, carefully selected for maximum absorption, minimum absorption interference, and good laser performance. In addition, they measured the PA signal on two laser transitions (10P(12), 10P(40)), for which all of the investigated gases exhibit negligible absorption, to verify the constant background signal. Therefore, the spectra to monitor ethylene (10P(14), 10P(16)), ethanol (9P(8), 9P(32)), methanol (9P(34), 9P(36)), and CO_2 (10P(20), 9R(20)) comprise ten different transitions. Thus cross references are possible and the background signal, which is the same for these lines, can be subtracted. This extension to several laser lines yields better detection limits and selectivity, although the time for one full measurement increases with the number of lines.

6. General schematic

The block diagram of the laser photoacoustic spectrometer, based on the general schematic shown in Fig. 2, is presented in Fig. 9. The cw, tunable CO_2-laser beam is chopped, focused by a ZnSe lens, and introduced in the PA cell. After passage through the PA cell, the power of the laser beam is measured by a laser radiometer Rk-5700 from Laser Probe Inc. with a measuring head RkT-30. Its digital output is introduced in the data acquisition interface module together with the output from the lock-in amplifier. All experimental data are processed and stored by a computer. The frequency stabilized, line tunable CO_2 laser will be described in the next section.

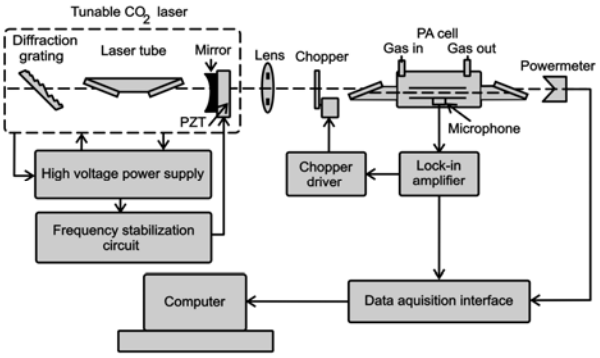

Fig. 9. Block diagram of the laser photoacoustic spectrometer.

We decided to use an extracavity arrangement because it has several advantages. In spite of a lower laser power available to excite the absorbing gas in the PA cell, a smaller coherent photoacoustic background signal makes it possible to increase the overall sensitivity of the instrument. This was proved by comparing our results with those obtained with intracavity arrangements (see Table 6, Section 8). Also, the dynamic range of the PA method is considerably reduced by intracavity operation. Optical saturation may occur for molecules with high absorption cross section while uncontrollable signal changes may be obtained at higher overall absorption in the PA cell, because the loss of light intensity influences the gain of the laser. This effect may cause erroneous results when the sample concentration changes are large. Therefore, high-sensitivity single- and multipass extracavity PA detectors offer a simpler alternative to intracavity devices.

Various modulation methods are applied in PA spectroscopy. It is necessary to distinguish between the modulation of incident radiation and that of sample absorption [35]. The first schemes include the widely used amplitude modulation of the incident radiation by mechanical choppers, electro-optic and acousto-optic modulators as well as the modulation of the laser emission itself by pulsed excitation, Q-switching, and mode-locking. On the other hand, frequency or wavelength modulation of the incident radiation provides the advantage of eliminating the continuum background PA signal caused by wavelength-independent absorption, e.g., by the cell window. The absorption characteristics of the sample can be modulated based on the Zeeman or Stark effect, i.e., by applying modulated magnetic or electric fields to the sample. Consequently, the absorption wavelength of the sample is varied, which corresponds to a wavelength modulation method. The continuum background is suppressed as a result. For example, a reduction of the background by a factor of 500 was achieved by Stark modulation compared with the one obtained in the same PA cell with conventional amplitude modulation by a chopper [56]. However, it should be noted that the application of the Stark modulation scheme in trace gas detection is restricted to molecules with a permanent electric dipole moment like ammonia (NH_3), nitric oxide (NO), etc. Nevertheless, a considerable increase in sensitivity and, even more important, in selectivity in multicomponent mixtures can be achieved.

The light beam was modulated with a high quality, low vibration noise and variable speed (4-4000 Hz) mechanical chopper model DigiRad C-980 or C-995 (30 slot aperture) operated at the appropriate resonant frequency of the cell (564 Hz). The laser beam diameter is typically 5 mm at the point of insertion of the chopper blade and is nearly equal to the width of the chopper aperture. An approximately square waveform was produced with a modulation depth of 100% and a duty cycle of 50% so that the average power measured by the powermeter at the exit of the PA cell is half the cw value. By enclosing the chopper wheel in a housing with a small hole (10 mm) allowing the laser beam to pass, chopper-induced sound vibrations in air that can be transmitted to the microphone detector as noise interference are reduced. A phase reference signal is provided for use with a lock-in amplifier.

The generated acoustic waves are detected by microphones mounted in the cell wall, whose signal is fed to a lock-in amplifier locked to the modulation frequency. The lock-in amplifier is a highly flexible signal recovery and analysis instrument, as it is able to measure accurately a single-frequency signal obscured by noise sources many thousands of times larger than itself. It rejects random noise, transients, incoherent discrete frequency interference and harmonics of measurement frequency. A lock-in measures an ac signal and produces a dc output proportional to the ac signal. Because the dc output level is usually greater than the ac input, a lock-in is termed an amplifier. The lock-in can also gauge the phase relationship of two signals at the same frequency. A demodulator, or phase-sensitive detector (PSD), is the basis for a lock-in amplifier. This circuit rectifies the signals coming in at the desired frequency. The PSD output is also a function of the phase angle between the input signal and the amplifier's internal reference signal generated by a phased-locked loop locked to an external reference (chopper). We used a dual-phase, digital lock-in amplifier Stanford Research Systems model SR 830 with the following characteristics: full scale sensitivity, 2 nV - 1 V; input noise, 6 nV (rms)/$\sqrt{\text{Hz}}$ at 1 kHz; dynamic reserve, greater than 100 dB; frequency range, 1 mHz –

102 kHz; time constants, 10 μs – 30 s (reference > 200 Hz), or up to 30000 s (reference < 200 Hz).

The diverging infrared laser beam is converged by a ZnSe focusing lens (f = 400 mm). In this way, a slightly focused laser beam is passed through the photoacoustic cell without wall interactions. The laser beam diameter D (or its radius, w), which is a very important issue in LPAS, is calculated at different locations on the beam's propagation path (Fig. 10). A too large beam compared to the inner diameter of the resonant tube could increase the coherent photoacoustical background signal to impracticable values. The calculation will be made in three steps: a) inside the laser cavity; b) between the laser coupling mirror and the focusing lens, and c) after the focusing lens (including at the center of the PA cell and at the Brewster windows of the cell).

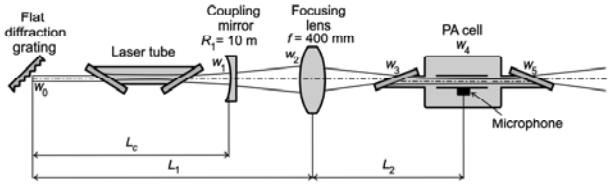

Fig. 10. Geometry of the laser beam from its waist to the exit of the PA cell.

The laser resonator has a stable-type configuration, being made of a diffraction grating equivalent to a totally reflecting flat mirror and a coupling concave spherical mirror with the radius of curvature R_1 = 10 m. We calculate the parameters of the ideal gaussian beam inside and outside the laser resonator, i.e., for M^2 = 1. The beam waist, positioned at the surface of the diffraction grating, has a radius given by:

$$w_0^4 = \left(\frac{\lambda}{\pi}\right)^2 L_c\left(R_1 - L_c\right) \tag{39}$$

For a cavity length L_c = 690 mm, R_1 = 10 m, and λ = 10.53 μm, we get w_0 = 2.91 mm or a beam waist diameter D_{01} = $2w_0$ = 5.83 mm. Based on this value of the beam waist, we can determine the Rayleigh range and the beam divergence half angle: $z_{R1} = \pi w_0^2/\lambda$ = 2535 mm and $\theta = \lambda/\pi w_0$ = 1.15 mrad (the full angle is 2.3 mrad). The beam spot on the coupling mirror has a radius given by:

$$w_1^4 = \left(\frac{\lambda R_1}{\pi}\right)^2 \frac{L_c}{R_1 - L_c} \tag{40}$$

resulting in w_1 = 3.02 mm or a beam diameter of $2w_1$ = 6.04 mm. A similar calculation indicates a beam diameter at the exit window of the laser tube (corresponding to $z \cong$ 600 mm from the diffraction grating) of w(600 mm) ≅ 3.0 mm or D(600 mm) ≅ 6.0 mm. Because the diameter of the discharge tube is 7.0 mm, the exit window acts as a round aperture forcing the laser to oscillate close to the TEM_{00} mode ($M_2 \cong 1$).

The beam radius at the entrance of the focusing lens can be calculated with the free space propagation law of a gaussian beam:

$$w(z) = w_0\left[1 + \left(\frac{z}{z_R}\right)^2\right]^{1/2} \tag{41}$$

where z is the longitudinal coordinate measured from the waist plane, located at the diffraction grating. For $z = L_1$ = 1060 mm, we have w_2 = 3.16 mm or a beam diameter of $2w_2$ = 6.32 mm.

After the focusing lens, we shall follow the treatment of Nemes [63] regarding the beam transformation through the general system free space - lens - free space. The usual notations are used, with the subscript 1 for the beam parameters before the lens, and the subscript 2 for the beam parameters after the lens. According to Fig. 11, the optical system consists of a free space propagation across a distance $L_1 = f + \Delta_1$, followed by the thin converging lens with focal distance f, and a second free space propagation of length $L_2 = f + \Delta_2$. The main spatial parameters such as the beam diameter at the new waist, D_{02}, the beam divergence half angle, θ_2, the waist position D_{2w} ($f + \Delta_{2w}$ from the lens), and the Rayleigh distance, z_{R2}, can be calculated by using the following relations:

$$D_{02} = \frac{D_{01} f}{\left(z_{R1}^2 + \Delta_1^2\right)^{1/2}} \tag{42}$$

$$\theta_2 = \frac{\theta_1\left(z_{R1}^2 + \Delta_1^2\right)^{1/2}}{f} \tag{43}$$

$$\Delta_{2w} = \frac{\Delta_1 f^2}{z_{R1}^2 + \Delta_1^2} \tag{44}$$

$$z_{R2} = \frac{z_{R1} f^2}{z_{R1}^2 + \Delta_1^2} \tag{45}$$

With f = 400 mm and $\Delta_1 = L_1 - f$ = 660 mm, we get: D_{02} = 0.89 mm, θ_2 = 7.53 mrad, Δ_{2w} = 15.39 mm, and z_{R2} = 59.12 mm. With the new beam parameters, the free space propagation law of the gaussian beam becomes:

$$w(z) = \frac{D_{02}}{2}\left[1 + \left(\frac{z}{z_{R2}}\right)^2\right]^{1/2} \tag{46}$$

where now z is the longitudinal coordinate measured from the second waist, after the focusing lens. When the PA cell is placed with its center at a distance L_2 = 450 mm from the lens, we can determine the laser beam diameters at the two Brewster windows (z_3 = 190 mm, z_5 = 710 mm): $2w_3$ = 3.51mm and $2w_5$ = 4.53 mm, respectively, and at the PA

cell center (z_4 = 450 mm): $2w_4$ = 1.03 mm. It follows that as the laser beam travels across the PA cell, its diameter is small enough compared with the diameter of the resonant tube (7 mm) to avoid wall absorptions, which ensures that the chosen geometry minimizes the coherent photoacoustical background signal, as intended.

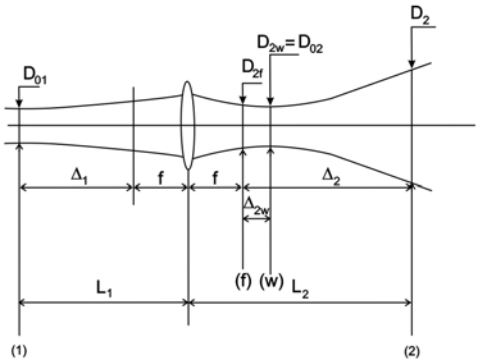

Fig. 11. Schematic of the ideal optical system free space - thin lens - free space used in spatial beam characterization. (1) - Input plane where the incoming beam waist is located. (2) - Arbitrary output plane. (f) - Back focal plane of the lens. (w) - Waist plane of the beam after the lens. d_1, d_2 - Lengths of the free space propagation. f - Focal lengths of the thin focusing lens. The distances Δ_1, Δ_2, and the beam diameters D_1, D_2, corresponding to different locations are marked on the figure. Distances and diameters not to scale.

The pertinent questions we set out to answer in assessing the performance of our PA cell were whether the chosen geometry minimized the coherent background signal, and how sensitive the background and calibration were to slight beam deviations from the intended path. Obviously, if the calibration would vary significantly with small movements of the beam, the accuracy of measurements made with the PA cell would be adversely affected unless the cell alignment was very carefully adjusted and rigidly fixed.

The variation of the background and calibration with transversal or longitudinal translation of the PA cell against the propagation beam direction is very small as long as the laser beam does not strike the walls of the cell. The optimum position of the PA cell against the focusing lens (the center of the resonant tube, i.e. the position of the microphones) is 450 mm (for a focusing length of 400 mm). On extending this optimum distance by 30 mm, the signal is decreased by 0.14%, while when shortening the distance by 60 mm, the signal decreases by 0.61%. The dependence of both signal and background signal on the transversal position of the resonant tube relative to the laser beam is similarly low. We found that the cell calibration and background were virtually invariable for reasonably small longitudinal or transversal movements of the cell.

As the angle of incidence deviates from the Brewster angle θ_B (θ_B = arctan$n$ = 67.38° for ZnSe), the window reflectivity becomes nonzero, and the reflected beam can heat the walls of the cell, making a further contribution to the background signal. The dependence on the angle of incidence of the reflectance for a plane wave polarized parallel to the plane of incidence (P polarization) is given by Fresnel's law:

$$R_p = \left(\frac{n_1 \cos\theta_2 - n_2 \cos\theta_1}{n_1 \cos\theta_2 + n_2 \cos\theta_1} \right)^2 \tag{47}$$

where n_1 = 1 is the refractive index for air, n_2 = 2.4 is the refractive index for ZnSe, $\theta_1 = \theta$ is the angle of incidence, θ_2 is the angle of refraction, and $n_1 \sin\theta_1 = n_2 \sin\theta_2$ (Snell's law). This dependence is illustrated in Fig. 12.

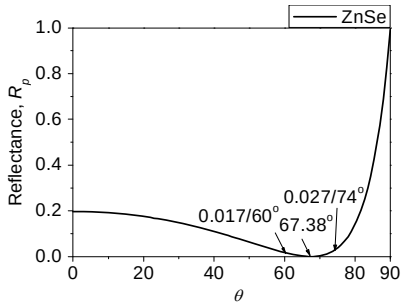

Fig. 12. Reflectance of the parallel polarization component as a function of the angle of incidence.

As the angle of incidence deviates from θ_B, the window reflectance becomes nonzero, and the refracted beam can heat the walls of the cell, making a further contribution to the background signal. Nevertheless, for a ±10% variation of the angle of incidence relative to the Brewster angle, the reflectance increases from zero to only 2.7% and 1.7%, respectively, meaning that a small deviation from the Brewster angle will not change dramatically the reflectance or the angle of refraction.

Another variable we investigated was the polarization angle of the beam. The cell response in terms of background signal displays a rather broad flat minimum, provided the incidence angle on the window ensures a minimum reflection loss. The data indicate that a deviation of several degrees from vertical polarization can be tolerated. In conclusion, we found that the calibration and background signal were not extremely sensitive to slight misalignments of the beam.

Several authors employed an iris diaphragm in close proximity of the PA cell entrance window to provide spatial filtering in order to reduce the background noise signal caused by off-axis radiation impinging on the internal wall of the chamber. With such a diaphragm, we found that the background signal increased significantly owing to laser beam diffraction at the edges of the aperture. Using high quality optical components (diffraction grating, coupling mirror, lens and windows) together with a well controlled laser beam makes the insertion of an iris diaphragm in the PA instrument unnecessary.

A general view of the two parallel measurement lines with laser photoacoustic sensors is shown in Fig. 13.

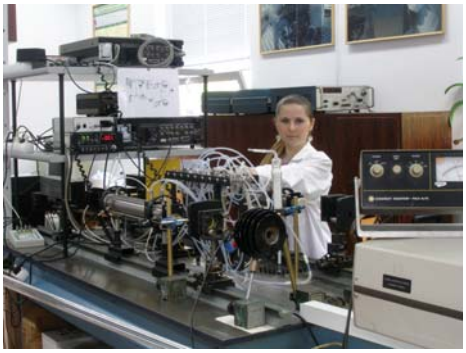

Fig. 13. General view of the PA sensors (two parallel measurement lines).

7. Frequency stabilized, line tunable CO_2 laser

We have designed, constructed and optimized a rugged sealed-off carbon dioxide laser, step-tunable on more than 60 vibrational-rotational lines and frequency stabilized by the use of plasma tube impedance variations detected as voltage fluctuations (the optovoltaic method). The glass tube has an inner diameter of 7 mm and a discharge length of 53 mm. At both ends of the tube we attached ZnSe windows at Brewster angle. The laser is water cooled around the discharge tube. The dc discharge is driven by a high-voltage power supply. The end reflectors of the laser cavity are a piezoelectrically driven, partially (85%) reflecting ZnSe mirror at one end and a line-selecting grating (135 lines/mm, blazed at 10.6 μm) at the other. Piezoelectric ceramics such as lead zirconate titanate (PZT) can be used.

A free-running or unstabilized laser is subject to many perturbations of its frequency. First of all, changes in cavity length affect the frequency of an oscillating mode ($\Delta\nu/\nu = \Delta L/L$), so keeping a constant length is the prime objective in frequency stabilization schemes. Possible perturbations of the cavity length can be divided into two groups: external effects (thermal variations of the spacer material, changes in atmospheric conditions, mechanical vibrations, variations in the position of optical components and in magnetic fields) and internal effects, which are generally related to the discharge noise.

Active power stabilization based on a piezo-driven out-coupling mirror is used in our laser. The principle of the stabilization schemes is based on a comparison between the frequency of a single frequency laser (single-mode, single-line) and some stable point of reference. If the laser frequency is different from that of the benchmark, an error-sensing discriminant is used to derive a signal proportional to the deviation. This error signal is used to control the laser oscillating frequency and retune it to the reference one. Such a servo-loop (closed loop feedback) locks the laser frequency to that of the reference. For moderate stability, the CO_2 laser line profile can be used as the discriminating curve [64]. This method is more appropriate for the CO_2 laser than for other lasers because the CO_2 vibrational-rotational line profile is narrow and has much steeper slopes than, for example, that of the neon line in a He-Ne laser. The error signal is produced by allowing the laser resonance cavity to "ride" around the steep part of the line profile slope, and its amplitude is dependent on the change in cavity mirror separation. This scheme requires internal frequency modulation (jittering) of the laser in order to sense the sign of the derived error signal. Stabilization is then obtained by re-establishing the required separation with a servo-system.

The CO_2 laser is frequency stabilized to the center of the curve representing its output power *versus* frequency (the molecular resonance) upon the variation of plasma tube impedance, when the optical power extracted from the medium is modulated [65]. In this closed-loop active stabilization, the cavity length is controlled by a piezoelectrically driven mirror along the cavity axis, which responds to the sum of a DC control voltage, plus a small jitter signal at some convenient frequency (~ 500 Hz). As can be seen in Fig. 14, where a curve of laser line gain *versus* frequency is drawn, the small cavity jitter induces a sinusoidal variation in laser output as the cavity mode scans across the transition gain profile, which is compared in phase to the jitter voltage.

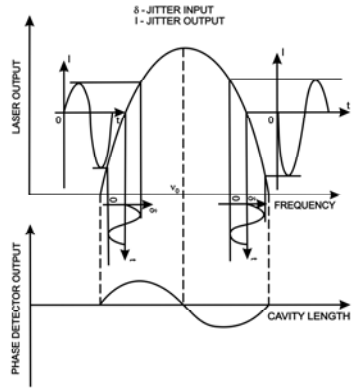

Fig. 14. Generation of the error-frequency signal.

The error signal generated by the phase detector can serve to drive the cavity resonance to the center of the laser gain curve. In this way, the electronic feedback loop seeks the center of the lasing gain profile, the lock-in point being the zero crossing of the phase detector response. If the mean mode frequency is lower than the line center frequency, the phase of the observed laser intensity variation is opposite to the one we have where the mode frequency is higher than the line center frequency. The amplitude of the jitter output increases with the frequency offset from the line center.

In lieu of using an IR detector to sense the laser intensity variation, the cavity length is adjusted using the optovoltaic effect. As the internal laser radiation field intensity is altered by changing the resonant cavity alignment, the discharge impedance, which is proportional to the slope of the curve of laser output power *versus* frequency, is also modulated. The impedance variation is determined by exciting the plasma tube with a high-speed current-regulated power supply and measuring the resulting variation in the voltage drop across the plasma

tube (the optovoltaic effect). An intensity variation of 1% is sufficient to change the discharge impedance significantly (~ 0.1%). By using a current regulated power supply, the voltage impedance fluctuation is detected as an AC component of the voltage drop across the plasma tube.

Before any attempt is made to stabilize the frequency of a laser, a single frequency output must be ensured. For this purpose, a laser operating in the lowest transversal mode (TEM_{00}) must be designed [66]. The single line operation of the CO_2 laser is achieved with a dispersive element (diffraction grating). The cavity length of L_c = 690 mm corresponds to a separation between two longitudinal modes of $\Delta\nu = c/2L_c$ = 217 MHz. Calculating the collisional broadening in a mixture of CO_2, N_2, He, Xe, and H_2 at a total pressure of 34 mbar gives a collisional full linewidth at half maximum (FWHM) $\Delta\nu_c$ = 119 MHz. We therefore conclude that a single frequency operation is obtained when a longitudinal mode is tuned on the top of the gain curve ($\Delta\nu > \Delta\nu_c/2$).

To increase the number of oscillating lines, especially those with a smaller gain, and obtain reliable long term operation at a single specific wavelength, some form of wavelength selection introduced in the optical cavity is generally required. As optical dispersion is incorporated by using a diffraction grating or Brewster-angle prisms within the laser cavity, the laser can be made to oscillate on only one vibrational-rotational line, otherwise the particular transition on which the CO_2 laser operates depends on the length of the resonator. That is why the total reflecting mirror must be replaced by a diffraction grating, which is tilted about its groove axis to the blaze angle and acts as a frequency selective reflector. Light diffracted into the first order maximum is returned along the optical axis and taken as laser output, while light in other orders as well as any other wavelength is returned off-axis and gets lost. Another advantage of a laser resonator with a grating is that the laser can be tuned over the entire oscillating linewidth from the line center.

We used a flat diffraction grating with 135 grooves/mm, blazed at 10.6 μm and having a peak efficiency of 96%, mounted in a Littrow configuration. With such a grating, the vibrational-rotational lines emitted by the CO_2 laser in the range P(50) – 10.9329 μm and R(44) – 9.1549 μm can be selected by controlling the grating angle in the range 47°33’32’’ to 38°10’02’’, which can be set to the desired laser transition with a micrometric screw. This grating presents a good dispersion, as the P(18) and P(20) lines (10.4 μm band) are separated by a 6’38’’ angular difference (as compared with 2’49’’ for a diffraction grating with 75 grooves/mm).

To meet the frequency stability requirements, the laser cavity must be so constructed as to reduce the effects of ambient vibration and thermal variations on the output frequency of the laser. This places less stringent demands on the performance of the servo-system controlling the laser frequency. To minimize the thermal length changes ($\Delta L/L = \alpha\Delta T$) in the mirror support structure, a material with a low expansion coefficient has to be used for the spacers between the endplates of the cavity which carry the mirrors. Such a material is Invar, which has an expansion coefficient α = 1.26x10^{-6}/°C. To obtain a passive instability of 3x10^{-8} for the laser frequency, the temperature variation must not exceed 0.024°C. Such constant temperature is hard to maintain, especially in longer lasers, where high power inputs and high heat dissipation cause large temperature instabilities.

Stiffness is a most desirable attribute for minimizing fractional changes in the cavity length. Special measures were taken against mechanical vibrations (by eliminating high frequency vibrations), variations in the position of optical components (by supporting rigidly any intracavity element) as well as to prevent magnetic fields and acoustically borne vibrations, which can be reduced by shielding the laser with some form of enclosure. The design of the remaining structure was chosen so as to avoid the lowering of the basic first resonance. The joints between the elements of the structure, especially the joints perpendicular to the laser axis, were so designed that they did not have any low frequency resonances. To have a spring constant of the joint high enough and to avoid joints using only the spring force of a few screws to connect significant masses, we used large contact areas under compressional stress. We chose a cylindrical shape for the mechanical structure, including the housing, because of its high resistance to bending deformation. A section through the laser cavity assembly is given in Fig. 15 and a photo of the mechanical structure, laser tube, and control panel is presented in Fig. 16.

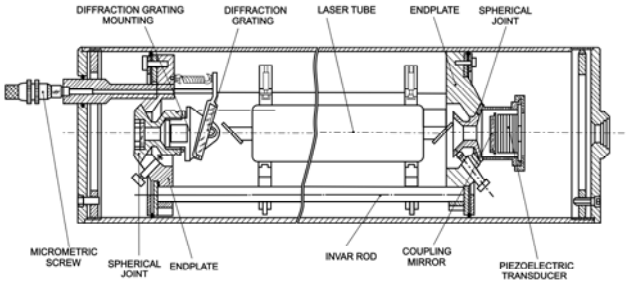

Fig. 15. Longitudinal section through the laser cavity assembly.

Fig. 16. Homebuilt frequency stabilized CO_2 laser model LIR-25 SF.

To keep the weight unchanged and still maintain the required thermal characteristics, the endplates of the cavity

which carry the mirror and the diffraction grating were primarily constructed of aluminum. The three invar rods are potted into the aluminum frame so as to ensure intimate contact between the invar rods and the rigid aluminum structure. To remove the problems associated with weak spring-type controls, the mirror holders were designed ruggedly. The mirrors can be adjusted in angle by sliding two stainless steel spherical joints with respect to one another. As the mirrors are adjusted into their final position, the adjustment screws clamp the mirror holder tightly so that no inadvertent movement is possible.

The diffraction grating is mounted in a similar holder and is rotated by a micrometric screw (0 – 25 mm), as shown in Fig. 17. The laser tube was rigidly mounted in the cavity with two concentric rings, the inner one being adjusted by three screws. This system allows the laser tube axis to fall into line with the mirror centers and provides good transverse stability.

Fig. 17. Diffraction grating-drive mechanism.

To achieve active stabilization, an automatic frequency control circuit (lock-in stabilizer) is used to maintain an axial mode on the top of the gain curve. The block diagram of the frequency stabilization system based on plasma tube impedance variations is shown in Fig. 18. A sinusoidal signal with a rough frequency of 500 Hz derived from the pilot oscillator is applied to the piezoelectric transducer, resulting in a simultaneous frequency and amplitude modulation of the laser output, dependent on the amplitude of the sinusoidal signal.

The ac voltage drop across the tube is passed through a tuned amplifier and then synchronously detected. The demodulation of the ac signal is performed in the phase-sensitive detector, with phase (continuously adjustable) determined by the phase shift circuit. The demodulator output is processed by the operational integrator and a high voltage dc amplifier. The dc bias together with this error correction signal is applied to the piezoelectric transducer, thus closing the feedback loop. The error signal generated by the phase detector serves to drive the cavity resonance to the center of the laser gain curve and compensates for the effects of slow drift.

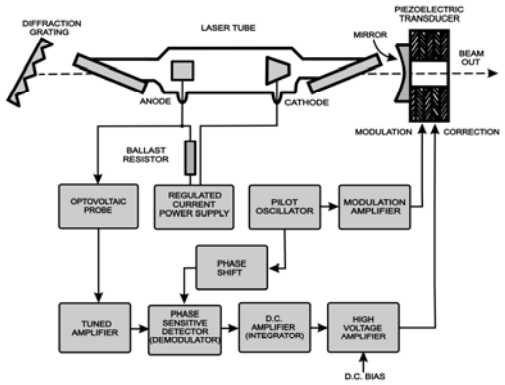

Fig. 18. Block-diagram of the automatic frequency control electronics.

There are fifteen functional modules grouped into three main blocks in accordance with the specific function they play in the operation of the frequency stabilized CO_2 laser:

1. a high speed current regulated power supply, which excites the CW CO_2 laser tube;
2. a servo control system, which controls the length of the resonant cavity;
3. a logic electronic system which allows an efficient operative control and monitoring of the frequency stabilized CO_2 operation.

The high-speed current regulated power supply includes three modules namely: the power supply converter – PSC, the power supply feedback – PSF, and the power supply rectifier PSR. The high frequency of the converter makes it possible to minimize the electronic components that are used in making the high voltage transformer and the low pass filter of the high voltage rectifier.

The modulation signal that is needed to scan the laser line profile is generated by a pilot oscillator and applied to the piezoelectric transducer through a modulation amplifier. Both circuits are placed on the same functional module OMA (Oscillator & Modulation Amplifier). For cw CO_2 lasers excited by current regulated power supplies, the modulation signal which appears in the emitted radiation can be measured according to the optovoltaic effect using a simple band pass filter like that noted with OVP (Optovoltaic Probe). The detected optovoltaic signal is amplified through a two-stage tuned AC amplifier – ACA. The amplified optovoltaic signal is introduced in the phase sensitive detector (PSD module) together with a phase adjustable component of the reference signal from the modulation oscillator.

The error signal is obtained in the output of the electronic dc amplifier module DCA, by processing the output signal of the phase sensitive detector. The DCA module has two modes of operation, namely: (a) gain of ten amplifier with integrating time constant of 1 second; (b) high gain integrator with output slewing rate of about 6V/s per volt of input. The first mode allows the observation of smoothed output of the demodulator (stabilization discriminator), while the second one is used

in closed loop stabilization to observe the error signal. A high voltage amplifier (HVA) that works on the principle of a switching high voltage power supply drives the piezoelectric transducer under the control of the error signal.

The logic electronic system includes four specialized modules, namely: a low voltage stabilized power supply (SPS), a logic drive circuit (LDC), a power meter circuit for laser radiation (PMC), and a beam controller (BCS). Every parameter and state that are monitored or selected in the operation of the frequency stabilized CO_2 laser LIR-25 SF are displayed on the rear panel of the laser (Fig. 16) by means of nine light emitting diodes (LED) driven by the panel display circuit (PDC). The output beam of the laser can be sent to either the powermeter head or the exit by a two-position reflecting mirror, controlled by a beam shutter circuit and a beam selector switch placed on the rear panel.

A visible HeNe laser is used for aligning the discharge tube and the CO_2 laser resonator consisting of a flat diffraction grating (135 lines/mm) and a ZnSe concave (10 m radius of curvature) coupling mirror (15% transmission). By measuring the micrometer screw indications for the two intense spots reflected back by the diffraction grating and knowing the slope of the line determined by the wavelength dependence of the micrometer screw position, the latter can unambiguously be determined for different vibrational-rotational lines of the CO_2 laser (Fig. 19). Optimum laser power is finally adjusted using the screws supporting the optical resonator components. The wavelength of the emission line is checked by a grating monochromator (Hilger & Watts model D330/D331 Mk.11, with a D339 grating, 75 lines/mm) equipped with a thermopile.

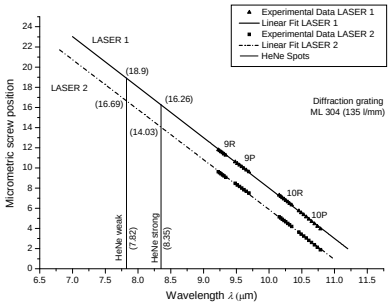

Fig. 19. Alignment of the CO_2 laser resonator.

The tunability of our CO_2 laser is presented in Fig. 20. We observed the oscillation of 62 different vibrational-rotational lines in both the 10.4 μm and 9.4 μm bands. In this way, the laser was line tunable between 9.2 μm and 10.8 μm with powers varying between 1 and 6.5 W depending on the emitted laser transition. More than 20 lines had output powers in excess of 5 W (see Table 3). The long-term frequency instability was $\Delta\nu/\nu = 3\text{x}10^{-8}$ or $\Delta\nu$ = 1 MHz (3×10^{-5} cm^{-1}). By using an additional feedback loop for laser power stabilization, the power instability was reduced from 1% to as low as 0.23% for a period of 2 minutes [67].

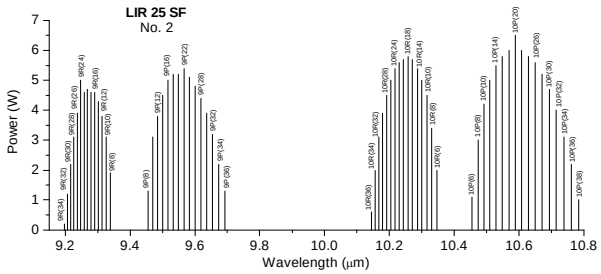

Fig. 20. Tunability of the CO_2 laser with diffraction grating.

Table 3. Characteristics of the line-tunable, frequency-stabilized CO_2-laser LIR-25 SF (No. 2).

Line	Wavelength in air (μm)	Micrometric screw position	Monochromator screw position	Laser power P_L (W)	Discharge current I (mA)
10P(38)	10.784	1.88	6762.7	1.0	9
10P(36)	10.761	2.01	6748.1	2.2	9
10P(34)	10.738	2.135	6733.7	3.1	10
10P(32)	10.715	2.26	6719.6	4.0	12
10P(30)	10.693	2.37	6705.7	4.7	12
10P(28)	10.671	2.49	6692.0	5.2	13
10P(26)	10.650	2.605	6678.6	5.6	13
10P(24)	10.629	2.72	6665.4	5.8	14
10P(22)	10.608	2.82	6652.4	6.0	14
10P(20)	10.588	2.93	6639.6	6.5	14
10P(18)	10.568	3.04	6627.1	6.0	14
10P(16)	10.548	3.14	6614.8	5.8	13
10P(14)	10.529	3.245	6602.7	5.5	13
10P(12)	10.510	3.34	6590.8	5.0	13
10P(10)	10.491	3.435	6579.1	4.2	13
10P(8)	10.473	3.535	6567.6	3.0	10

10P(6)	10.455	3.63	6556.4	1.1	8
10R(6)	10.346	4.195	6488.1	2.0	8
10R(8)	10.330	4.27	6478.3	3.4	9
10R(10)	10.315	4.35	6468.8	4.5	11
10R(12)	10.300	4.415	6459.4	5.0	12
10R(14)	10.286	4.495	6450.2	5.4	12
10R(16)	10.271	4.57	6441.2	5.7	13
10R(18)	10.257	4.64	6432.4	5.8	14
10R(20)	10.243	4.71	6423.7	5.7	14
10R(22)	10.230	4.775	6415.3	5.6	14
10R(24)	10.217	4.84	6407.1	5.4	14
10R(26)	10.204	4.905	6399.0	5.0	13
10R(28)	10.191	4.97	6391.1	4.5	12
10R(30)	10.179	5.03	6383.4	3.9	12
10R(32)	10.167	5.095	6375.9	3.1	11
10R(34)	10.155	5.155	6368.6	2.0	10
10R(36)	10.144	5.205	6361.4	0.6	9
9P(36)	9.692	7.44	6077.8	1.3	9
9P(34)	9.673	7.54	6066.0	2.2	10
9P(32)	9.654	7.63	6054.4	3.2	10
9P(30)	9.636	7.715	6042.9	3.9	11
9P(28)	9.618	7.80	6031.7	4.4	11
9P(26)	9.600	7.88	6020.6	4.8	12
9P(24)	9.583	7.97	6009.7	5.1	12
9P(22)	9.566	8.05	5999.0	5.4	13
9P(20)	9.549	8.13	5988.5	5.2	13
9P(18)	9.533	8.21	5978.2	5.2	13
9P(16)	9.517	8.28	5968.1	5.0	13
9P(14)	9.501	8.35	5958.1	4.5	12
9P(12)	9.485	8.42	5948.4	3.8	11
9P(10)	9.470	8.49	5938.8	3.1	10
9P(8)	9.455	8.57	5929.4	1.3	8
9R(8)	9.339	9.06	5856.5	1.9	8
9R(10)	9.326	9.145	5848.7	3.1	9
9R(12)	9.314	9.20	5841.1	3.8	10
9R(14)	9.302	9.255	5833.7	4.3	11
9R(16)	9.291	9.31	5826.4	4.6	11
9R(18)	9.279	9.365	5819.3	4.6	12
9R(20)	9.268	9.42	5812.3	4.7	12
9R(22)	9.258	9.47	5805.5	4.6	12
9R(24)	9.247	9.52	5798.9	5.0	13
9R(26)	9.237	9.57	5792.4	3.9	11
9R(28)	9.227	9.615	5786.1	3.1	10
9R(30)	9.217	9.665	5780.0	2.2	10
9R(32)	9.207	9.685	5773.9	1.2	9
9R(34)	9.198	9.715	5768.1	0.2	9

8. Photoacoustic cell

In the literature the PA cells are often characterized as "nonresonant" or "resonant". This terminology is misleading, because any PA cell can be operated at an acoustic resonance or far from its resonance. Thus, it is preferable to label the system in terms of its nonresonant or resonant mode of operation.

To design an optimum acoustically resonant PA cell to be used in CO_2-laser photoacoustic spectroscopy, the following requirements have to be met:

(i) the fraction of laser energy absorbed by the gas must be maximized by increasing either the incident laser power (but maintaining a large signal-to-noise ratio) or the optical density of the gas (Eq. 2);

(ii) cell responsivity needs to be as high as possible, because the voltage response is proportional to it (Eq. 29);

(iii) the microphone responsivity has to be as high as possible, and the use of many microphones is advisable (Eqs. 30 and 31);

(iv) the design must make it possible to operate the cell at an acoustic resonance, and the resonance frequency must lie between 400 and 1000 Hz, where the microphone noise is minimal;
(v) the quality factor Q of the acoustic resonance must not exceed 50 in order to decrease the influence of small deviations from the resonance frequency;
(vi) the electrical noise and the coherent acoustic background noise must be as low as possible; this can be done by using low noise microphones, good acoustic and vibration isolation, low noise electronics, and good electronic isolation (no ground loops, proper shielding);
(vii) the coherent photoacoustic background signal due to the heating of the walls and windows must be minimized by using optical components of very high quality and introducing acoustic baffles;
(viii) the cell must enable continuous gas flow operation, and consequently not only the cell windows, but also the gas inlets and outlets have to be positioned at pressure nodes of the resonance;
(ix) the cell must have low gas consumption and fast response, and the cell volume has to be sufficiently small to prevent prohibitive dilution when the produced trace gas is flowed through the cell volume by a continuous gas stream;
(x) the adsorption and desorption rates on the surfaces in direct contact with the sample gas that can influence particularly measurements on sealed-off samples must be minimized by using special cell materials and reducing the surface-to-volume ratio;
(xi) the effect of the loss mechanisms which we can control must be minimized by an appropriate system design.

Various ways to design (cylindrical geometry, H geometry, T geometry, or using a Helmholtz resonator) and operate (longitudinal, azimuthal, radial, or Helmholtz resonances) resonant PA cells have been studied [27]. Furthermore, PA cells for multipass [69, 61] or intracavity operation [70, 37] were designed. The effect of window heating in the amplitude modulation schemes has been minimized by introducing acoustic baffles [43], developing windowless cells [55, 71, 52], or using tunable air columns [51]. In many cases the window-heating signal can be markedly reduced by positioning the entrance and exit of the light beam at nodes of the mode being excited.

A cylindrical cell operated at a radial resonance and having Brewster windows mounted at the pressure nodes of the first radial mode, as presented by Gerlach and Amer [55], does not fulfill all these requirements. Therefore, an open resonant cell excited in its first longitudinal acoustic mode was developed to fulfill most of these requirements.

The H-type longitudinally resonant cell was chosen to form the core of our measuring instrument. Dividing the PA cell into a central chamber and two buffer chambers adjacent to the Brewster windows, a design which lowered significantly the coherent photoacoustic background noise, was first proposed by Tonelli *et al*. [68]. The characteristics of this type of PA cell have been discussed by Nodov [72], Kritchman *et al*. [41], and Harren *et al*. [37]. Its main advantages are: (a) stable operation at a relatively low frequency; a quality factor of about 20, i.e., much lower than that of a radial resonator, which makes it less sensitive to environmental changes; the efficient conversion of radial to longitudinal modes and the relatively long wavelength guarantee a sufficiently high photoacoustic amplitude; (b) a longitudinal resonator is not noticeably influenced by the gas flow at the desired flow rate of several l/h; noise by gas flow phenomena is negligible for properly positioned inlet and outlet ports; (c) window noise is minimal if the windows are located at a quarter wavelength from the ends of the resonator tube; (d) the construction is rugged and simple and can be achieved with low adhesion materials.

Following these guidelines, a PA cell was designed, constructed, and tested. An H-type cylindrical cell designed for resonant photoacoustic spectroscopy in gases is shown in Fig. 21. The longitudinal resonant cell is a cylinder with microphones located at the loop position of the first longitudinal mode (the maximum pressure amplitude). Some general considerations imply that the coherent photoacoustic background signal caused by window heating is decreased if the beam enters the cell at the pressure nodes of the resonance. The advantage of mounting the windows at the pressure nodes is well demonstrated, and the window heating signal is decreased by the Q factor. The laser beam enters and exits the cell at the Brewster angle. It is more advantageous to have the beam pass through the windows at the Brewster angle (θ_B), as θ_B is nearly constant over a wide range of wavelengths, and variations of θ_B with wavelength can be tolerated since reflectivity increases very slowly for small deviations from θ_B (see Fig. 12).

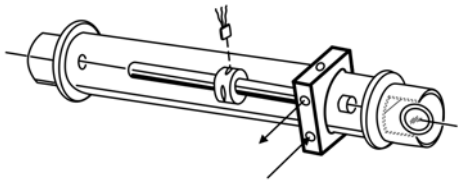

Fig. 21. Schematic of the PA cell designed for the first longitudinal resonance mode.

The influence of scattered light onto the PA background signal can be minimized by using a highly reflecting polished material, with a good thermally conducting substrate. Bijnen *et al*. [51] investigated different materials for the resonant tube and found that the background signal decreased for polished stainless steel, polished brass, and polished, gold-coated copper in a ratio of 6:2:1, respectively. In the case of the CO_2 laser, the best performance was obtained by employing a copper tube with a polished gold coating as resonator material. Because of the excellent heat-conducting properties, the absorbed heat can be quickly dispersed in the copper tube. The gold coating was used not only to optimize laser

radiation reflection, but also to obtain a noncorrosive surface to withstand aggressive gases.

Many polar compounds (e. g. ammonia) are highly adsorptive and produce an error in real time concentration measurements by adhering to the detector surfaces. These molecules interact strongly with most metals and many insulating materials. Ammonia is a good model compound for these molecules as it shows the characteristic adsorptive behavior that is not a health hazard at low concentrations. The rate of ammonia adsorption on the gas handling surfaces depends on the surface material and temperature, and on the mixture concentration, flow rate, and pressure. Comparing the ammonia results with those for ethylene, which interacts weakly with most surfaces, provides a measure of the cell-sample interaction. Beck [57] evaluated the suitability of several surface materials for minimizing sample adsorption loss. Four materials– 304 stainless steel, gold, paraffin wax, and Teflon–were tested using ammonia as a sample. The results show that both metals interact strongly with the sample. Teflon coating (thickness <25 μm) was found to provide accurate real time response for ammonia sample flows. Also, no signal decay is observed following flow termination. Additionally, the coatings must not degrade the acoustic response of the cell. The Teflon coating actually increases the cell Q by a small amount (1 percent). This is attributed to the smooth slick surface obtained by Teflon coating which would decrease any surface frictional or scattering loss of acoustic energy. Rooth *et al*. [47] tested the following wall materials – stainless steel 304, gold (on Ni-coated stainless steel), Teflon PTFE, and Teflon PFA – in contact with the gas. Stainless steel proved to be an almost unsaturable reservoir for ammonia at pptV levels. The number of stored molecules exceeded by a factor of 10 or more the number of potential locations on the total geometric surface. Despite its inferior properties in terms of adsorption, Olafsson *et al*. [59] used a stainless steel cell for detecting NH_3 and found that an operating temperature of 100°C combined with water vapors led to a very significant reduction of NH_3 adsorption. Apparently, the water molecules stick to the walls even more efficiently than NH_3, and the cell walls are effectively coated with water. Later on, the sample cell was constructed with Teflon as wall material [73].

Since an open pipe efficiently picks up and amplifies noise from the environment, it should be surrounded by an enclosure. In order to ensure high acoustic reflections at the pipe ends, a sudden change of the cross section is necessary. Therefore, the resonator pipe should open up into a larger volume or to buffers with a much larger cross section. The buffers can be optimized to minimize flow noise and/or window signals. The length of the two buffers accounting for half the resonator length is chosen such as to minimize the acoustic background signal originating from absorption by the ZnSe windows. Open pipes were introduced for PA detection as early as 1977 [27], and the most sensitive PA detectors currently used are based on open resonant pipes. In resonant cells, window signals can be diminished by using $\lambda/4$ buffers next to the windows. These buffers, placed perpendicular to the resonator axis near the windows, are tuned to the resonator frequency and act as interference filters for the window signals (the coupling of the window signals into the resonator is reduced by large buffer volumes that act as interference dampers).

It was found both theoretically and experimentally that the signal amplitude decreases drastically when buffer length $L_{buf} < \lambda/8$ [51]; the resonance frequency and quality factor, for both the window and gas signals, are not much affected by changing the buffer length. The length of the buffer is optimal for window signal suppression when $L = 2L_{buf}$ ($L >> r$) (L and r stand for resonator length and radius). The dependence of the gas absorption p_g and window absorption pressure p_w on the ratio of the buffer and resonator radii is:

$$p_g \propto \frac{\sqrt{L}}{r}\left(1-\frac{r^2}{r_{buf}^2}\right) \tag{48}$$

$$p_w \propto \frac{r}{r_{buf}\sqrt{L}} \tag{49}$$

The ratio between the gas absorption signal and window signal then becomes:

$$\frac{p_g}{p_w} \propto \left(\frac{r_{buf}}{r}\right)^2 L \tag{50}$$

The optimal buffer length, resulting in an optimal suppression of the photoacoustic background signal, is $\lambda/4$. Choosing a buffer length of $\lambda/8$ has the advantage of a shorter cell, and a good, though not optimal, suppression of the window signal is still possible in this case. If the volume and overall size of the buffers pose no problem, their radii have to be large for optimal operation. A practical radius can be deduced to be $r_{buf} \approx 3r$. The gas absorption amplitude is barely influenced above this value. A small radius for the resonator of the resonant cell is advantageous as it enhances gas absorption. The limit for the resonator radius is mainly determined by the wings of the gaussian laser beam profile hitting the wall; r should roughly be at least three times the radius of the laser beam to reduce wall absorption to an acceptable level.

Our PA cell design, based on the above considerations, is shown in Fig. 22 in cross sectional longitudinal view. The PA cell is made of stainless steel and Teflon to reduce the outgassing problems and consists of an acoustic resonator (pipe), windows, gas inlets and outlets, and microphones. It also contains an acoustic filter to suppress the flow and window noise. ZnSe windows at the Brewster angle are glued with epoxy (Torr-Seal) to their respective mounts. The resonant conditions are obtained as longitudinal standing waves in an open tube (resonator) are placed coaxially inside a larger chamber. We use an open end tube type of resonator, excited in its first longitudinal mode. To achieve a larger signal (eqs. 26 and 27), we chose a long absorption path length (L = 300

mm) and an inner diameter of the pipe of $2r$ = 7 mm ($r \cong 1.5w_5$, see Fig. 11). The fundamental longitudinal wave, therefore, has a nominal wavelength $\lambda_s = 2L$ = 600 mm (and a resonance frequency f_0 = 564 Hz). The effective wavelength is ~1% longer than the nominal value, in accordance with predictions of Eq. (5). The two buffer volumes placed near the Brewster windows have a length L_{buf} = 75 mm ($\lambda/8$) and a diameter $2r_{buf}$ = 57 mm ($r_{buf} \cong 8r$). The inner wall of the stainless steel resonator tube is polished. It is centered inside the outer stainless steel tube with Teflon spacers. A massive spacer is positioned at one end to prevent bypassing of gas in the flow system; the other is partially open to avoid the formation of closed volumes. Gas is admitted and exhausted through two ports located near the ends of the resonator tube. The perturbation of the acoustic resonator amplitude by the gas flow noise is thus minimized.

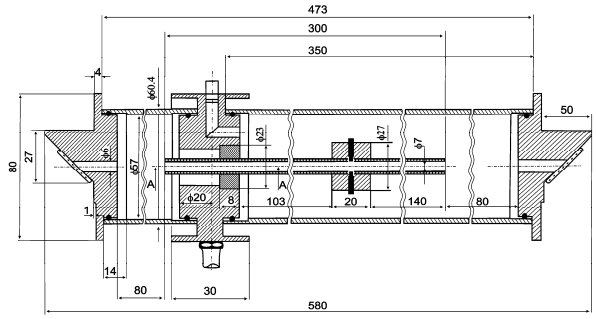

Fig. 22. Resonant photoacoustic cell with buffer volumes.

The total cell volume is approximately 1.0 dm^3 (total length 450 mm, and inner diameter 57 mm, minus inner mechanical parts). For flowing conditions, however, it is advantageous to reduce the active volume of the cell. Especially if the flow rate is smaller than 1 l/h (16.6 sccm), the replenish time for the 1.0 dm^3 cell becomes impractical. The buffer volume at the entrance port of the cell affects the renewal time τ considerably. The buffer volume is approximately 200 cm^3, yielding a time constant of 12 min ($\tau = V/R_{flow}$ = (200 cm^3)/(16.6 cm^3/min) = 12 min). By reducing the buffer volume to 24 cm^3, with $r_{buf} \cong 3r$ (diameter 20 mm, length 75 mm), a τ of 1.5 min is obtained. However, an increased acoustical noise level was observed, due to the gas flow.

In photoacoustic measurements in the gas phase, microphones are usually employed as sensing elements of the acoustic waves generated by the heat deposition of the absorbing molecules. Although high-quality condenser microphones offer the best noise performance, they are rarely used in photoacoustic gas detection because of their large size, lower robustness, and relatively high price. The most common microphones employed are miniature electret devices originally developed as hearing aids. The choice of a miniature microphone is particularly advantageous since it can be readily incorporated in the resonant cavity without significantly degrading the Q of the resonance. The frequency response of electret microphones extends beyond 10 kHz, and the response to incident pressure waves is linear over many orders of magnitude.

In our PA cells there are four Knowles electret EK-3033 or EK-23024 miniature microphones in series (sensitivity 20 mV/Pa each at 560 Hz) mounted flush with the wall. They are situated at the loops of the standing wave pattern, at an angle of 90^o to one another. The microphones are coupled to the resonator by holes (1 mm diameter) positioned on the central perimeter of the resonator. The battery-powered microphones are mounted in a Teflon ring pulled over the resonator tube (Fig. 23). It is of significant importance to prevent gas leakage from inside the resonator tube along the Teflon microphone holder, since minute spacing between the holder and resonator tube produces a dramatic decrease of the microphone signal and the Q value. The electrical output from these microphones is summed and the signal is selectively amplified by a two-phase lock-in amplifier tuned to the chopper frequency.

Fig. 23. Teflon ring used to mount the microphones flush with the tube wall.

The resonance curve of our PA cell (cell response in rms volts) was recorded as a function of laser beam chopping frequency and the results are plotted in Fig. 24. An accurate method is to construct the resonance curve point by point. In this case, the acoustic signal is measured at different fixed frequencies thus avoiding potential problems arising from the slow formation of a steady state standing wave in the resonator and the finite time resolution of the lock-in amplifier. It is evident from these data that the cell resonance curve is fairly broad, implying that the absorption measurements would not be considerably affected if the frequency of the laser modulation or the cell resonance itself were to shift by a few hertz. PA cells exhibiting narrow resonances (as in the case of excitation of the radial modes) require tight control of both temperature and laser modulation frequency to avoid responsivity losses during the experiment.

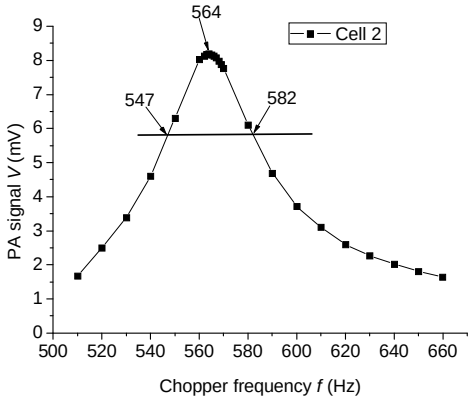

Fig. 24. Resonance curve for the first longitudinal mode of the PA cell.

The acoustic resonator is characterized by the quality factor Q, which is defined as the ratio of the resonance frequency to the frequency bandwidth between half power points. The amplitude of the microphone signal is $1/\sqrt{2}$ of the maximum amplitude at these points, because the energy of the standing wave is proportional to the square of the induced pressure. The quality factor was measured by filling the PA cell with 1 ppmV of ethylene buffered in nitrogen at a total pressure of 1 atm and by tuning the modulation frequency in 10 Hz increments (2 Hz increments near the top of the curve) across the resonance profile to estimate the half width, as described above. For this PA cell, the profile width at half intensity was 35 Hz, yielding a quality factor Q = 16.1 (Eq. 15) at a resonance frequency f_0 = 564 Hz. The experimentally determined resonance is not completely symmetric, as the curve rises steeply on one side and becomes less steep on the other side of the maximum. This asymmetry is caused by a coherent superposition of the standing acoustic waves in the detection region of the microphones [74].

The calibration of the PA system is usually performed with a reference gas. We calibrated our PA cell with the widely used reference gas ethylene (C_2H_4), whose absorption coefficients are accurately known at CO_2-laser wavelengths. Ethylene is well suited for this purpose, since it interacts only weakly with common cell surface materials. Ethylene is chemically inert, has the same molecular weight as nitrogen and possesses no permanent dipole moment which means negligible adsorption on the cell walls. Furthermore, its spectrum within the CO_2-laser wavelength range is highly structured. In particular it exhibits a characteristic absorption peak at the 10P(14) laser transition at 949.49 cm^{-1} which is caused by the proximity of the Q branch of the ν_7 vibration of C_2H_4 centered at 948.7715 cm^{-1}. We used a commercially prepared, certified mixture containing 0.96 ppmV C_2H_4 in pure nitrogen throughout our investigations. For calibration we examined this reference mixture at a total pressure p of approximately 1013 mbar and a temperature $T \cong 23^oC$ and using the commonly accepted value of the absorption coefficient of 30.4 $cm^{-1}atm^{-1}$ at the 10P(14) line of the $^{12}C^{16}O_2$ laser. For shorter time intervals (by changing the calibration gas mixture after a careful vacuum cleaning of the PA cell), the variation of the cell constant was smaller than 2%. The calibration also depends to some extent on the modulation waveform, since only the fundamental Fourier component of that waveform is resonant with, and hence significantly excites, the first longitudinal mode.

Using this PA cell and an optimized experimental arrangement we measured a cell responsivity R = 300 V cm/W. With the total responsivity of the four microphones $S_{M\ tot}$ = 80 mV/Pa (20 mV/Pa each) (Eq. 30), a cell constant C = 3750 Pa cm/W can be calculated (Eq. 28). A comparison of these PA cell parameters with other results reported in the literature is presented in Table 4. Different photoacoustic resonator designs such as longitudinal organ pipe resonators excited in the first longitudinal mode, closed longitudinal resonators excited in the second longitudinal mode, and cylindrical resonators excited in the first radial mode were used by various authors (Fig. 25). As can be noticed from the table, the cell responsivity we obtained is one of the best values that have been reported up to now.

Based on the measured noises, background signals, and cell responsivity, all parameters characterizing the PA instrument can be evaluated (see Table 5). Some of them depend on the CO_2 laser and the PA cell, while others are determined by either the coherent acoustic background noise or the coherent photoacoustic background signal.

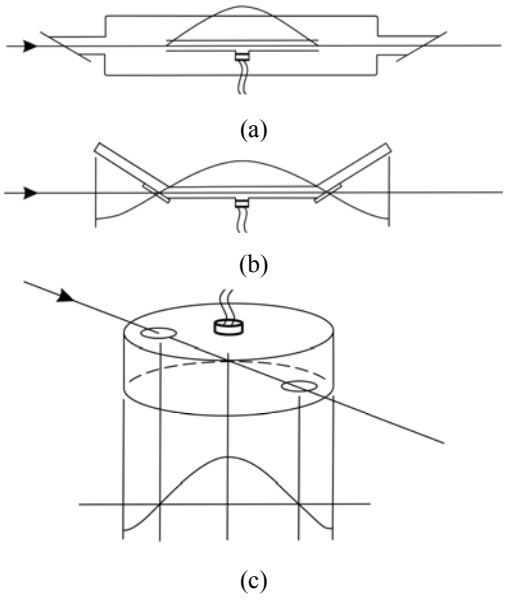

Fig. 25. Different photoacoustic resonator designs: (a) longitudinal organ pipe resonator, excited in the first longitudinal mode; (b) closed longitudinal resonator excited in the second longitudinal mode; (c) cylindrical resonator excited in the first radial mode.

Table 4. Comparison of our results with different PA cells.

Authors	Excitation mode	PA cell characteristics	R (V cm/W)	C (Pa cm/W)
Our results	First longitudinal mode	L = 30 cm, f_0 = 564 Hz, 4 microphones, S_M = 80 mV/Pa, Q = 16.1	280	3500
Crane 1978 [75]	Nonresonant operation	L = 20 cm, f = 33.3 Hz, 1 microphone	16.3	
Gerlach, Amer 1980 [55]	First radial mode	6.54x15.56 cm^2, f_0 = 2.7 kHz, 1 microphone, S_M = 11mV/Pa + preamplif.x10, Q = 560	26.5	241
Hubert 1983 [36]	Nonresonant operation	L = 20 cm, f = 695 Hz, 1 microphone	121[a]	
Ryan *et al*. 1983 [76]	First longitudinal mode	L = 30 cm, f_0 = 695 Hz, 1 microphone, Q = 17.4	56	
Gandurin *et al*. 1986 [77]	Nonresonant operation	L = 15 cm, 2r = 1.5 cm, 1 microphone, S_M = 50 mV/Pa	1-10	(20-200)[b]
Bernegger, Sigrist 1987 [49]	Second longitudinal mode	L = 60 cm, f_0 = 555 Hz, 1 microphone, Q = 52		1990
Sauren *et al.* 1989 [78]	First longitudinal mode	L = 10 cm, f_0 = 1608 Hz, 1 microphone, S_M = 10 mV/Pa	(39)	3900
Rooth *et al.* 1990 [47]	First longitudinal mode	L = 30 cm, f_0 = 556 Hz, 4 microphones	114	
Harren *et al.* 1990 [79]	First longitudinal mode	L = 30 cm, f_0 = 560 Hz, 4 microphones, S_M = 40 mV/Pa, Q = 16.4	(200)	5000
Harren *et al.* 1990 [37]	First longitudinal mode	L = 30 cm, f_0 = 560 Hz, 4 microphones, S_M = 40 mV/Pa, Q = 20	(160)	4000
Harren *et al.* 1990 [37]	First longitudinal mode (intracavity operation)	L = 10 cm, f_0 = 1653 Hz, 1 microphone, S_M = 10 mV/Pa, Q = 31.8	(37)	3700
Meyer, Sigrist 1990 [19]	First radial mode	4.18x16 cm^2, f_0 = 2.65 kHz, 1 microphone, S_M = 12.5 mV/Pa Q = 340	3.5	(280)
Thöny, Sigrist 1995 [53]	Resonance in vicinity of the first radial mode	4.18x16 cm^2, f_0 = 2.86 kHz, 2 microphones, S_M = 25 mV/Pa Q = 168	1.72	(69)
Bijnen *et al*. 1996 [51]	First longitudinal mode	L = 15 cm, f_0 = 1030 Hz, 1 microphone, S_M = 1000 mV/Pa, Q = 40	(2000)	2000
Fink *et al.* 1996 [80]	First longitudinal mode (intracavity operation)	f_0 = 1986 Hz, 1 microphone, S_M = 26 mV/Pa,	(52)	2000
Harren *et al.* 1997 [20]	Second longitudinal mode	L = 45 cm, f_0 = 555 Hz, 1 microphone, S_M = 1000 mV/Pa, Q = 43	(1.64)	1640
Harren *et al.* 1997 [20]	First longitudinal mode	L = 10 cm, f_0 = 1600 Hz, 3 microphones, S_M = 60 mV/Pa, Q = 32	(270)	4500
Henningsen Melander, 1997 [81]	Nonresonant operation, pulsed excitation	Cell volume = 1 cm^3, f = 1600 Hz	1.45	
Nägele, Sigrist, 2000 [61]	First longitudinal mode in a multipass resonant PA cell	5x12 cm^2, f_0 = 1250 Hz, 16 microphones, S_M = 160 mV/Pa, Q = 70	260	(1625)
Pushkarsky *et al*. 2002 [39]	First longitudinal mode	f_0 = 1915 Hz, 1 microphone, S_M = 22 mV/Pa, Q = 49.7	(71.5)	3250[c]

[a] The value of 50 V cm/W reported for a rms signal of 162 mV was corrected for a peak-to-peak signal of 402 mV.

[b] In brackets are the values we deduced using the authors' specifications for microphone responsivity.

[c] These authors calculated the cell constant by using a PA signal $\sqrt{2}$ x rms instead of a $2\sqrt{2}$ x rms signal; as a result, their cell constant (and responsivity) value is half the one we obtained by our methodology of calculus.

Table 5. PA cell parameters.

Resonance frequency, f_0 (Hz)	564
Quality factor[a], Q	16.1
Cell responsivity[b], R (V cm/W)	280
Microphone responsivity[c], S_M (V/Pa)	4 x20x10^{-3} = 8x10^{-2}
Cell constant[d], C (Pa cm/W)	3.5x10^{3}
Pressure amplitude response[e], p/P_L (Pa/W)	10^{-1}
Limiting sensitivity of the cell[f], S_{cell} (W cm^{-1})	2.6x10^{-8}
Limiting sensitivity of the system[g], S_{sys} (cm^{-1}) (at 4.4 W laser power)	5.9x10^{-9}
Limiting measurable concentration of ethylene[h], c_{lim} (ppbV)	0.2
Minimum measurable signal in nitrogen[i], V_{min} (μV) (root mean square)	12
Minimum detectable pressure amplitude[j], p_{min} (Pa)	4.2x10^{-4}
Minimum detectable concentration[k], c_{min} (ppbV)	0.9
Minimum detectable absorptivity[l], α_{min} (cm^{-1})	2.7x10^{-8}
Minimum detectable absorption cross-section per molecule[m], σ_{min} (cm^2)	1.1x10^{-27}
Cell sensitivity for 1 ppbV of C_2H_4 at 1 W of unchopped laser power[n], V_{ppb} (μV at 1 ppbV)	3.0

[a] This quality factor value corresponds to a full bandwidth at the 0.707 amplitude points of $\Delta f = f_0/Q \cong 35$ Hz

[b] The cell responsivity is the signal per unit power per unit absorption coefficient; in our case, the signal per unit power is 11.6 mV/4.0 W = 2.9x10^{-3} V/W (rms value) or 8.2x10^{-3} V/W (peak-to-peak value) for 0.96 ppmV of C_2H_4 (the absorption coefficient $\alpha^* = 30.4$ cm^{-1} atm^{-1} x 0.96x10^{-6} atm = 2.92x10^{-5} cm^{-1}, where $\alpha = 30.4$ cm^{-1} atm^{-1} is the absorption coefficient of C_2H_4 at 10P(14) line of the CO_2 laser), so that R = 8.2x10^{-3} V/W/2.92x10^{-5} cm^{-1} ≅ 280 V cm/W; the same responsivity was obtained with the etalon mixture of 10 ppmV of C_2H_4 in N_2: R = 8.4x10^{-2} V/W/3x10^{-4} cm^{-1} ≅ 280 V cm/W

[c] The microphone responsivity is determined from the Knowles data-sheet for the microphone type 3033: 54 dB (≅500) attenuation at 564 Hz from 1 V/0.1 Pa, leading to $S_M \cong 20$ mV/Pa

[d] The cell constant is the pressure amplitude per unit absorption coefficient per unit power: $C = R/S_M$

[e] The pressure amplitude response per unit incident power for 1 ppmV of C_2H_4 is $p/P_L = C\alpha^*$

[f] The limiting sensitivity of the cell is $S_{cell} = 2\sqrt{2}\ V_N^{ac}\ /R$ (several authors, e.g., Harren *et al*. [37] used the rms value of the voltage instead of its peak-to-peak value, resulting in a limiting sensitivity of the cell and of the system and the limiting measurable concentration of ethylene lower by a factor of 2.84; other authors, e.g., Kosterev *et al.* [82] used a parameter named "sensitivity to absorption", defined as $D = \alpha_{\min}^{el} P_L / \sqrt{\Delta f} = S_{cell} / \sqrt{\Delta f}$, where $\alpha_{\min}^{el}$ is the absorption coefficient corresponding to the coherent acoustical background noise-equivalent signal V_N^{ac} , P_L is the laser excitation power, and Δf is the detection bandwidth).

[g] The limiting sensitivity of the system or the microphone noise-limited minimum detectable absorption coefficient (the equivalent bulk absorption coefficient in the gas) is $S_{sys} = S_{cell}/P_L$ (the minimum detectable absorption strength is defined as the strength that gives a SNR at the transducer output equal to one).

[h] The limiting sensitivity of the system gives a limiting measurable concentration of ethylene of $c_{lim} = S_{sys}/\alpha$.

[i] The minimum measurable signal in nitrogen, as determined by the coherent photoacoustical background signal, is $V_{min} = V_N^b$ (nitrogen) x P_L.

[j] The minimum detectable peak-to-peak pressure amplitude can be determined by dividing the minimum measurable signal in nitrogen by the responsivity of the microphone: $p_{min} = 2\sqrt{2}\ V_{min}/S_M$.

[k] The minimum measurable signal in nitrogen, limited by the synchronous background signal, gives a minimum detectable concentration $c_{min} = 2\sqrt{2}\ V_{min}/\alpha 2P_{meas}R$, where P_{meas} is the measured laser power after chopper: $P_L = 2P_{meas}$.

[l] The minimum detectable absorption coefficient or the equivalent absorption coefficient of C_2H_4 for a minimum detectable concentration (the absorption coefficient corresponding to the synchronous background signal) is $\alpha_{min} = c_{min}\alpha = 2\sqrt{2}\ V_N^b/R$ (or the ratio between the peak-to-peak value of the synchronous background signal and the cell responsivity).

[m] The minimum detectable absorption cross-section per molecule of ethylene determined by the synchronous background signal is the ratio between the equivalent absorption coefficient of C_2H_4 for minimum detectable concentration and the

number of absorbing molecules per unit volume: $\sigma_{min} = \alpha_{min}/N_{tot}$, where N_{tot} is the number of absorbing molecules per cubic centimeter ($N_{tot} = 2.5\text{x}10^{19}$ cm^{-3} at 1013 mbar and 20^{o}C).

[n] Knowing the cell responsivity, we can determine the sensitivity of the photoacoustic cell (the rms voltage amplitude measured by the lock-in amplifier) to measure 1 ppb of a given gas at a given laser frequency with 1 W of unchopped laser power: $2\sqrt{2}\ V_{ppb} = \alpha P_L R c$ ($\alpha = 30.4$ cm^{-1} atm^{-1}, $P_L = 1$ W, $R = 280$ V cm/W, and $c = 10^{-9}$ atm).

Several factors influence the lowest levels at which selected compounds can be detected by CO_2 laser spectroscopic techniques, within prescribed confidence limits, in a multicomponent mixture. These factors, some of which are interdependent, include (1) the sensitivity or minimum detectable absorptivity α_{min} (cm^{-1}) of the particular CO_2 laser detection technique employed; (2) the absorption coefficients and spectral uniqueness of both the compounds of interest and interferences; (3) the total number of compounds that absorb within the wavelength regions of the CO_2 laser output; (4) the wavelengths and number of CO_2 laser lines used for monitoring; and (5) the output power of the laser at each of these lines when the photoacoustic technique is employed.

The minimum concentrations of various vapors that can be detected under interference-free conditions by the CO_2 laser photoacoustic technique are given by the relationship $c_{min} = \alpha_{min}/\alpha(\lambda)$. Here α_{min} is the minimum detectable absorptivity value for the photoacoustic detection system in units of cm^{-1}, and $\alpha(\lambda)$ is the absorption coefficient in units of cm^{-1}atm^{-1} of the vapor of interest at the CO_2 laser monitoring wavelength. In order to determine the concentrations of the various gas mixture components, it is necessary to know the absolute absorption coefficients for every gas component at the laser wavelengths. Our CO_2 laser photoacoustic system with a α_{min} value of 2.7×10^{-8} cm^{-1} should provide interference-free minimum detectable concentrations between 0.9 ppbV and 270 ppbV for vapors with usual absorption coefficients of 30-0.1 cm^{-1}atm^{-1}.

A comparison of the results we obtained by using an extracavity PA cell and the experimental parameters measured using intracavity PA cells is given in Table 6. If we take into consideration only the parameters determined by the coherent acoustical background noise (SNR = 1), then the minimum detectable absorptivity S_{sys} (cm^{-1}) is much lower (1-2 orders of magnitude) in the intracavity arrangements due to the increased laser power. Unfortunately, only SNR is often considered in the literature, which yields an extrapolated detection limit that may be considerably too small. In reality, other background signals such as window absorption limit the ultimate sensitivity. These background signals must always be taken into consideration, as they can only be reduced, but not eliminated. In real PA instruments, the minimum measurable signal V_{min} is higher in extracavity PA cells (3 times in our case) and much higher in intracavity PA cells (hundreds or even thousands of times) than the coherent acoustic background noise V_N^{ac}. From this table it clearly follows that the best sensitivity is obtained with our extracavity PA instrument, with α_{min} (cm^{-1}) being better by one or two orders of magnitude than in intracavity arrangements.

Table 6. Comparison of our results (extracavity PA cell) with the experimental parameters determined with intracavity PA cells.

Parameter	Our results	Harren *et al*. 1990 [37]	Fink *et al*. 1996 [80]
PA cell and CO_2 laser			
R (V cm/W)	280	37	52
$S_{M\,tot}$ (mV/Pa)	80	10	26
C (Pa cm/W)	3500	3700	2000
P_L (W)	4.4	100	40
p/P_L (Pa/W)	10^{-1}	1.1×10^{-1}	6×10^{-2}
Parameters determined by the coherent acoustic background noise (SNR = 1)			
V_N^{ac} (rms)[a] (μV)	2.6	0.5	0.81[b]
S_{cell} (W cm^{-1})	2.6×10^{-8}	4.0×10^{-8} [c]	4.4×10^{-8}
S_{sys} (cm^{-1})	5.9×10^{-9}	5.1×10^{-10} [d]	1.1×10^{-9}
c_{lim} (pptV)	200	17[e]	34
Parameters determined by the coherent photoacoustic background signal (SBR = 1)			
V_N^b (rms) (μV/W)	2.7	1.5	26
V_{min} (rms) (μV)	12	117[d]	1040
p_{min} (Pa)	4.2×10^{-4}	3.3×10^{-2}	1.1×10^{-1}
c_{min} (ppbV)	0.9	3.8	46
α_{min} (cm^{-1})	2.7×10^{-8}	1.2×10^{-7}	1.4×10^{-6}

[a] For a bandwidth of 1 Hz.

[b] The authors claim that they determined a coherent acoustical background noise of 0.1 μV, but their measured S_{sys} and c_{lim} correspond to V_N^{ac} = 0.81 μV.

[c] The value of S_{cell} = 1.4×10^{-8} cm^{-1}, as cited by the authors, was corrected for a peak-to-peak value of the coherent acoustical background noise.

[d] A factor of 0.78 was introduced either in the absorption coefficient of ethylene or in the intracavity laser power to compensate for the influence of saturation; the value of S_{sys} = 1.8×10^{-10} cm^{-1} claimed by the authors was corrected for a peak-to-peak value of the coherent acoustical background noise.

[e] The value of 6 pptV claimed by authors was corrected for a peak-to-peak value of the coherent acoustical background noise

To keep the flow noise at a sufficiently low level, the flow must be in the laminar regime. Another practical requirement is the time response, which is determined by the gas sample exchange rate in the resonant cell. In addition, a delay occurs because the gas flows from the inlet to the resonant cell first through the acoustic filter. A response time of < 1 s and a delay of < 10 s may occur in the continuous flow mode. Taking into account the largest dimension and the limiting value of the Reynolds number ($Re \leq 2300$ for laminar flow), the flow velocity should not exceed 1.7 m/s. This value is far too large, since it would give a flow rate of 4.8 l/min (large gas consumption). As an operating value a flow rate of up to 0.5 l/min was used. With this value, the maximum flow velocity was about 15 cm/s, the Reynolds number $Re < 200$, and the calculated response time $\tau < 0.7$ s. The response time determined from the rise time of the PA signal is longer due to gas mixing in the buffer volumes of the cell. Nevertheless, the measured response times are below 10 s for nonadsorbing gases. Adsorption on the PA cell may increase the response time significantly. Note that the adsorption effect can be effectively reduced by using appropriate wall materials and higher wall temperatures. The adsorption effects can prevent accurate determination of the vapor pressure, since even with an *in situ* sample the vapor pressure will equilibrate between the rate of vapor emission and rate of plating out.

Let us consider the system to be a cell with constant volume. For an ideal gas, $dT/dE = (nC_v)^{-1}$, so that $dp/dE = R/(C_vV)$. Here T is the temperature, p is the pressure, E is the absorbed energy, n is the number of moles of the gas, C_v is the molar heat capacity at constant volume of the gas mixture, R is the gas constant, and V is the volume of the cell. For a real photoacoustic system the contents of the cell do not completely equilibrate at the modulation frequency; thus the above equations are a simplification. However, they do emphasize the basic constraints for maximizing the photoacoustic signal; (1) the gas mixture in the cell should have the lowest possible molar heat capacity, and (2) the effective volume of the cell should be as small as possible. The latter is also advantageous when the sample amount is limited. The ideal conditions for PA spectroscopy are a gas mixture consisting of a small amount of sample buffered in a large amount of a nonabsorbing gas with a low C_v, such as rare gases, inside a cell with the smallest possible volume. Since the laser beam has cylindrical symmetry, the best way to minimize the volume is to use a cylindrically symmetric cell with an internal diameter barely larger than the diameter of the laser beam.

Cylindrical cells, without additions, such as baffles, gas valves, sample fingers, or microphone tubes, and having a diameter of less than about 1/4 of wavelength, behave as simple pipes. Since the speed of sound is inversely proportional to the mass density of the gas (see Eq. 6), the frequency is lower for a more massive gas. The speed of sound is effectively independent of the total buffer gas pressure. Some works suggest that using the heavier noble gases as buffers increases the signal-to-noise level in acoustically resonant PA spectroscopy [45].

Davidsson *et al*. [83] investigated the importance of window noise and the role of acoustic baffles in photoacoustic spectroscopy. Small amounts of dirt or imperfections can cause heating at the windows and thus the production of a photoacoustic background signal. Window absorption is a major problem for intracavity photoacoustic spectroscopy because of the high light intensity inside the cavity. The signature of window noise is that it is laser frequency independent; its intensity tracks the intensity of the exciting radiation. This signal can actually mask the signal of interest (see spectrum D in Fig. 26). It was shown that the window noise should decrease with increasing modulation frequency [84], which suggests that a relatively high modulation frequency is advantageous. The approach to this problem is to keep the windows as clean as possible and place acoustic baffles between the windows and the body of the sample cell where the microphones are mounted.

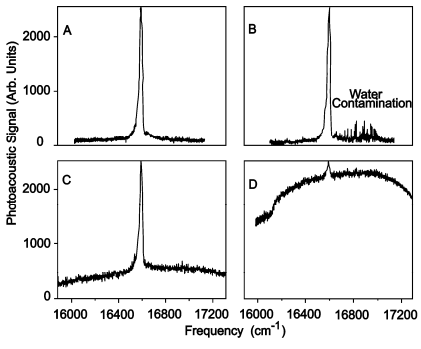

Fig. 26. Photoacoustic spectra: (A) clean windows on baffled cell; (B) clean windows on unbaffled cell; (C) dirty windows on baffled cell; (D) dirty windows on unbaffled cell [82].

The acoustic baffles hinder the propagation of the window noise into the central region of the cell near the microphones. In an attempt to quantify the usefulness of the baffles, four spectra are shown in Fig. 26. These spectra illustrate the microphone signal versus laser frequency. For both the baffled and unbaffled cells, a longitudinal resonance frequency was used. From this figure it is immediately obvious how important it is to have clean windows. If the sample makes it difficult to keep the windows clean, a cell with baffles will perform much better than one without them. Even with clean windows, the baffles give a flatter base line.

The random noise level visible on the base lines of spectra A and B in Fig. 26 is probably due to a combination of the ambient lab noise, noise from the microphones, associated electronics, and the fluctuations of the laser itself. The ultimate limit of a microphone's sensitivity is set by the random thermal fluctuations in the sample and of the microphone diaphragm. In practice, the random fluctuations of the laser do not seem to be critical. Also, the combined electronic noise of the lock-in, preamplifier, and FET amplifier in the microphones totaled about 3 μV. This is at least a factor of 10 less than the noise level observed in the spectra. The noise that is visible in the spectra stems almost exclusively from thermal fluctuations and ambient lab noise. One of the major ambient noise sources is the mechanical chopper. In practice, this seems to set the detection limit. Acoustically isolating the chopper improves the noise, but replacing it with a nonmechanical modulator is better still, as it also speeds up modulation.

In an attempt to reduce the effects of microphone noise, the output of two microphones was summed in the low-noise preamplifier. Two microphones seem better than one when observing the noise level, but the difference is not as obvious in the spectra that were taken. However, the absolute signal level does increase with an increasing number of microphones; when the sample is weakly absorbing, more microphones are an advantage.

High isolation against window absorption may be obtained by introducing acoustic baffles between the windows and the resonator. However, the resonator also introduces additional noise. Pressure fluctuations from turbulence in the gas and acoustic flux reaching the resonator from the surroundings will be amplified along with the signal. Furthermore the amplification provided by a resonator is accompanied by an increased sensitivity to parameters which affect the resonance frequency, such as gas composition, temperature, and pressure.

Besides cleaning the cell windows, a very careful rinsing of the inner walls of the cell is also very important. If the inner of the cell is not properly cleaned before a measurement, a considerable drift of the photoacoustic background signal is observed if the gas flow is interrupted. This fact demonstrates that the desorption of IR-absorbing gases and vapors from the cell walls can make a large contribution to the background signal. That is why no measurement started until after the PA cell had been rinsed with pure nitrogen till the coherent photoacoustical background noise reached the minimum value of 2.7 μV/W.

To distinguish the gas absorption signal from other signals (e.g., from the walls, windows, or interfering gases), one has to switch the CO_2 laser to other laser lines. However, repositioning the laser beam to its original wavelength can change the configuration of the laser cavity (deviation in grating position, thermal drift) and result in irreproducible absorption signals if the operation is not carefully conducted. Using a CO_2 laser stabilized on the top of the gain curve ensures that both the laser frequency and output power are reestablished with high accuracy when the laser operation is changed from one line to another.

9. The gas handling system

Whenever monitoring is performed by flowing the gas mixture through a cell, a crucial question is whether the measured signal, which represents the trace gas concentration in the interaction region, also reflects the concentration at the source. On their way to the cell, the different components of a gas mixture may react with one another, form clusters or aerosols, and react with or be adsorbed on particles present, or on the sampling line and cell walls. Adsorption problems are particularly severe for polar molecules with large dipole moments, such as water and ammonia, but they can be reduced by a proper choice of materials.

The vacuum/gas handling system is an important element in these measurements owing to its role in ensuring PA cell and gas purity. The Teflon/stainless steel system can perform several functions without necessitating any disconnections. It can be used to pump out the cell, mix gases in the desired proportions, and monitor the total pressure of gases. Whenever possible, the PA cell was employed in the gas flow mode of operation to minimize any tendency for the vapor to stick to the cell walls and the effects of the subsequent outgassing of contaminants, which would otherwise lead to increasing background signals during an experimental run.

To design an efficient vacuum/gas handling system to be used in LPAS, one must make sure that the following operations can be carried out:

(i) evacuation by the vacuum system of the entire gas handling system, including the PA cell, either totally or in different sections;
(ii) controlled introduction of a gas or gas mixture either for rinsing the PA cell and the gas handling system with pure nitrogen or for calibrating the PA spectrometer with a certified gas mixture;
(iii) pressure measurement in the PA cell and in different sections of the system;
(iv) safe insertion in the gas handling system of a sample cuvette (usually made of Pyrex glass) or aluminum-coated plastic bag with the trace gas sample;
(v) filtration of certain gases (carbon dioxide and water vapors), which interfere with the trace gas to be measured;

(vi) controlled introduction of the trace gas to be measured from the sample cuvette or bag into the PA cell by a nonabsorbing gas (nitrogen or synthetic air) acting as carrier;
(vii) controlled change of the sample and carrier gas flow rates within a broad range (10-1000 sccm);
(viii) simultaneous measurement of two sample gases (e.g., ethylene and ammonia);
(ix) quick monitoring of the trace gas concentration in the sample gas by ensuring a response time on the order of minutes or even seconds.

A vacuum/gas handling system to be used in PA experiments was designed and implemented based on these guidelines. The schematic of the gas handling chain is shown in Fig. 27, while a general view of the valves and distribution system is given in Fig. 28.

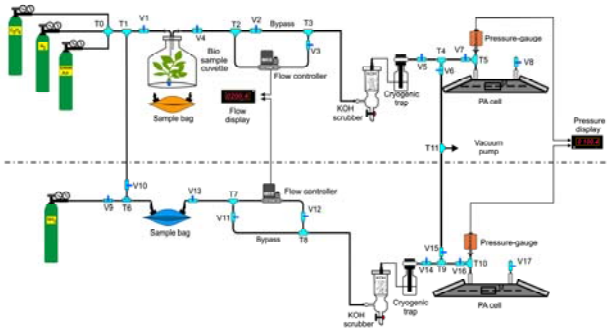

Fig. 27. Gas handling system.

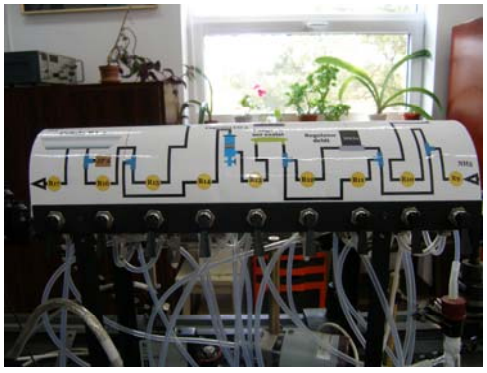

Fig. 28. General view of the gas mixing station.

Gas transport lines throughout the gas mixing station were made of Teflon (Swagelok PFA-T6M-1M-30M, 6 mm inner diameter and 1 mm wall thickness) to minimize adsorption and contamination. The toggle valves V1-V17 (Swagelok SS-1GS6mm) and union tees T1-T11 (Swagelok SS-6MO-3) were made of stainless steel. No valve grease was used. The PA cell gas inlet and outlet were connected to the gas handling system with Swagelok fittings (male connectors SS-6MO-1-2RT). Connections to the inlet and outlet valves of the PA cell were made via flexible Teflon tubing so as to minimize the coupling of mechanical vibrations to the PA cell. The flexible lines also make it possible to position the PA cell during optical alignment.

The pressure of the gases added to the PA cell was determined by means of three Baratron pressure gauges (MKS Instruments, Inc.): 622A (0-1000 mbar), 122A (0-1000 mbar), and 122A (0-100 mbar), connected to a digital two-channel unit PDR-C-2C.

We use thermal mass flowmeters, or mass flow controllers (MFC), to deliver stable and known gas flows to the PA cell. The most critical processes will require flow measurement accuracies of 1% or better in the range 1000 to 10 sccm ($7x10^{-4}$ to $7x10^{-6}$ mol/sec; 1 sccm at 0^oC = $7.436x10^{-7}$ mol/sec). The digital MFCs sense the mass flow from the temperature difference between two temperature sensors in thermal contact with the gas stream and then process the information digitally with a microcontroller. The analog sensor output is amplified and digitized before it is sent to a microprocessor to compute the final control valve position. The gas flow in our gas handling system is adjusted by two gas flow controllers, MKS 1179A (0 - 1000 sccm) and MKS 2259CC (0 - 200 sccm), which are connected to a digital four-channel instrument MKS 247C.

By using an adequate scrubber for CO_2 filtration, the CO_2 interference problem can be resolved. The CO_2 scrubber must neither alter the ethylene concentration level, nor introduce new interfering gases. By using a CO_2 trap with a volume of 88 cm^3 filled with fresh KOH pellets, we succeeded to reduce the CO_2 content in the exhaled breath of a healthy nonsmoking young person from 1.7% (equivalent to a ethylene concentration of 1.2 ppmV) to 220 ppmV (equivalent to a ethylene concentration of 15 ppbV), that is a reduction factor of 80. The water vapors are additionally filtered by a cryogenic trap filled with liquid nitrogen.

The following gases were used throughout the experiments:

- ethylene: Linde Gaz Romania, 0.96 ppmV (±5%) C_2H_4 diluted in nitrogen 5.0 (purity 99.999%) and 9.88 ppmV (±2%) C_2H_4 diluted in nitrogen 6.0 (purity 99.9999%)
- nitrogen: Linde Gaz Romania, nitrogen 5.0 (purity 99.999%) and 6.0 (purity 99.9999%);
- synthetic air: Linde Gaz Romania, 20% oxygen and 80% nitrogen (impurities: hydrocarbons max. 0.1 ppmV, nitrogen oxides max. 0.1 ppmV);
- carbon dioxide: Linde Gaz Romania, purity 99.95% (impurities: oils max. 1 ppmV);
- ammonia: Linde Gaz Romania, purity 99.98% and 9.66 ppmV (±5%) NH_3 diluted in nitrogen 6.0 (purity 99.9999%).

The flow rate was usually set at a low value of 30-100 sccm in all experiments in order to eliminate the acoustic noise of the gas flow, and all measurements were carried out with the PA cell at atmospheric pressure. Flow noise increases upwards of 10 l/h (167 sccm) were found to limit the minimum response time of the detector. The flow velocity minimizes the accumulation of the produced gases in the sampling cell. The carrier gas we used was

either nitrogen or synthetic air, and its flow rate through the system was monitored by the calibrated flowmeter. Provision is made for bypassing the flowmeter with the gas mixture flow prior to a measurement to equilibrate the feedline surfaces. This ensures that the measured rise times are an exclusive function of the cell characteristics. A measurement is initiated by diverting the gas flow from the bypass through the flowmeter and PA cell and monitoring the photoacoustic signal rise that follows.

As far as the sampling procedure is concerned, we use an extractive method, based on the collection of trace gas samples by some type of container or collecting medium and subsequent analysis in the laboratory. A problem may arise at this point due to some alterations of the gas composition caused by adsorption and desorption processes on the inner surface of the collecting container. The breath samples we analyzed were obtained from volunteers who agreed to provide such samples at certain time intervals. The volunteers were asked to exhale into a sample bag with a normal exhalation flow rate. The breath samples were collected in 0.75-liter aluminum-coated bags (Quintron, Milwaukee, Wisconsin USA) equipped with valves that sealed them after filling (Fig. 29). The bags were inserted into a modified version of the gas handling system (Fig. 30), which ensured better control by means of two independently adjusted flow controllers of the upstream pressure and the flow rate through the sample bag.

Fig. 29. Aluminum-coated plastic bag with sample gas.

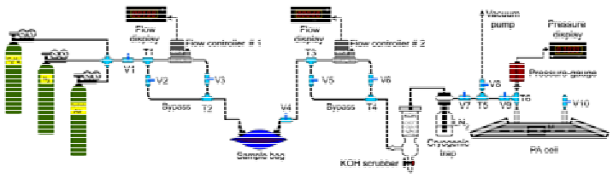

Fig. 30. Modified version of the gas handling system.

The rate of change in concentration of a species i in a flowing cell is given by:

$$\frac{dC_i(t)}{dt} = \frac{R_{flow}}{V}\left[F_i - C_i(t)\right] \tag{51}$$

where R_{flow} is the gas flow rate (liter/min or sccm), F_i is the feed concentration of species i, and V is the cell volume. This equation assumes that the adsorption rate of i is zero, and that gas mixing inside the cell is instantaneous. Integrating Eq. (51) with the initial condition that $C_i(0) = 0$ gives

$$C_i(t) = F_i\left[1 - \exp\left(-R_{flow}t/V\right)\right] \tag{52}$$

where $\tau = V/R_{flow}$ is the renewal time constant.

The solid line in Fig. 31 shows the rise time curve predicted by Eq. (52) for the experimental parameter values: V = 1200 cm^3 and R_{flow} = 100 sccm. The total renewal time of the gas content in the system (sampling cell, scrubber, and photoacoustic cell) is τ = 12 min (1/e time). This τ value is small compared to the time response of certain biological samples (e.g., the C_2H_4 production of a single flower, 0.02-0.3 nl/g/h) [79].

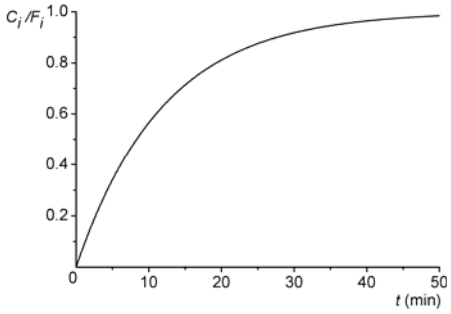

Fig. 31. Time response of the PA spectrometer for a gas flow rate of 100 sccm.

10. Data acquisition and processing

The acquisition and processing of the recorded data was done with Keithley TestPoint software. TestPoint data acquisition software provides a development environment in which data acquisition applications can be generated. A graphical editor is provided for creating a user interface, or "panel", which the user sees and interacts with as the application executes. A user panel is made of pictorial elements that represent such things as switches, variable controls, numerical, text and selection boxes, bar displays, graphs, and strip charts. In addition, an application editor is provided, which ensures some interactive means of specifying how the visual elements on the user panel interact with the data sources and processing functions to achieve application goals. TestPoint uses an automated textual description of the operations carried out by each user panel element.

We developed a modular software architecture aimed at controlling the experiments, collecting data, and preprocessing information. It helps automate the process of collecting and processing experimental results. The software controls the chopper frequency, transfers powermeter readings, normalizes data, and automatically stores files. It allows the user to set parameters such as the PA cell responsivity (a constant used to normalize raw data), gas absorption coefficient, number of averaged samples at every measurement point, sample acquisition rate, and total number of measurement points. This software interfaces the following instruments:

- lock-in amplifier;

- chopper;
- laser powermeter;
- gas flowmeter.

The software user interface allows the user to set or read input data and instantaneous values for the PA voltage (rms), average laser power after chopper, and trace gas concentration. Users may set experimental parameters for the PA cell responsivity and gas absorption coefficient. They are also provided with a text input to write a description of the experiments or take other notes. The user interface also provides data visualization (Fig. 32).

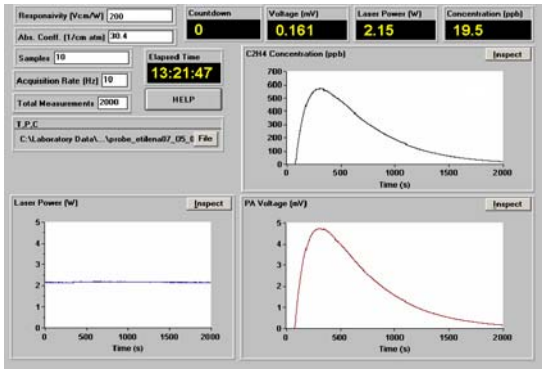

Fig. 32. Software user interface used to record trace gas concentrations.

The software user interface contains three graphs which display in real time the following parameters:

- CO_2 laser power level;
- PA signal;
- trace gas concentration.

Another window (countdown) indicates the number of remaining measurement points.

All settings and properties are stored to disk from session to session. In addition, a file may be automatically generated when running an experiment, including:

- **Laser power** stores powermeter readings of power incident on the sample as a function of time;
- **PA signal** stores the instantaneous values of the PA signal measured by the lock-in amplifier as a function of time;
- **Trace gas concentration** stores the time evolution of the trace gas concentration for a given laser wavelength.

12. Measurement of ethylene absorption coefficients

The ethylene absorption coefficients for various CO_2 laser transitions have been measured in various experiments. Discrepancies as high as ~15% have been found in the absolute IR values observed at many laser transitions. Such discrepancies are typical of many other gases and are partially associated with the difficulty of producing proper gas samples with known concentration levels. Unfortunately, large discrepancies are also found between measurements of the relative spectral signatures (the ratio between absorption coefficients at different wavelengths). Knowledge of the relative spectral signatures rather than absolute ones is sufficient for trace gas identification. We also note that it is rather problematic to obtain highly accurate measurements of the absolute values of the absorption coefficients of gases using the photoacoustic effect. The reason for this is the need of an absolute calibration of the cell. The calibrations cited in the literature are all based on *a priori* knowledge of the absorption coefficient of a gas at some selected wavelength. However, in all cases the absorption coefficient was actually known only to a few percent.

Photoacoustics is emerging as a standard technique for measuring extremely low absorptions independent of the path length and offers a degree of parameter control that cannot be attained by other methods. Radiation absorption by the gas creates a pressure signal which is sensed by the microphone. The resulting signal, processed by a phase sensitive detector, is directly proportional to the absorption coefficient and laser power (or laser power absorbed per unit volume). The sensitivity of the technique is such that absorptions of $<10^{-7}$ cm^{-1} can be measured over path lengths of a few tens of centimeters. The small volume of the chamber makes it possible to accurately control the gas parameters, and the system can be operated with static fills or in continuous gas flow mode.

The set of values of the absorption coefficients α, for all laser wavelengths, for a particular gas or vapor and at a common concentration is called the optoacoustic absorption spectrum or signature and is unique to a combination of vapor and laser. These signatures or "fingerprints" are absolute entities, unique only to the laser frequency and species, which provide the specifics of instrument performance in terms of detection limit and interference rejection.

To improve the measurement of ethylene absorption coefficients, a special procedure was followed. Prior to each run, the gas mixture was flowed at 100 sccm for several minutes to stabilize the boundary layer on the cell walls, since a certain amount of adsorption would occur and possibly influence background signals; after this conditioning period, the cell was closed off and used in measurement. For every gas fill with 0.96 ppmV ethylene buffered in pure nitrogen, the responsivity of the cell was determined supposing an absorption coefficient of 30.4 $cm^{-1}atm^{-1}$ at 10P(14) laser transition. After measurements at all laser lines, the cell responsivity was checked again, to eliminate any possibility of gas desorption during the measurement. The partial pressure of ethylene was enough to have significant PA signals for all laser lines and low enough to be far away from the saturation regime (observations were only made at a C_2H_4 concentration of 100 ppmV). The α values at each laser line were obtained from Eq. (29) using the measured PA signal and laser power (the cell responsivity and ethylene concentration were known). An average over several independent measurements at each line was used to

improve the overall accuracy of the results. The values to be presented are thought to be the best published to date.

The absolute magnitudes of the absorption coefficients were calculated as mean values of several independent measurements. An absorption coefficient corresponding to each CO_2 laser transition was determined from two sets of 50 different measurements. Every set of measurements was initiated by the frequency stabilization of a given line of the CO_2 laser. From one set of measurements to another, the closed loop of the frequency stabilization circuit was interrupted, the laser was tuned again to the top of the gain curve, and then the frequency stabilization was set and checked by watching the long term stability. Inside one set, 50 independent measurements were made at a rate of one per second to assess reproducibility. From one measurement to the next, the error measurement of the absorption coefficient was calculated as the ratio between the maximum difference (maximum value minus minimum value) and the average value. The final value of the ethylene absorption coefficient is given by the arithmetic mean of the two sets of measurements, while the absorption coefficient error is chosen as the larger value of the two sets. The same procedure was applied for every absorption coefficient of ethylene.

To measure the absorption coefficients of ethylene, the software user interface was modified to allow that the laser power, PA signal, and calculated absorption coefficients function on time (or number of measurements) be recorded on different panels (Fig. 33).

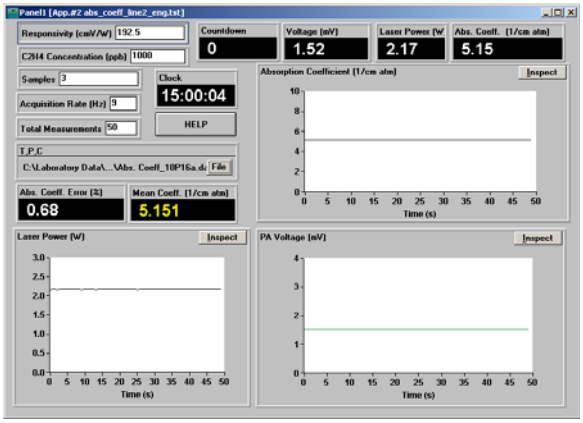

Fig. 33. Software user interface to measure the absorption coefficients of ethylene.

The results of our measurements are given in Fig. 34 and Table 7.

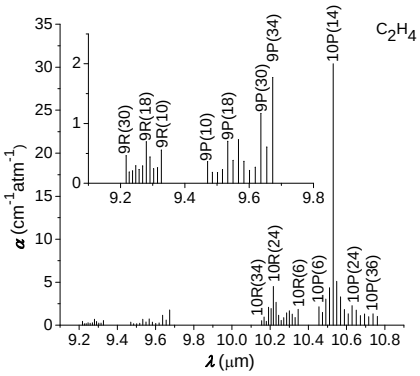

Fig. 34. Absorption coefficients of ethylene at CO_2 laser wavelengths. The inset shows an enlarged view of the measurements for the 9-μm band.

In Table 7, the wavelengths and frequencies of the CO_2 laser lines are those determined by Freed *et al*. [85]. Because of the large spacing between laser transitions (1.2-2 cm^{-1} apart), strong differences of absorption occur. Our results are compared to those of Brewer *et al*. [86] that were also obtained by a photoacoustic method. The difference between the two spectral patterns suggests problems in the measurement techniques (for example, frequency deviation from the laser line center, gas calibration, system purity, linearity, precision) and/or data analysis. The different temperatures and atmospheric pressures at which the measurements were made cannot account for the discrepancies, because Persson *et al*. [87] measured a change in absorption coefficient of only 5% at the 10P(14) line for a temperature change of 30 ^{o}C (negative temperature coefficient), while the changes caused by a pressure difference of 40 Torr are <5% for all CO_2 laser wavelengths.

The random coincidence between the emission and absorption lines will be such that some laser lines will lie close to the centers of the absorbing lines and others will be far away in the wings. The result is a spectral representation unique to that molecule. As a consequence of the superposition of different pressure-broadened C_2H_4 transitions (ν_7 vibration), a strong absorption is obtained at the 10P(14) laser line (absorption coefficient of 30.4 $cm^{-1}atm^{-1}$ at 949.479 cm^{-1}). C_2H_4 has weaker absorption coefficients at the 10P(12) and 10P(16) CO_2 laser transitions (4.36 $cm^{-1}atm^{-1}$ at 951.192 cm^{-1} and 5.10 $cm^{-1}atm^{-1}$ at 947.742 cm^{-1}, respectively). Also, in Fig. 34 ethylene is seen to possess moderately strong absorption profiles within the 9.4-μm band.

There is general agreement with the results of Brewer *et al.* [86] for the $00^{0}1$-$10^{0}0$ band. The difference between our results and those obtained by the above mentioned authors is less than 10% for the majority of the investigated lines while only for five lines the discrepancy is higher, between 10% and 20%. By contrast, the values determined in the present work are consistently higher in the $00^{0}1$-$02^{0}0$ band. The difference is larger by 10-50% for the P branch, while our values in the R branch are higher by a factor of 1.5-5.5 (the largest discrepancies are recorded for the 9R(28), 9R(30), and 9R(22) laser lines).

Table 7. Absorption coefficients of C_2H_4 at $^{12}C^{16}O_2$ laser wavelengths.

Spectral line	Wavelength (μm vac.) [85]	Wavenumber (cm^{-1}) [85]	$\alpha(C_2H_4)$ ($cm^{-1}atm^{-1}$) our results	$\alpha(C_2H_4)$ ($cm^{-1}atm^{-1}$) Brewer *et al.* [86]
10P(36)	10.764060	929.017436	1.04 ± 5.1%	1.20 ± 7.7%
10P(34)	10.741122	931.001413	1.33 ± 5.0%	1.40 ± 6.8%
10P(32)	10.718568	932.960421	0.985 ± 3.6%	1.10 ± 6.0%
10P(30)	10.696394	934.894496	1.31 ± 1.7%	1.35 ± 6.2%
10P(28)	10.674594	936.803747	1.12 ± 1.5%	1.19 ± 6.1%
10P(26)	10.653164	938.688257	1.76 ± 2.0%	1.78 ± 5.9%
10P(24)	10.632098	940.548098	2.28 ± 1.5%	2.29 ± 5.8%
10P(22)	10.611393	942.383336	1.32 ± 2.5%	1.37 ± 6.5%
10P(20)	10.591043	944.194029	1.82 ± 2.5%	1.84 ± 6.2%
10P(18)	10.571045	945.980229	3.29 ± 1.9%	3.32 ± 6.7%
10P(16)	10.551395	947.741978	5.10 ± 1.9%	5.07 ± 7.2%
10P(14)	10.532088	949.479313	30.4 ± 2.1%	30.4 ± 7.6%
10P(12)	10.513121	951.192263	4.36 ± 1.5%	4.31 ± 6.4%
10P(10)	10.494491	952.880849	3.04 ± 1.8%	2.98 ± 6.4%
10P(8)	10.476194	954.549086	1.51 ± 5.0%	1.52 ± 6.0%
10P(6)	10.458205	956.184982	2.15 ± 3.8%	2.06 ± 7.7%
10R(6)	10.349286	966.250160	1.86 ± 4.1%	1.81 ± 5.7%
10R(8)	10.333703	967.707233	0.889 ± 5.9%	0.924 ± 5.6%
10R(10)	10.318431	969.139547	1.29 ± 1.7%	1.31 ± 5.9%
10R(12)	10.303465	970.547244	1.68 ± 2.4%	1.66 ± 5.8%
10R(14)	10.288804	971.930258	1.44 ± 2.0%	1.41 ± 5.6%
10R(16)	10.274445	973.288516	0.886 ± 3.3%	0.914 ± 6.4%
10R(18)	10.260388	974.621939	0.560 ± 3.7%	0.617 ± 7.4%
10R(20)	10.246636	975.930439	1.17 ± 2.8%	1.09 ± 5.5%
10R(22)	10.233173	977.213922	2.67 ± 1.5%	2.55 ± 6.0%
10R(24)	10.224193	978.072285	4.51 ± 2.6%	4.33 ± 6.2%
10R(26)	10.207149	979.705420	1.94 ± 4.3%	1.89 ± 5.8%
10R(28)	10.194581	980.913210	2.10 ± 2.0%	2.02 ± 5.8%
10R(30)	10.182308	982.095530	0.458 ± 3.3%	0.553 ± 6.0%
10R(32)	10.170330	983.252249	0.954 ± 5.4%	1.02 ± 6.3%
10R(34)	10.158645	984.383225	0.530 ± 2.9%	0.634± 5.8%
9P(34)	9.675971	1033.48799	1.77 ± 4.4%	1.50 ± 5.7%
9P(32)	9.657416	1035.47361	0.604 ± 7.3%	0.563 ± 5.7%
9P(30)	9.639166	1037.43410	1.17 ± 4.9%	1.03 ± 6.5%
9P(28)	9.621219	1039.36931	0.268 ± 6.8%	0.202 ± 7.5%
9P(26)	9.603573	1041.27907	0.215 ± 1.7%	0.193 ± 5.8%
9P(24)	9.586227	1043.16323	0.366 ± 7.5%	0.332 ± 6.1%
9P(22)	9.569179	1045.02166	0.729 ± 3.5%	0.661 ± 5.7%
9P(20)	9.552428	1046.85421	0.383 ± 7.0%	0.359 ± 5.9%
9P(18)	9.535971	1048.66080	0.703 ± 4.8%	0.607 ± 6.3%
9P(16)	9.519808	1050.44128	0.230 ± 4.8%	0.177 ± 6.3%
9P(14)	9.503936	1052.19554	0.180 ± 3.0%	0.119 ± 9.8%
9P(12)	9.488354	1053.92350	0.181 ± 3.4%	0.124 ± 7.3%
9P(10)	9.473060	1055.62506	0.361 ± 5.2%	0.276 ± 5.7%
9R(10)	9.329369	1071.88376	0.522 ± 4.0%	0.308 ± 6.8%
9R(12)	9.317246	1073.27848	0.260 ± 7.0%	0.0904 ± 8.5%
9R(14)	9.305385	1074.64648	0.242 ± 6.0%	0.0654 ± 5.4%
9R(16)	9.293785	1075.98781	0.440 ± 5.5%	0.224 ± 6.6%
9R(18)	9.282443	1077.30251	0.694 ± 2.6%	0.448 ± 6.1%
9R(20)	9.271358	1078.59064	0.289 ± 2.8%	0.115 ± 8.7%
9R(22)	9.260526	1079.85225	0.229 ± 5.3%	0.0667 ± 5.4%
9R(24)	9.249945	1081.08742	0.292 ± 1.7%	0.119 ± 7.9%
9R(26)	9.239614	1082.29623	0.205 ± 7.0%	0.0720 ± 5.8%
9R(28)	9.229530	1083.47877	0.187 ± 3.8%	0.0342 ± 8.7%
9R(30)	9.219690	1084.63514	0.460 ± 4.9%	0.130 ± 7.4%

The present work was carried out using a methodology which gave the best possible control over the ethylene partial pressure and background signals. The background levels and calibration of the PA cell were checked before and after every experimental run. The present study is considered reliable, particularly in view of the careful attention that was paid to controlling the gas composition and noise signals. No apparent fault could be found with either the apparatus or methodology that would account for the discrepancy by factors of 2-5 from other reported data in the case of the CO_2 laser 9R lines.

In Table 8 we present average results of measurements of the absorption coefficients of ethylene relative to measurements at the strongly absorbed 10P(14) laser transition (this line acts as the normalizing value), $R_1 = \alpha(\lambda)/\alpha(\lambda = 10.532088\ \mu m)$. In the table we also compare our results with other existing data considered by us most reliable (R_2 for Brewer *et al*. [86] and R_3 for Persson *et al*. [87]).

Table 8. Relative spectral signature of ethylene at STP $R_i = \alpha(\lambda)/\alpha$ ($\lambda = 10.532088\ \mu m$).

Wavelength line	R_1 Our results	R_2 [86]	R_3 [87]	R_{med}	S (%)	S/R_{med} (%)
10P(10)	0.100	0.098	0.099	0.099	0.077	0.78
10P(12)	0.143	0.142	0.136	0.140	0.311	2.21
10P(14)	1	1	1	-	-	-
10P(16)	0.168	0.167	0.165	0.167	0.001	0.60
10P(18)	0.108	0.109	0.105	0.107	0.002	1.87
10P(20)	0.060	0.061	0.061	0.061	0.058	0.95
10P(22)	0.043	0.045	0.046	0.045	0.001	2.22
10P(24)	0.075	0.075	0.074	0.075	0.058	0.77
10P(26)	0.058	0.059	0.060	0.059	0.081	1.37
10P(28)	0.037	0.039	0.040	0.039	0.001	2.56
10P(30)	0.043	0.044	0.047	0.045	0.173	3.84
10R(10)	0.042	0.043	0.043	0.043	0.058	1.35
10R(12)	0.055	0.055	0.057	0.056	0.100	1.79
10R(14)	0.047	0.046	0.050	0.047	0.183	3.89
10R(16)	0.029	0.030	0.032	0.030	0.129	4.30
10R(18)	0.018	0.020	0.020	0.019	0.100	5.26
10R(20)	0.038	0.036	0.037	0.037	0.082	2.22
10R(22)	0.088	0.084	0.088	0.087	0.191	2.20
10R(24)	0.148	0.142	0.144	0.145	0.252	1.74
10R(26)	0.064	0.062	0.064	0.063	0.100	1.59
10R(28)	0.069	0.066	0.072	0.069	0.245	3.55
9P(14)	0.006	0.004	0.004	0.005	0.100	20.00
9P(16)	0.008	0.006	0.006	0.007	0.100	14.29
9P(18)	0.023	0.020	0.022	0.022	0.129	5.86
9P(20)	0.013	0.012	0.008	0.011	0.216	19.64
9P(22)	0.024	0.022	0.023	0.023	0.082	3.57
9P(24)	0.012	0.011	0.011	0.011	0.058	5.27
9P(26)	0.007	0.006	0.007	0.007	0.058	8.29

The results listed in Table 8 differ importantly from those shown in Table 7 in that they compare relative rather than absolute values. The discrepancies between the three sets for each probe line are indicated in the ratio S/R_{med} of the standard deviation S to the mean absorption coefficient R_{med}, where:

$$R_{med} = \frac{\sum_{i=1}^{n} R_i}{n} \tag{53}$$

$$S = \sqrt{\frac{\sum_{i=1}^{n} (\Delta R_i)^2}{n}}\, x100(\%) \tag{54}$$

The erratic discrepancies in S/R_{med} are smaller than 5% for all lines in the P and R branches at 10 μm, while for the P branch at 9 μm they are higher, but do not exceed 20%. No comparison was possible for the R branch at 9 μm, because Persson *et al*. [87] made no measurement at these wavelengths. The results generally show increasing measurement discrepancies at wavelengths furthest from the strong 10P(14) line and weakest in terms of absorptivity of the CO_2 laser lines. Note that the values provided in Table 8 were derived by three distinct experimental techniques: our results and those of Brewer *et al*. [86] were obtained by different photoacoustic methods, while Persson *et al*. [87] applied the White cell methodology (long path measurements). This comparison sustains the observation that significant agreement on

ethylene absorption coefficients remains elusive, especially at lower absorbing CO_2 laser lines.

13. Conclusions

Based on previous discussion and experience, PA spectroscopy, performed with tunable CO_2 lasers as radiation sources, offers the following main characteristics relevant to *in situ* trace gas monitoring:

(i) Its high sensitivity makes it possible to measure absorption coefficients on the order of 10^{-8} cm^{-1}, corresponding to densities of $\mu g/m^3$ or concentrations of ppbV (10^{-9}) for most substances.
(ii) The PA cell responsivity is independent of radiation wavelength.
(iii) A large number of gases and vapors are measurable with the same instrument.
(iv) It has high selectivity, meaning that it can clearly distinguish among various compounds.
(v) The experimental setup is rather simple, immune to interference, and, for example, does not require cryogenic cooling of the infrared detectors, etc.
(vi) Relative portability for *in situ* measurements (carried on mobile trailers in the troposphere or on balloon-borne systems to the stratosphere).
(vii) Operational simplicity and real time data analysis make it capable of performing quasi continuous measurements.
(viii) The calibration with certified gases and gas mixtures is straightforward and reliable.
(ix) Detection linearity and a wide dynamic range of at least 7 orders of magnitude are offered (from several pptV to tens of ppmV), i.e., the same apparatus can be used for low (immission) and high (emission) concentrations.
(x) Specially designed PA cells can perform continuous measurements on flowing gas mixtures, i.e., a much better temporal resolution can be achieved than the one provided by, *inter alia*, gas chromatography.

The outstanding features of the PA cell, most importantly its small size, simplicity, and robustness, cannot be fully utilized unless it is combined with a suitable laser source. The recent commercial availability of sealed-off, medium-power (<25 W), grating-tunable CO_2 lasers has paved the way to the development of instrumentation with excellent sensitivity and compact footprints that can be readily deployed in industrial or medical settings. Further improvements are possible by using resonant PA cells with high Q factors (limited, though, by fluctuations of the modulation frequency), multipass, or intracavity arrangements.

The applications of resonant PA spectroscopy include concentration measurements and trace gas analysis, accurate determinations of thermophysical properties, detections of dynamic processes such as gas mixing or chemical reactions, relaxation processes (determinations of collisional lifetimes of specified quantum states and routes of energy exchange in polyatomic molecules), spectroscopic experiments, studies of aerosols, etc. Trace-gas sensing is a rapidly developing field, in demand for applications such as process and air-quality measurements, atmospheric monitoring, breath diagnostics, biology and agriculture, chemistry, and security and workplace surveillance.

More than 250 different volatile organic compounds including air pollutants originating from the burning of fossil fuels, traffic, or natural sources can be identified and measured with a CO_2 laser based PA instrument. Such studies are prompted by the growing public concern about serious environmental problems such as acid rain, photochemical smog, stratospheric ozone depletion, and global climatic changes.

Breath analysis is a noninvasive medical diagnostic method that distinguishes among more than 200 compounds in exhaled breath. Many of these compounds, if measured accurately at very low concentration levels, typically in the range of few ppbV, can be used to identify particular medical conditions. Measuring human biomarkers in exhaled breath is expected to revolutionize diagnosis and management of many diseases and may soon lead to rapid, improved, lower-cost diagnosis, which will in turn ensure expanded life spans and an improved quality of life. For example, ammonia levels in the breath can be used to determine the exact time necessary for an optimal degree of dialysis for a patient with end-stage renal disease at every session.

Trace-gas detection techniques based on PA spectroscopy make it possible to discover and control plant physiology mechanisms such as those responsible for germination, blossoming, senescence, ripening, wounding effects, post anaerobic injury, etc. Many agriculturally interesting gases (ethylene, methane, water vapor concentration, carbon dioxide, ammonia, ozone) can be measured in situ and in real time with CO_2 and CO laser based photoacoustic spectrometers.

In chemistry, PA spectroscopy is useful in the monitoring of chemical processes (reaction rates, equilibrium constants, enthalpies), identification of different compounds (even isomers and radicals), and dimerization of fatty acid vapors.

The techniques of PA spectroscopy can be extended to the detection of a wide variety of industrial gases, including benzene, hydrogen cyanide, acetylene, carbon monoxide, and carbon dioxide, as well as a broad range of chemical warfare agents, including nerve gases (Sarin, Soman, Tabun), blistering agents (phosgene, mustard gas), and poisonous gases (hydrogen cyanide), explosives (TNT, PETN), and harmful drugs (heroin, morphine, narcotine).

Our previous research on LPAS [89-95] has led to the development of new applications in plant physiology (seed germination, ripening of climacteric fruits, plant response to pathogen infection) [96-98], measurement of gas absorption coefficients (ethylene, ammonia) [99], and medicine (cultures of human cells doped with heavy metals, ionizing radiation damage in living organisms, lipid peroxidation in lung epithelium following the

inhalation of cigarette smoke, exhaled breath from patients treated by anti-tumor radioisotope therapy) [100-103].

Other laser sources were successfully applied in photoacoustic spectroscopy. Recent developments in compact near-infrared (NIR) and IR all-solid-state tunable lasers, such as the tunable semiconductor lasers, quantum-cascade lasers, and devices utilizing non-linear optical mixing in non-linear crystals (OPOs, difference frequency generators (DFGs), optical parametric amplifiers (OPAs)), have significantly advanced the application of photoacoustic techniques in sensitive trace gas analysis.

Near-infrared diode lasers are becoming more and more popular due to recent development of cheap high-quality, compact sources having a spectral emission which falls in the absorption range of many molecules of great practical interest. The range of the available NIR diode lasers spans from about 0.8 to 2.1 μm. Many gases like methane, acetylene, CO, and CO_2 exhibit overtone absorptions in the 1.55-1.65 μm wavelength region which can be covered by a conventional external cavity diode laser (ECDL). Detection limits are lower compared with measurements in the fundamental absorption region but still sufficient for many applications. A combination of diode lasers with PA detection was used by various authors to detect ammonia [104, 105], methane [106], elemental carbon [107], toluene [108], and water vapor [109]. Different experimental arrangements such as external cavity diode lasers [110] or intracavity PA cells [111] were tested. At present, 1.6 μm diode lasers, coinciding with the first vibrational overtones and combination bands of molecules containing a CH bond, are those that – in the NIR range – provide the best trade-off between cost and molecular detection efficiency [112].

Recent progress with quantum-cascade lasers makes them attractive sources in the important 3- to 5-μm spectral range. This area is important not only because the characteristic absorption bands of, among others, CO, N_2O, HCl and CH_2O, lie herein, but also because there is an atmospheric transparent window in this range. Soon after the first appearance of these lasers, gas monitoring applications using various detection schemes were reported [113]. Quantum-cascade lasers were used to detect ammonia and water vapor at 8.5 μm [114], NO at 5.2 μm [115], $^{12}CH_4$, $^{13}CH_4$ and N_2O isotopomers at 8.1 μm [116], trace gases (CH_4, N_2O, H_2O) in laboratory air at 7.9 μm [117] and carbon dioxide, methanol and ammonia at 10.1/10.3 μm [118]. In contrast to semiconductor (diode) lasers, quantum-cascade lasers are unipolar light sources based on only one type of carrier, usually electrons, making intraband transitions between confined energy levels within the conduction band. The term "cascade" comes from the fact that the confined energy levels are arranged the way of a waterfall, so that electrons undergoing lasing transitions travel from one stage to the next, just like water does in a multiple-step water cascade. Therefore, one electron can emit sequentially up to *n* photons when *n* steps are present. The emission wavelength of a quantum-cascade laser is determined not by the semiconductor bandgap but by the quantum confinement in the quantum wells created by the quantum-well material and the barrier material. Therefore, quantum-cascade lasers can span a wide wavelength range using the same material system. Quantum-cascade lasers with wavelengths from 3.5 to 13 μm have been fabricated by use of the same material system (InGaAs wells and InAlAs barriers).

Widely tunable, narrowband optical parametric oscillator (OPO)-based laser sources were used for trace gas spectroscopy in the fundamental C-H stretch vibration region (3-5 μm) [119], to detect ethane at 3.34 μm [120,121], N_2O at 2.86 μm [122], or methane at 3.39 μm [123]. Most of today's commercial OPOs are based on BaB_2O_4 crystals (BBO) pumped by the third harmonic of a Nd:YAG laser and their IR tuning range is limited to approximately 2 μm. Difference frequency generation (DFG) is certainly the most promising technique for the extension of the tuning range of an existing tunable laser to the mid infrared (2.5-4.5 μm) [124]. Spectrometers using DFG were applied to monitoring, for example, formaldehyde in ambient air at 3.53 μm [125] and volcanic gases (CH_4, CO_2, HCl, SO_2, H_2O vapor) at 3.3-4.4 μm [126].

Extensions of various aspects of this work are currently being pursued in our laboratory.

References

[1] A. G. Bell, Am. J. Sci. **XX**, 305-324 (1880).
[2] A. G. Bell, Phil. Mag. J. Sci. **XI**, 510-528 (1881).
[3] J. Tyndall, Proc. R. Soc. **31**, 307-317 (1881).
[4] W. C. Röntgen, Ann. der Phys. und Chem. **1**, 155-159 (1881).
[5] W. H. Preece, Proc. R. Soc. **31**, 506-520 (1881).
[6] R. Kaiser, Can. J. Phys. **37**, 1499-1513 (1959).
[7] E. L. Kerr, J. Atwood, Appl. Opt. **7**, 915-921 (1968)
[8] L. B. Kreuzer, J. Appl. Phys. **42**, 2934-2943 (1971).
[9] L. B. Kreuzer, C. K. N. Patel, Science **173**, 45-47 (1971).
[10] L. B. Kreuzer, N. D. Kenyon, C. K. N. Patel, Science **177**, 347-349 (1972).
[11] C. F. Dewey Jr., R. D. Kamm, C. E. Hackett, Appl. Phys. Lett. **23**, 633-635 (1973).
[12] C. W. Bruce, R. G. Pinnick, Appl. Opt. **16**, 1762-1765 (1977).
[13] R. W. Terhune, J. E. Anderson, Opt. Lett. **1**, 70-72 (1977)
[14] C. K. N. Patel, A. C. Tam, Rev. Mod. Phys. **53**, 517-554 (1981).
[15] G. A. West, Rev. Sci. Instrum. **54**, 797-817 (1983).
[16] P. Hess, "Resonant photoacoustic spectroscopy", in Topics in Current Chemistry, Vol. **111**, Managing Editor F. L. Boschke, Springer, Berlin, 1-32 (1983).
[17] A. C. Tam, Rev. Mod. Phys. **58**, 381-431 (1986).
[18] M. W. Sigrist, J. Appl. Phys. **60**, R83-R121 (1986).
[19] P. L. Meyer, M. W. Sigrist, Rev. Sci. Instrum. **61**, 1779-1807 (1990).
[20] F. J. M. Harren, J. Reuss, "Spectroscopy, photoacoustic", in Encyclopedia of Applied Physics, Vol. **19**, Editor G. L. Trigg, VCH Publishers, New York, 413-435 (1997).

[21] F. J. M. Harren, G. Cotti, J. Oomens, S. te Lintel Hekkert, "Photoacoustic spectroscopy in trace gas monitoring", in Encyclopedia of Analytical Chemistry, edited by R. A. Meyers, Vol. **3**, Wiley, Chichester, UK, 2203-2226 (2000).
[22] A. Miklos, P. Hess, Z. Bozoki, Rev. Sci. Instrum. **72**, 1937-1955 (2001).
[23] M. W. Sigrist, Rev. Sci. Instrum. **74**, 486-490 (2003).
[24] T. Schmid, Anal. Bioanal. Chem. **384**, 1071-1086 (2006).
[25] Y. -H. Pao, Ed., "Optoacoustic Spectroscopy and Detection", Academic, New York 1977.
[26] A. Rosencwaig, "Photoacoustics and Photoacoustic Spectroscopy", Chemical Analysis **57**, Wiley, New York 1980.
[27] V. P. Zharov, V. S. Letokhov, "Laser Optoacoustic Spectroscopy", Springer Verlag, Berlin 1986.
[28] P. Hess, Ed., "Photoacoustic, Photothermal and Photochemical Processes in Gases", Topics in Current Physics **46**, Springer, Berlin 1989.
[29] A. Mandelis, Ed., "Progress in Photothermal and Photoacoustic Science and Technology", Vol. **1**, Elsevier, New York 1992.
[30] D. Bicanic, Ed., "Photoacoustic and Photothermal Phenomena III", Springer Series in Optical Sciences **69**, Springer, Berlin 1992.
[31] V. E. Gusev, A. A. Karabutov, "Laser Optoacoustics", AIP, New York 1993.
[32] M. W. Sigrist, Ed., "Air Monitoring by Spectroscopic Techniques", Vol. **127** of Wiley Chemical Analysis Series, Wiley, New York 1994.
[33] A. Mandelis, Ed., "Progress in Photothermal and Photoacoustic Science and Technology", Vol. **2**, Prentice Hall, Englewood Cliffs, N. J. 1994.
[34] A. Mandelis, P. Hess, Eds., "Progress in Photothermal and Photoacoustic Science and Technology", Vol. **3**, SPIE, Bellingham, Wash. 1997.
[35] M. W. Sigrist, S. Bernegger, P. L. Meyer, "Atmospheric and exhaust air monitoring by laser photoacoustic spectroscopy", Ch. 7, Vol. **46** of Topics in Current Physics "Photoacoustic, photothermal and photochemical processes in gases", Editor P. Hess, Springer Verlag, Berlin, 173-211 (1989).
[36] M. H. Hubert, "Laser optoacustic detector measurement of signatures of a selection of environmental contaminants", Ultra Lasertech Inc., Mississauga, Canada, Rep. No. 83-715-1, 1-107 (1983).
[37] F. J. M. Harren, F. G. C. Bijnen, J. Reuss, L. A. C. J. Voesenek, C. W. P. M. Blom, Appl. Phys. B **50**, 137-144 (1990).
[38] J. Reid, J. Shewchun, B. K. Garside, E. A. Balik, Appl. Opt. **17**, 300-307 (1978).
[39] M. B. Pushkarsky, M. E Weber, O. Baghdassarian, L. R. Narasimhan, C. K. N. Patel, Appl. Phys. B **75**, 391-396 (2002).
[40] R. Gerlach, N. M. Amer, Appl. Phys. Lett. **32**, 228-231 (1978).
[41] E. Kritchman, S. Shtrikman, M. Slatkine, J. Opt. Soc. Am. **68**, 1257-1271 (1978).
[42] R. D. Kamm, J. Appl. Phys. **47**, 3550-3558 (1976).
[43] C. F. Dewey, "Design of optoacoustic systems", Chap. 3 in Optoacoustic Spectroscopy and Detection, Ed. Y. -H. Pao, Academic, New York, 1977.
[44] P. M. Morse, K. U. Ingard, "Theoretical Acoustics", Princeton University Press, Princeton, N.J. 1986.
[45] L. J. Thomas III, M. J. Kelly, N. M. Amer, Appl. Phys. Lett. **32**, 736-738 (1978).
[46] M. A. Gondal, Appl. Opt. **36**, 3195-3201 (1997).
[47] R. A. Rooth, A. J. L. Verhage, L. W. Wouters, Appl. Opt. **29**, 3643-3653 (1990).
[48] R. H. Johnson, R. Gerlach, L. J. Thomas III, N. M. Amer, Appl. Opt. **21**, 81-89 (1982).
[49] S. Bernegger, M. W. Sigrist, Appl. Phys. B **44**, 125-132 (1987).
[50] L. B. Kreuzer, "The physics of signal generation and detection", Chap. 1 in Optoacoustic Spectroscopy and Detection, Ed. Y. -H. Pao, Academic, New York, 1977.
[51] F. G. Bijnen, J. Reuss, F. J. M. Harren, Rev. Sci. Instrum. **67**, 2914-2923 (1996).
[52] G. Z. Angeli, A. M. Solyom, A. Miklos, D. D. Bicanic, Anal. Chem. **64**, 155-158 (1992).
[53] A. Thöny, M. W. Sigrist, Infrared Phys. Technol. **36**, 585-615 (1995).
[54] T. Groot, "Trace gas exchange by rice, soil and pears. A study based on laser photoacoustic spectroscopy", PhD Thesis, University of Nijmegen, The Netherlands, 2002.
[55] R. Gerlach, N. M. Amer, Appl. Phys. **23**, 319-326 (1980).
[56] M. J. Kavaya, J. S. Margolis, M. S. Shumate, Appl. Opt. **18**, 2602-2606 (1979).
[57] S. M. Beck, Appl. Opt. **24**, 1761-1763 (1985).
[58] P. Perlmutter, S. Shtrikman, M. Slatkine, Appl. Opt. **18**, 2267-2274 (1979).
[59] A. Olaffson, M. Hammerich, J. Bülow, J. Henningsen, Appl. Phys. B **49**, 91-97 (1989).
[60] J. Henningsen, A. Olaffson, M. Hammerich, "Trace gas detection with infrared gas lasers", in Applied Laser Spectroscopy, Ed. W. Demtröder, M. Inguscio, Plenum Press, New York, 403-416 (1990).
[61] M. Nägele, M. W. Sigrist, Appl. Phys. B **70**, 895-901 (2000).
[62] M. A. Moekli, C. Hilbes, M. W. Sigrist, Appl. Phys. B **67**, 449-458 (1998).
[63] G. Nemes, "Laser beam characterization", ASTiGMAT Technical Text TT_032105 (2005).
[64] D. C. Dumitras, D. C. Dutu, N. Comaniciu, V. Draganescu, R. Alexandrescu, I. Morjan, Rev. Roum. Phys. **26**, 485-498 (1981).
[65] D. C. Dutu, V. Draganescu, N. Comaniciu, D. C. Dumitras, Rev. Roum. Phys. **30**, 127-130 (1985).
[66] D. C. Dumitras, D. C. Dutu, N. Comaniciu, V. Draganescu, Rev. Roum. Phys. **21**, 559-568 (1976).

[67] D. C. Dumitras, D. Sporea, D. C. A. Dutu, "Set-up for power calibration transfer at CO_2 laser wavelength", Proc. SPIE **6344** "Advanced Laser Technologies 2005" (Invited), Editors I. A. Schcherbakov, Kexin Xu, Qingyue Wang, A. V. Priezzhev, V. I. Pustovoy, 643-653 (2006).
[68] M Tonelli, P. Minguzzi, A. Di Lieto, "Intermodulated optoacoustic spectroscopy", J. Physique (Colloque C6) **44**, 553-557 (1983).
[69] K. P. Koch, W. Lahmann, Appl. Phys. Lett. **32**, 289-291 (1978).
[70] K. H. Fung, H. -B. Lin, Appl. Opt. **25**, 749-752 (1986).
[71] A. Miklos, A. Lörincz, Appl. Phys. B **48**, 213-218 (1989).
[72] E. Nodov, Appl. Opt. **17**, 1110-1119 (1978).
[73] A. Olafsson, M. Hammerich, J. Henningsen, Appl. Opt. **31**, 2657-2668 (1992).
[74] A. Karbach, P. Hess, J. Chem. Phys. **83**, 1075-1084 (1985).
[75] R. A. Crane, Appl. Opt. **17**, 2097-2102 (1978).
[76] J. S. Ryan, M. H. Hubert, R. A. Crane, Appl. Opt. **22**, 711-717 (1983).
[77] A. L. Gandurin, S. B. Gerasimov, A. A. Zheltukhin, I. P. Konovalov, S. T. Kornilov, G. F. Mel'nik, Yu. Yu. Mikhalevich, D. D. Ogurok, V. A. Petrishchev, S. N. Chirikov, Zhurnal Prikl. Spektrosk. **45**, 337-343 (1986).
[78] H. Sauren, D. Bicanic, H. Jelink, J. Reuss, J. Appl. Phys. **66**, 5085-5087 (1989).
[79] F. J. M. Harren, J. Reuss, E. J. Woltering, D. D. Bicanic, Appl. Spectrosc. **44**, 1360-1368 (1990).
[80] T. Fink, S. Büscher, R. Gäbler, Q. Yu, A. Dax, W. Urban, Rev. Sci. Instrum. **67**, 4000-4004 (1996).
[81] J. Henningsen, N. Melander, Appl. Opt. **36**, 7037-7045 (1997).
[82] A. A. Kosterev, Y. A. Bakhirkin, F. K. Tittel, Appl. Phys. B **80**, 133-138 (2005).
[83] J. Davidson, J. H. Gutow, R. N. Zare, J. Phys. Chem. **94**, 4069-4073 (1990).
[84] L. -G. Rosengren, Appl. Opt. **14**, 1960-1976 (1975).
[85] C. Freed, L. C. Bradley, R. G. O'Donnell, IEEE J. Quantum Electron. **QE-16**, 1195-1206 (1980).
[86] R. J. Brewer, C. W. Bruce, J. L. Mater, Appl. Opt. **21**, 4092-4100 (1982).
[87] U. Persson, B. Marthinsson, J. Johansson, S. T. Eng, Appl. Opt. **19**, 1711-1715 (1980).
[88] J. Henningsen, A. Olafsson, Phys. Scripta **T58**, 94-99 (1995).
[89] D. C. Dumitras, R. Alexandrescu, I. Morjan, "Laser absorption measurements using photoacoustic detection", Proceedings of the 10-th International FASE Symposium, Ed. D. Rucinski, ICPE Publishing House, Bucharest, 189-192 (1993).
[90] D. C. A. Dutu, D. C. Dumitras, S. Cristescu, L. Sarkozy, Rom. Reports in Phys. **46**, 639-644 (1994).
[91] D. C. A. Dutu, S. Cristescu, D. C. Dumitras, Proc. SPIE **2461**, 308-316 (1994).
[92] D. C. Dumitras, D.C.A. Dutu, S. Cristescu, C. Mujat, Proc. SPIE **2778**, 670-671 (1996).
[93] D. C. Dumitras, D. C. A. Dutu, S. Cristescu, C. Mujat, Optoelectronica **4**, 21-27 (1996).
[94] S. Cristescu, D. C. Dumitras, D. C. A. Dutu, C. Mujat, Rom. Reports in Phys. **49**, 757-768 (1997).
[95] S. Cristescu, D. C. Dumitras, D. C. A. Dutu, Proc. SPIE **4068**, 263-272 (2000).
[96] S. Cristescu, D. C. Dumitras, D. C.A. Dutu, Proc. SPIE **3405**, 627-631 (1998).
[97] S. Cristescu, D. C. Dumitras, A. Godeanu, "Role of ethylene in the germination metabolism of ricinus communis", American Institute of Physics Conference Proceedings **463**, 652-654 (1999).
[98] A. Lai, L. DeDominicis, M. Francucci, M. Giorgi, G Giubileo, D. C. Dumitras, Proc. SPIE **5131**, 295-299 (2003).
[99] S. Cristescu, D. C. Dumitras, D. C. A. Dutu, Proc. SPIE **4070**, 457-464 (2000).
[100] G. Giubileo, L. DeDominicis, C. C. Lombardi, C. Mancini, A. Antonini, D. C. Dumitras, Proc. SPIE **5147**, 219-225 (2003).
[101] G. Giubileo, A. Puiu, D. C. Dumitras, Proc. SPIE **5486**, 280-286 (2004).
[102] D. C. Dumitras, A. Puiu, R. Cernat**,** G. Giubileo, A. Lai, Molecular Crystals and Liquid Crystals Journal **418**, 217/[945]-227/[955] (2004).
[103] D. C. Dumitras, G. Giubileo, A. Puiu, Proc. SPIE **5850**, 111-121 (2005).
[104] M. Fehér, Y. Jiang, J. P. Maier, A. Miklós, Appl. Opt. **33**, 1655-1658 (1994).
[105] A. Schmohl, A. Miklós, P. Hess, Appl. Opt. **41**, 1815-1823 (2002).
[106] S. Schäfer, M. Mashni, J. Sneider, A. Miklós, P. Hess, H. Pitz, K. -U. Pleban, V. Ebert, Appl. Phys. B **66**, 511-516 (1998).
[107] A. Petzold,, R. Niessner, Appl. Phys. Lett. **66**, 1285-1287 (1995).
[108] A. Beenen, R. Niessner, Analyst **123**, 543-545 (1998).
[109] Z. Bozóki, J. Sneider, Z. Gingl, A. Mohácsi, M. Szakáll, G. Szabó, Meas. Sci. Technol. **10**, 999-1003 (1999).
[110] J. Sneider, Z. Bozóki, G. Szabó, Z. Bor, Opt. Eng. **36**, 482-486 (1997).
[111] Z. Bozóki, J. Sneider, G. Szabó, A. Miklós, M. Serényi, G. Nagy, M. Fehér, Appl. Phys. B **63**, 399-401 (1996).
[112] A. Boschetti, D. Bassi, E. Iacob, S. Iannotta, L. Ricci, M. Scotoni, Appl. Phys. B **74**, 273-278 (2002).
[113] S. W. Sharpe, J. F. Kelly, J. S. Hartman, C. Gmachl, F. Capasso, D. L. Sivco, J. N. Baillargeon, A. Y. Cho, Opt. Lett. **23**, 1396-1398 (1998).
[114] B. A. Paldus, T. G. Spence, R. N. Zare, J. Oomens, F. J. M. Harren, D. H. Parker, C. Gmachl, F. Cappasso, D. L. Sivco, J. N. Baillargeon, A. L. Hutchinson, A. Y. Cho, Opt. Lett. **24**, 178-180 (1999).
[115] L. Menzel, A. A. Kosterev, R. F. Curl, F. K. Titel, C. Gmachl, F. Capasso, D. L. Sivco, J. N.

Baillargeon, A. L. Hutchinson, A. Y. Cho, W. Urban, Appl. Phys. B **72**, 859-863 (2001).
[116] G. Gagliardi, F. Tamassia, P. De Natale, C. Gmachl, F. Capasso, D. L. Sivco, J. N. Baillargeon, A. L. Hutchinson, A. Y. Cho, Eur. Phys. J. D **19**, 327-331 (2002).
[117] A. A. Kosterev, F. K. Tittel, "Chemical sensors based on quantum cascade lasers", IEEE J. Quantum Electron. **38**, 582-591(2002).
[118] D. Hofstetter, M. Beck, J. Faist, M. Nägele, M. W. Sigrist, "Photoacoustic spectroscopy with quantum cascade distributed-feedback lasers", Opt. Lett. **26**, 887-889 (2001).
[119] A. Bohren, M. W. Sigrist, Infrared Phys. Technol. **38**, 423-435 (1997).
[120] F. Kühnemann, K. Schneider, A. Hecker, A. A. E. Martis, W. Urban, S. Schiller, J. Mlynek, Appl. Phys. B **66**, 741-745 (1998).
[121] M. van Herpen, S. te Lintel Hekkert, S. E. Bisson, F. J. M. Harren, Opt. Lett. **27**, 640-642 (2002).
[122] D. Costopoulos, A. Miklós, P. Hess, Appl. Phys. B **75**, 385-389 (2002).
[123] A. Miklós, C.-H. Lim, W.-W. Hsiang, G.-C. Liang, A. H. Kung, A. Schmohl, P. Hess, "Appl. Opt. **41**, 2985-2993 (2002).
[124] C. Fischer, M. W. Sigrist, Appl. Phys. B **75**, 305-310 (2002).
[125] D. Rehle, D. Leleux, M. Erdelyi, F. Tittel, M. Fraser, S. Friedfeld, Appl. Phys. B **72**, 947-952 (2001).
[126] D. Richter, M. Erdelyi, R. F. Curl, F. K Tittel, C. Oppenheimer, H. J. Duffell, M. Burton, Opt. Lasers Eng. **37**, 171-186 (2002).

*Corresponding author: dan.dumitras@inflpr.ro